Spectrum of Fires in an LNG Facility

Assessments, Models and Consideration in Risk Evaluations

Final Technical Report

Developed under

Contract Number: DTRS56-04-T-0005

Submitted to

The U.S. Department of Transportation
Pipeline & Hazardous Materials Safety Administration
400 Seventh Street, S.W.
Washington, DC 20059

by

Technology & Management Systems, Inc.
102 Drake Road
Burlington, MA 01803

5th December 2006

REPORT DOCUMENTATION PAGE	Form Approved OMB No. 0704-0188

1. AGENCY USE ONLY (Leave Blank)	2. REPORT DATE	3. REPORT TYPE AND DATES COVERED
	June, 2006	Final Report: October 2004 – November 2006

4. TITLE AND SUBTITLE	5. FUNDING NUMBERS
Spectrum of Fires in an LNG Facility **Assessments, Models and Considerations in Risk Evaluations**	Contract Number **DTRS56-04-T-0005**
6. AUTHOR(S) **Phani K. Raj**	
7. PERFORMING ORGANIZATION NAME(S) AND ADDRESS(ES) Technology & Management Systems, Inc. 102 Drake Road, BURLINGTON, MA 01803	8. PERFORMING ORGANIZATION'S REPORT NUMBER
9. SPONSORING/MONITORING AGENCY NAME(S) AND ADDRESS)ES) U.S. Department of Transportation, Pipeline & Hazardous Materials Safety Administration 400 Seventh Street, S.W., WASHINGTON, DC 20590	10. SPONSORING/MONITORING AGENCY REPORT NUMBER
11. SUPPLEMENTARY NOTES	
12a. DISTRIBUTION/AVAILABILITY STATEMENT	12b. DISTRIBUTION CODE

13. ABSTRACT (Maximum 200 words)

The models used at present to evaluate the potential hazard areas around large LNG fires were developed with field test data from smaller diameter (1.8 m to 15 m) fires. These models are, however, applied to predict hazard distances from fires much larger in size compared to the experimental fires. Recent publication of the results from a series of tests conducted in 1987 with 35 m diameter LNG fires indicates that large LNG fires tend to generate significant amount of black soot. The black soot is postulated to be generated from incomplete and inefficient combustion of fuel vapors due to reduced oxygen diffusion into the combustion zone near the core of the fire. This phenomenon (of black soot production) in large LNG fires reduces the radiant heat hazard expectations in areas surrounding such fires.

In this project a review was undertaken of the different types and sizes of fires that could occur in a LNG facility and from ship releases, either due to accidental releases or from deliberate acts. The models associated with each of the fire scenarios have been reviewed. A new generation LNG pool fire model ("PoFMISE") has been developed based on data from a number of tests with both LNG and other hydrocarbon fluids. This model is applicable to small as well as large LNG fires and includes the formation of smoke and the consequent diminution of radiant heat output from the fire. The results of the model agree with experimental results for mean emissive power for fires of less than 35 m. Results for larger fires indicate substantial reduction in mean emissive power with almost 50% reduction for a 300 m diameter fire compared to the values used in current models. This implies that the currently predicted hazard distances for large fires are high (by factors of 2 to 3, after accounting for atmospheric absorption).

The report also provides guidance with an illustrative procedure to calculate the risk from different types and sizes of fires that may occur in a LNG facility.

14. SUBJECT TERMS	15. NUMBER OF PAGES
LNG Fire, Emissive Power, Radiant Heat Flux, Atmospheric Absorption, Spectral Radiance, Burn injury, Pool Fire, Vapor Fiore, Jet Fire, Fireball	117
	16. PRICE CODE

17. SECURITY CLASSIFICATION OF REPORT	18. SECURITY CLASSIFICATION OF THIS PAGE	19. SECURITY CLASSIFICATION OF ABSTRACT	20. LIMITATION OF ABSTRACT
Unclassified	Unclassified	Unclassified	None Unclassified

NSN 7540-01-280-5500 Standard Form 298 (Rev. 2-89)

Acknowledgment

The work reported in this report was developed under the US DOT Contract number DTRS56-04-T-0005. The work was jointly sponsored and funded on an equal basis by the Pipeline and Hazardous Materials Safety Administration ("PHMSA"), a modal administration within US DOT, and the Distrigas of Massachusetts Corporation, LLC ("DOMAC"). The work was performed by Technology & Management Systems, Inc ("TMS"). Dr. Phani K. Raj was the project manager, principal analyst and author of this report. Mrs. Geetha Raj performed all work related of coding, debugging and developing the user interface for the computer program that is based on the model development work accomplished in this project.

Dr. Raj expresses his thanks to several persons who made this work possible. First, he acknowledges with sincere thanks to PHMSA and DOMAC for their financial support for this project. Mr. Stanley Kastanas, Mr. Charles Helm, and Mr. Frank Licari of PHMSA provided significant encouragement during the course of this project. Thanks are also due to Mr. Francis Katulak and Mr. Anthony Scaraggi of DOMAC for assisting in a tour of an operating LNG facility, participating in illuminating discussions on realistic fire scenarios and for the support in facilitating the gathering of literature references. The engaging and fruitful discussions with all PHMSA and DOMAC personnel during presentations of the technical progress in the project work helped in the development of new tools in this project; the author thanks them all for their input and efforts in spite of very busy schedules.

Sincere thanks are also due to Mr. Benedict Weis, Dr. Hugues Malvos of Gaz de France, for providing an opportunity to review the original data from the Montoir 35 m diameter LNG tests and discussions on the various issues related to LNG industry. Dr. Raj also expresses his thanks to Dr. Malvos, Mr. Dominique Nedelka and Mr. Michael Godeau, all of Gaz de France for the interesting and fruitful technical discussions that helped in the formulation of the model indicated in this report.

The author also expresses his gratitude for all other technical peers who provided valuable inputs to the model with their questions during the presentation of parts of the model in the May 2005 AIChE conference; they are many to name them individually. Finally, the interest in the subject shown and the encouragement provided by Mr. Robert Smith of the Office of Sponsored Research, PHMSA is gratefully acknowledged.

Table of Contents

List of Tables

List of Figures

Executive Summary

The Pipeline and Hazardous Materials Safety Administration ("PHMSA"), a modal agency of the US DOT, has the principal safety oversight and inspection responsibilities under the pipeline safety laws (49 U.S.C. 60101 *et seq*.). Oversight of the design and safe operation of on-shore liquefied natural gas (LNG) facilities is within the purview of this agency. PHMSA's mission is to ensure continued safety in all aspects related to LNG facilities, in the current rapid expansion of the industry. The design, operation and maintenance requirements for LNG facilities are stipulated in 49CFR, Part 193. These regulations have gone a long way to ensure that no LNG leaks/releases occur from material defects, natural phenomena and machinery attrition; if one should occur there are enough safeguards to minimize the effects on plants and the surroundings. However, since 9/11/2001 a new threat poses significant concerns. Many of the potential release scenarios that would have not been a cause of concern (based on assessments of mechanical failures of structures, piping and equipment due to usage or fatigue, age, natural forces and acts of God) need to be reexamined from the perspective of sabotage caused failures.

The primary concerns of hazards to both people and infrastructure are those caused by fires of different sizes resulting from different scenarios of LNG releases either at storage terminals or from transportation vessels. Understanding, modeling and developing appropriate consequence assessment tools (for example, computer programs to calculate the hazard zones) for a spectrum of fire scenarios are essential before proper and additional safeguards can be employed. Also, these analytical or computer based tools will aid in assessing the system-wide risks, especially those caused by fires.

E-1 Purpose of the study

PHMSA's stated goal is to perform relevant research in partnership with industry. In keeping with this goal and in response to an identified need to develop research applicable to LNG industry, PHMSA and Distrigas of Massachusetts Corporation. LLC, (representing the industry participation) jointly sponsored and funded the project reported in this report.

The project discussed in this report was undertaken to,

1 Identify the various types of fires that may occur in a LNG facility either from accidents or caused by intentional acts of terror and evaluate the state of knowledge related to determining the hazards posed by each type and size of fire.

2 Develop mathematical models and to improve existing models taking into account data from field experiments involving 35 m diameter LNG fires on land that became available since the original models were developed. These data indicated a fire characteristic that were not known before and which indicated a considerable reduction in radiant heat hazard extent of larger fires (compared to the current model predictions).

E-2 The Scope of work

The scope of the work performed in this project includes the following:

1 Developing, in consultation with the industry, a set of credible scenarios of LNG release in a facility

2 Reviewing the state of the art in modeling and calculating the hazards from fires identified in the release scenarios

3 Developing or improving mathematical models, based on experimental data, describing these fires and facilitating the evaluation of potential hazard areas, and

4 Identifying an approach ("protocol") to use the models in an assessment of the risks posed to the public from these fires.

E-3 Project achievements & findings

The current regulatory requirements in 49 CFR, part 193 and the specifications in the NFPA 59A Standard for assessing the potential hazard zones around "design spills" in LNG facilities have been reviewed in this report. Also, the specifications in a risk-based regulation in Europe (EN 1473) for LNG facilities have been reviewed.

Discussions with industry representatives and participation in several LNG forums resulted in the compilation of several "credible" scenarios of fires in on-shore LNG facilities. These include (i) the jet fires due to small or medium leaks of gas or liquid from transfer piping, (ii) pool fires due to the spill of LNG on to ground, contained in impoundments (required by code and regulations), (iii) vapor fires arising from the ignition of a dispersed vapor cloud ignited at some downwind distance from the source and after the cloud has dispersed for a considerable, (iv) fireball type burning which occurs when a vapor cloud of high vapor concentration (which occurs at the early stages of dispersion of vapor generated by LNG spill) is ignited. In addition, the expanding pool fire, arising from spill of LNG on water, from either the unloading arm or from the tank through hull puncture of a LNG ship, and its immediate ignition is also identified.

The review of the data and findings from past LNG fire experiments discussed in Chapter 2 of this report indicate that the hazard from smaller fires is well understood (and current models represent the hazard realistically). However, it is seen that there is a size dependent phenomenon, namely production of large quantity of black smoke that occurs in LNG fires above certain diameter, which tends to reduce the severity of the thermal radiation hazard. The formation of smoke in large LNG fires acts as a shield around the fire (obscures the inner burning core) and consequently reduces the radiant heat output from the fire to the surroundings. Mathematical models for calculating the fire radiant heat hazards that are currently used by both the government and the LNG industry do not take the effect of smoke shielding into account when determining the hazard zones around large LNG pool fires. Another phenomenon that has not been considered and which has been found in more recent experiments is the burning of a dispersed vapor cloud in the form of a fireball. This phenomenon has been observed when a

LNG vapor cloud is ignited during its early dispersion when much of the cloud has higher vapor concentration (significantly higher than the upper flammability limit).

The experimental data on pool fires up to 35 m diameter fire indicate that the mean emissive surface power (MSEP) of LNG fire increases initially as the fire diameter increases, up to about 20 m diameter, and subsequently begins to decrease, perhaps due to the above described smoke production phenomenon. The mean emissive power is defined on the basis of a specific geometrical description of the fire as a right circular cylinder whose height is set equal to the visible height of the fire and which is given by a correlation (Thomas' correlation). On this basis, the maximum value of the fire geometry average emissive power is 225 kW/m^2 (recorded in the 15 m diameter LNG fire tests on water). The mean emissive power for a 35 m diameter LNG fire on land is reported to be 165 kW/m^2. Figure E-1 shows the summary of these mean emissive power results.

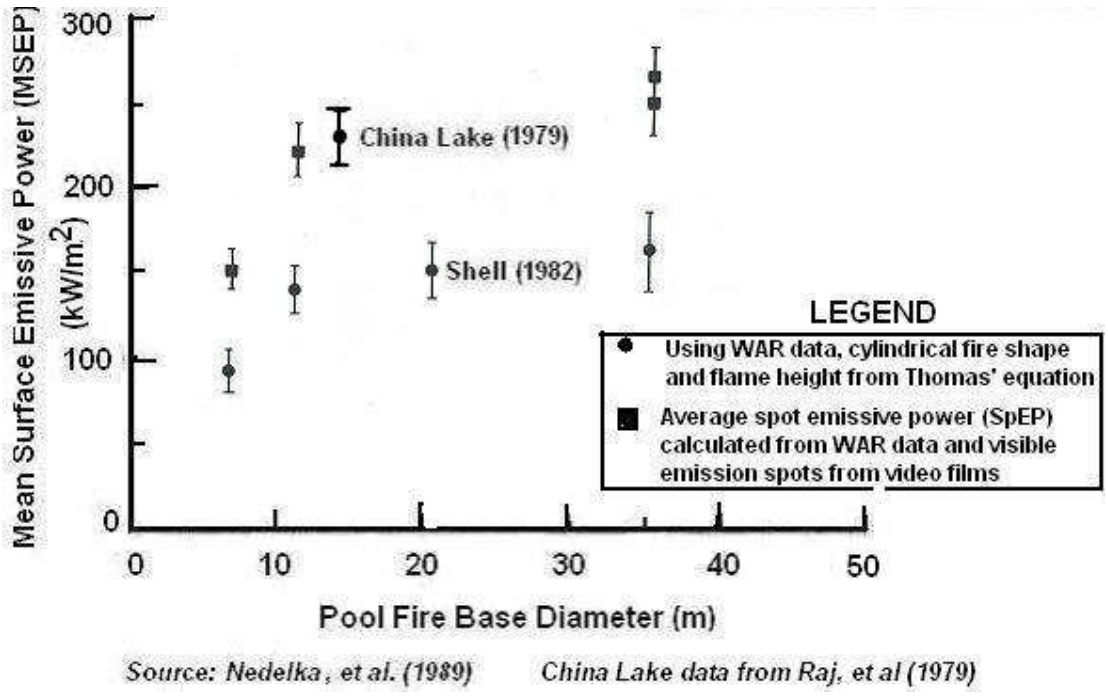

Figure E-1: Experimental data on mean surface emissive power (MSEP) variation with fire size

In addition, the experimental data from the 35 m diameter tests of LNG fire on land (conducted in Montoir France in 1987) indicate that the surface emissive power (SEP) of a large fire varies significantly between the bottom parts of the fire and the top part of the fire. In fact, a variation of SEP by a factor of about 5 between the bottom and top of fire has been observed. The statistical distribution of the data gathered in these test series by a movable narrow angle radiometer is shown in Figure E-2. It is clearly seen that the emissive power in the bottom parts of the fire is more "concentrated" and in the top parts there is more data scatter (due to intermittency in smoke shielding effect). It is also seen from spectral measurements taken at

about 4 m above the ground surface that the fire emission is similar to that of a black body except for absorption in the water vapor and CO_2 bands. In addition, it is also seen from a review of the films of the test that the fire has a base height over which the burning seems to be very intense and bright and it is only on top of this "base zone" is there any smoke production. Based on the spectral measurements in the Montoir tests and from the spectral data obtained in the China Lake LNG fires-on-water-tests it is determined that the optical path length for a LNG fire is 13.5 m and that the effective blackbody temperature in the fire is 1547 K (corresponding to a blackbody emissive power of 325 kW/m^2). The uncertainty in the above temperature estimation is calculated to be 0% to-2.5 % (i.e., the estimated temperature can be in the range of 1547 K to 1512 K). A fire of diameter equal to the optical path length (or its inverse the extinction coefficient) in the brightest part of the fire will have an effective emissivity (ration of actual emissive power to that of the blackbody emissive power) of $\varepsilon = \{1\text{-}e^{-1}\} = 0.6321$. (A fire of diameter equal to about 3.5 times the optical path length could be considered as a black radiator).

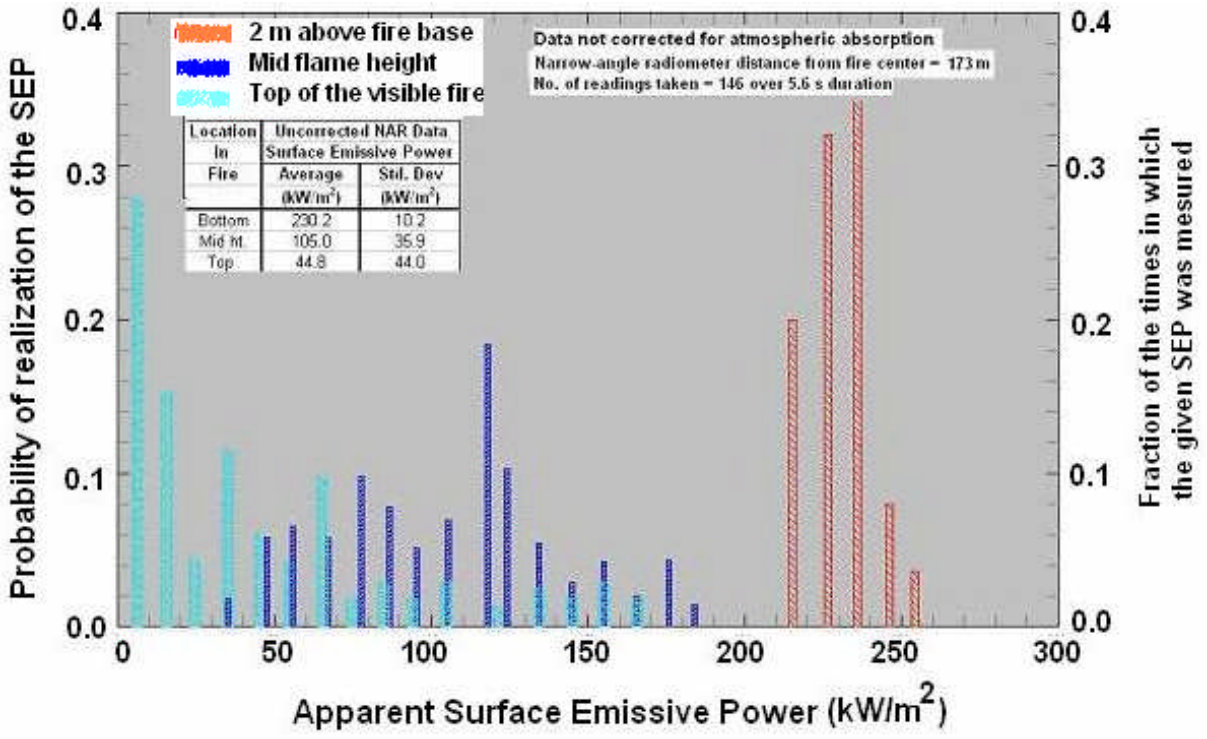

Figure E-2: Statistics of apparent SpEP (NAR data) – for different locations along the fire plume axis

Current generation models that are being used to calculate the radiant heat flux levels at different distances from the fire are found to be overly conservative in that they do not take into account the radiant emission reduction observed in large LNG fires. Therefore, a large LNG pool fire model has been developed which takes into account the production rate of smoke, the variation of emissive power from bottom to the top of the "visible" fire and the presence of and

variation with size of the bottom "bright burning" zone. This model, termed the Pool Fire Model Including Smoke Effects ("PoFMISE") is described in Chapter 4. The model uses correlations developed from tests with crude oil fires of up to 17 m diameter for the fraction of the fuel that gets converted to smoke. It also utilizes other correlations for the smoke optical properties (extinction coefficient, extinction cross section, etc.) obtained from relatively small scale, laboratory experiments. Using the model the fire-geometry-based mean surface emissive power (MSEP) for LNG fires of various diameters has been calculated. These results are presented in Table E-1.

It is seen that the PoFMISE model results agree very closely with the mean values obtained in the experiments to date. In addition, the model results indicate that as the fire diameter is of the size 100 m and larger the mean emissive power reduces significantly compared to those that are used in current models such as LNGFIRE 3 model (190 kW/m^2). This implies that the hazard distances predicted for a specified flux level would be smaller when the PoFMISE model is used compared to those from other models such as LNGFIRE 3. The results shown in Table E-1 also indicate that the bottom "clean burning" zone length is about 25% of the visible length for a 15 m diameter fire whereas for a 300 m diameter fire it is less than 9%. The latter is in keeping observations from very large oil fires on water where only a very small part of the fire is visible (because of the "clean burning" zone).

As a part of the overall goal of calculating the risks to the population from a LNG facility a methodology of evaluating the risks from potentially large LNG pool fires is illustrated in Appendix C of this report. This methodology describes the various phases in the performance of a risk assessment, the identification of fire scenarios and their organization in the order of primary and secondary events, and the development of the various probabilities of occurrence of the scenarios. Also, illustrated is the calculation of the consequence areas and people exposure to hazardous radiant heat flux after considering the mitigating and shadow effects of buildings and structures, and the atmospheric absorption of radiant heat. Determination of the risk by considering different categories of population (the elderly, the physically challenged, the children and normal adults), population density, density of buildings and other shelter providing structures, etc. are illustrated. No numerical values, of either the probabilities of occurrence of fire events or the consequence areas for different size fires in different wind and weather conditions have been determined. Also not performed in this report are any site-specific calculations.

The study results are expected to lead to a better understanding of the types of fires that may occur in a LNG facility. In addition, the PoFMISE model developed in this project will lead to a more accurate description of large LNG fires. The utility of this model lies in the fact that it provides a better description of the real conditions that occur in large LNG and other hydrocarbon fires and therefore can provide better estimates of the real hazard distances from the fires without compromising public safety. The results of this study may contribute to the scientific debate to better understand the hazards of large fires instead of using the current models that were developed using small fire data and extrapolation. Finally, the results of this study may lead to modifications in industry consensus standards or US DOT regulations related to the calculation of LNG fire hazard areas since the model developed in this report is easy to use, captures the fire behavior characteristics of large LNG fires and has been validated by data currently available from experiments.

Table E-1
Comparison of model predicted MSEP with experimental data

Fire Diameter (m)	Substrate on which LNG boils	Soot mass yield (Y)* (%)	Soot Concentration (C_S) (kg/m^3)	Fractional length of the "Clean burning zone" (ψ)	Soot Transmissivity (τ_S) = 10^{-2} x	MSEP over the visible fire plume height (E_{avg})		Remarks
						PoFMISE model result (kW/m^2)	From field tests (kW/m^2)	
15	Water	12.7	3.328 x 10^{-4}	0.196	66.40	172	185-224	China Lake tests Raj, et al [1979]
20	Land	13.0	3.419 x 10^{-4}	0.180	57.12	183	140-180	Mizner & Eyre [1983]
35	Land	13.7	3.595x 10^{-4}	0.150	35.70	177	175±30	Montoir tests GDF [1987]
100	Land	14.9	3.926 x 10^{-4}	0.093	4.00	113	-----	Potential size of future pool fire tests
300	Water	16.2	4.272 x 10^{-4}	0.033	0.00277	90	-----	Estimated pool size from one tank content spill from LNG ship

Assumed parameter values; **r = 17.17 for CH_4 ;** **β = 0.06 ;** **k_m = 130 m^2/kg ;** **E_{max}= 325 kW/m^2 ;** **T_a = 293 K**

*** Notarianni correlation for smoke yield;** **Optical path scale length at bottom of LNG fire = 13.5 m**

E-4 Uncertainty Analysis

An uncertainty analysis was undertaken to determine the sensitivity of the model results to changes in values of parameters used in the model. The model contains three significant parameters whose values are not known completely, especially for methane diffusion fires. These parameters include (i) the fraction of the fuel that gets converted in to smoke, (ii) the size of the smoke particles represented by the soot specific extinction coefficient (κ_m) and the "profile" of the curve of variation of the local mean surface emissive power with height above the base of the fire (represented by the index "n" of the visibility probability distribution with height). For the fraction of fuel converted to smoke as a function of the size of the fire, experimental values obtained from 17 m diameter crude oil fires has been used. This value represents the best fit to the measured NAR data from the 35 m diameter LNG fire tests in Montoir. The extinction coefficient values (κ_m) were perturbed from 100 m^2/kg to 1000 m^2/kg (130 m^2/kg is the value for laboratory size propane diffusion fire). The index (n) on the fire core visibility probability (p) distribution was varied from 1 to 4. The results, in terms of the overall mean surface emissive power (MSEP), obtained from the model for these parameter variations were compared with the 35 m diameter experimental data for the same MSEP. Based on this comparison it is concluded that a combination of n=3 and κ_m = 130, n=2, κ_m=200 best represent the values of the parameters. These combinations of parameter values not only track the measured vertical distribution of the SEP but also predict very closely the measured overall MSEP (165 kW/m^2). However, it is noticed that the κ_m = 200 is higher than the value for laboratory scale propane fire (and one expects κ_m to be less for methane fire). It is entirely possible that in a large diffusion fire the size of the smoke particles are bigger thereby leading to a higher κ_m value. The correct values of these parameters can only be determined from additional laboratory and field scale experiments.

E-5 Conclusions from the study

The major conclusions from this study are:

1 A semi empirical model to predict the thermal radiation output from large hydrocarbon liquid fuel pool fires has been developed, which takes into consideration the formation of smoke, its effect (by shrouding the inner burning region) in reducing the thermal output into the surroundings.

2 The model assumes a constant emissive power zone at the bottom of the fire. The height of this zone varies with the properties of the fuel, the size of the fire and the evaporation rate. The variation of the emissive power with height above this zone has been modeled by assuming a probability distribution for the fraction of the time the inner core of burning fire is visible through the smoke shroud.

3 The results of the model have been compared with the only available (narrow angle radiometer) data for the measured variation of the emissive power with height. The model results track this variation reasonably well, given the uncertainties in the model assumptions and in the data.

4 The model also predicts the measured mean emissive power from 15 m and 35 m LNG fire tests within the accuracy that can be ascribed to the model.

5 The model is more realistic in its treatment of the actual dynamics and phenomena observed in all large hydrocarbon fuel fires, including the very important one relating to smoke production and obscuration of the burning regions of the fire. In this regard it is, perhaps, superior to any of the existing single-mean-emissive-power models.

6 The use of the model and other fire models in a risk analysis has been illustrated with a protocol for risk calculations.

The use of the model developed has significant implications for the calculation of realistic hazard distances as opposed to the significantly large hazard distance predictions of the currently used LNG fire models.

E-6 Recommendations from the study

Based on the assessments performed in this project and the large fire model developed, the following recommendations are put forth.

1 Laboratory studies should be performed to obtain certain key parameter values for LNG vapor burning in air. These include the fraction of the fuel mass that gets converted to smoke particles as a function of combustion temperature and fuel-air (or oxygen) concentration ratio. Similarly, laboratory studies should be performed to obtain the optical properties of smoke produced in diffusion fires of methane in air.

2 Additional field tests with LNG fires of sizes larger than 35 m diameter should be conducted to determine the large diameter effects and to verify whether large fires have reduced heat emission compared to smaller size (< 35 m) LNG fires. Dike fires on land and unconfined spill fires on water should be conducted.

3 The PoFMISE model developed in this project should be included in any revisions to the 49 CFR, part 193 regulations, since the model represents the best data available for large LNG fires and includes many of the phenomena seen in large fires. Current model recommended for use in the regulations does not include these important phenomena.

4 Effects of passive and active mitigation techniques (such as dike walls, sub surface sumps, water curtains, water application directly to the fire plume to reduce temperature and affect combustion processes) in reducing fire thermal hazard effects should be evaluated both theoretically and experimentally. This effort should be initiated with a detailed review of the available techniques, their effects and their incorporation into a fire radiant heat flux model.

5 An integrated fire hazard model should be developed which includes the characteristics of large LNG fires (and radiant heat from such fires with due consideration to the variation of emissive power with height), the spectral characteristics of emission from various parts of

the fire, the absorption in the atmosphere of the intensity of fire emission in different wavelengths, the characteristics of the intervening objects between the fire and the heat receiving object, the thermal characteristics of the receiver and the proper consideration of the hazard to the object based on its susceptibility to heat input and duration of exposure.

6 A database of probabilities of different types of releases of LNG from both fixed plant equipment and from shipping and transportation incident should be developed.

7 A realistic risk assessment procedure that considers the probabilities of occurrence of different types and sizes of LNG fires, many of the phenomena, parameters and models identified in this report and other considerations (such as the effects of mitigation technology) should be developed. The application to a generic plant or transportation condition should be demonstrated with an example calculation.

8 A set of criteria should be developed for the acceptability of risk results in evaluating the safety of a LNG plant or LNG transportation, relative to public safety**.**

Chapter 1
Introduction

1.1 Background

The liquefied natural gas (LNG) industry in the U.S. has been providing services safely for over 30 years without any incidents that have affected the public. At present only four marine import (base load) and land-based storage terminals are operating in the US, the ones in Everett, MA, Cove Point, MD, Elba Is., GA and Lake Charles, LA. In addition, an LNG export terminal has also been operating in Kenai, AL for over two decades. More recently, an off shore marine terminal has been commissioned in the Gulf of Mexico and operated by Excelerate Inc. Because of the projected shortfall in supply of domestic natural gas to service the increasing demand for natural gas fuel in the US, several marine LNG import facilities are proposed for construction in the US and applications are pending before the Federal Energy Regulatory Commission (FERC) and the US Maritime Administration (MARAD), respectively, for on-shore and off-shore facilities.

The Pipeline and Hazardous Materials Safety Administration (PHMSA) of the US Department of Transportation (US DOT) has the principal safety oversight and inspection responsibilities for on-shore LNG terminals under the pipeline safety laws (49 U.S.C. 60101 *et seq*.). PHMSA wants to ensure continued safety in all aspects of design and operation of LNG facilities in the current expansion of the industry. The requirements for design, operations and maintenance stipulated in 49CFR, Part 193 for LNG facilities have gone a long way to ensure that no LNG leaks/releases occur from material defects, natural phenomena and machinery attrition. If one should occur there are sufficient safeguards to minimize the effects on plants and the surrounding populations. However, since 9/11/2001 a new threat poses significant concerns. Many of the potential release scenarios that would have not been a cause of concern (based on assessments of mechanical failures of structures, piping and equipment due to usage or fatigue, age, natural forces and acts of God) need to be reexamined from the perspective of sabotage and terrorist action caused failures.

The primary concern is of safety from LNG fires to the general public and the infrastructure (both inside the facility as well as out of the facility property). Large fires may have impact outside the plant boundary, whereas smaller fires could have adverse effects on machinery and process equipment within the LNG facility. While large fires may have off-site effects, their occurrence is extremely rate[1]. Therefore, the level of potential fire hazards to the neighbors (both people and infrastructure) of a LNG plant can be gauged only by the scientific methods of risk assessment. A similar argument can also be made for LNG transportation (in ships, highway trucks or other modes). LNG fire risk assessments involve considerations of both the probabilities of events (that can lead to fires) as well as the considerations of different sizes of fires and their effects (consequences) on objects and people within and outside the plant

[1] World-wide, several tens of LNG facilities have been operating for over 3 decades. Not a single large fire has occurred, anywhere in the world, in any LNG terminal/storage facility. This enviable record cannot be matched by other fuel storage or import or production facilities.

boundary. Understanding, modeling and developing appropriate consequence assessment tools (ex, computer programs to calculate the hazard zones) for a spectrum of fire scenarios are therefore essential for not only understanding the risks such fires pose but also to evaluate the effectiveness, in terms of risk reduction, of mitigation and safeguarding measures. These analytical or computer based tools will aid in assessing the system-wide risks, especially those caused by fires.

PHMSA has realized that assessment of risks to the public from LNG releases from either land based terminals or during transportation requires the knowledge of the type of fires that could occur, their characteristics and the extent of hazard that each type of fire would pose. Assessment of the magnitude of the hazards requires mathematical modeling of the various realistic phenomena that influence the fire characteristics and radiant heat output from such fires. It is with this intent of cataloging and characterizing various types and sizes of LNG fires that may occur in a LNG facility and in LNG transportation that PHMSA initiated the work described in this report.

Technology & Management Systems, Inc (TMS), was awarded a joint Government and Industry, cost-share type of contract to conduct the research described in this report under. The project was funded 50% by US DOT, Pipeline and Hazardous Materials Safety Administration (PHMSA), Washington, DC under the contract number DTRS56-04-T-0005 and the other 50% by Distrigas of Massachusetts Corporation, LLC., Everett, MA. Dr. Phani K. Raj was the project manager and principal analyst for the project at TMS.

1.2 Objectives of the project

The objectives of the research discussed in this report were to:

- Identify various scenarios of LNG fires that may occur in LNG import/storage terminals (and from ships).
- Develop additional models for such fires as may occur and which the current models do not address completely or properly.
- Develop protocols for and approaches to using the fire models in conducting an assessment of the risks from fires in either LNG import/storage terminals or LNG in transportation.

1.3 Scope of work

To achieve the above objectives, the project was conducted under the following four tasks.

Task 1: Discussion with the LNG industry, and the development of a list of credible and potential LNG release scenarios resulting in LNG fires.

Task 2: Review of the literature on modeling LNG fires identified in task 1.

Task 3: Improvement/development of the mathematical models describing the fire characteristics and the extent of hazard from different types of fires. Also, computerizing any new models developed.

Task 4: Development of protocols for using the fire models in performing risk assessment of LNG release from storage terminals or transport ships.

1.4 Credible and potential LNG fire scenarios in LNG terminals and in LNG transportation

Informal discussions were undertaken with several knowledgeable members of the LNG industry, both during personal meetings and over the telephone regarding past historical accidents involving LNG releases and potential release scenarios that could lead to the occurrence of a fire. The discussions involved potential release scenarios covering both on-shore terminals and shipping operations (near receiving terminals and in docks). In one case, a site visit was undertaken to an operating, large, on-shore LNG import and storage terminal for discussion with operators and a review of potential scenarios of LNG fires due to accidents as well by the intentional acts of terrorists.

Table 1-1 illustrates the potential LNG release and fire scenarios that were identified during the discussions with LNG terminal operators. The causes of LNG release and the types of fires that may potentially occur and the hazards that these fires may pose are also indicated in this Table. Figure 1-1 shows the spectrum of different types of potential fires from LNG releases in on-shore storage facilities, and LNG ships. The generic types of fires that can occur in a LNG facility include (i) the jet fires (due to liquid releases in the form of a jet from a pipeline or the tank), (ii) liquid pool fires which form when the released LNG pools on land or water and is ignited while the liquid pool persists, (iii) concentrated vapor burning in the form of a short lived fireball and, (iv) vapor flash fire - deflagration type burning of a dispersed vapor cloud; a vapor cloud is formed by the release of liquid on to land (or water) and is dispersed by the wind when the vapor cloud is unignited at the source of vapor. In a particular scenario of LNG release, one or more of these generic types of fires can result depending upon the time of ignition relative to the time of release and the local environmental conditions. Pool fires can be of the high aspect ratio type (if the liquid is in a trench and is ignited) or of the constant size (diameter) type as in the case of LNG contained within an impoundment (sump or dike), or of the temporally expanding type as would be the case for an expanding LNG pool on water. When dispersed LNG vapor clouds are ignited in the open, in general, an upwind moving flash fire results (for leading edge ignition) with a deflagration type burning, which has a turbulent flame speed of the order of several meters per second, the flame speed being dependent on the wind conditions. It is anticipated that the flame speed for vapor burning can increase (accelerate) in the presence of obstructions, the acceleration in normal outdoor obstructions may not be sufficient to cause high over pressures and their concomitant hazard.

In Chapter 2 the literature related to modeling the above different spectrum of fires is reviewed. Specific attention is directed at the ability of the models to consider the realistic situations that arise in LNG facilities and shipping and calculate the extent of hazards from each type of fire. Past experimental findings are also discussed.

Table 1-1
Fire Scenarios due to releases from on-shore LNG terminals and ships

#	Cause of LNG release	Types of fires	Potential hazards
1	Transfer piping, valve or gasket leak	Principally a liquid jet fire. Very likely to be a very small diameter jet fire with limited distance of fire plume	Jet fire impinging on an object will have the torch effect of heating the object to high temperature, locally. Whether the object fails or not depends on the duration of exposure and the thermal properties of the object. A person exposed (with flame contact) to a jet fire will suffer severe burns. Radiant heat effects will be relatively small.
2	Leak from a hole on the side of transfer pipe caused by an accidental collision of a vehicle or debris with the pipeline.	Jet fire which whose size (diameter and flame distance) will depend upon the size of hole and the back-pressure in the pipe.	
3	Puncture in vaporizer piping	Pool fire if enough liquid pools under the release location or is directed to a sump and ignites. Vapor fire, if the vapors are dispersed and meet an ignition source. Depending upon confinement by pipes and other structures vapor cloud explosion may occur under certain circumstances	Pool fires pose radiant heat hazards outside the fire. Distance to hazard depends upon the size of fire and its location relative to other objects and the dike. Vapor cloud hazard can occur within the property line or outside the properly line. In general only a transient flash fire will result with no over pressures. Objects within the path of the propagating fire may suffer thermal damage. People within the fire path will experience severe burns. People outside the path of the flash fire will experience transient radiant heat. In general, persons outside the vapor cloud will not suffer serious injuries.
4	Release from the ship-to-shore transfer piping within the facility during LNG transfer operations or during withdrawal from the storage tank (released LNG directed into an impoundment or sump)	Jet fire from the rupture in the pipeline, if the rupture is small. Channel fire in the liquid channel to the impoundment area. Pool fire in the impoundment (sump) into which the liquid spill is channeled, if the release is large and not all released liquid is consumed in the jet or channel fire	Potential hazards from pool fire radiant heat to structures within and outside the facility. Also, potential burn hazards to people within and outside the facility. Jet fire and channel fire hazards are expected to be confined to within the facility.

5	Release due to a missile penetration of the side of a LNG storage tank	Pool fire in the impoundment. Possible pool fire outside the facility. Vapor cloud fire if no immediate ignition, of the vapor cloud formed, but its ignition at a later time or at a distance from the source of vapor.	Pool fire radiant heat hazards. Deflagration vapor fire hazards. Potential vapor cloud fire acceleration (and corresponding overpressure) in areas where the vapor cloud has spread to and then ignited in the presence of obstructions or structures.
6	Liquid exposure to the atmosphere and its subsequent ignition due to the collapse of the storage tank roof (impact by a very heavy and high momentum object such as a small plane)	Pool fire on top of the storage tank	Pool fire radiant heat hazard
7	Release at the jetty from the improper connection between the connecting arm (Chiksan arm) and the ship's transfer piping. The improper coupling may be due to misalignment, a bad gasket, or a human error cause	Vapor fire from spill evaporating on water without ignition. Pool fire on water if the spill is large and is ignited. Pool fire on dock ground if spill occurs on land and is ignited	Vapor cloud fire radiant heat hazard Pool fire radiant heat hazard Radiant heat effects on local structures, next to the jetty.
8	Large releases on or under water from a LNG ship due to a ship-to-ship collision incident or due to acts of terror on the LNG ship	Fireball type burning of the large vapor cloud formed (and ignited) immediately after the release of LNG on to and into water Expanding pool fire of LNG on water Dispersed vapor cloud fire if ignition occurs after significant time of cloud dispersion	Radiant heat hazards from both the fire ball and pool fire Radiant heat hazard from the deflagration type burning of the vapor cloud.
9	Hose rupture at an LNG loading (truck) station	If ignition occurs immediately a jet fire from the hose end will occur. This fire will last until the supply of LNG is terminated by the shut off valve. In the absence of immediate ignition, part of the the LNG released will flash to vapor which will get dispersed by the wind and the remainder liquid will flow into sump and will further evaporate or if ignition occurs form a pool fire. The dispersing vapor, if ignited by a down wind ignition source will result in a flash vapor fire of very short duration.	Vapor cloud fire radiant heat hazard Pool fire radiant heat hazard Radiant heat effects on local structures, next to the truck loading sttion.

10	Overfilling storage tank or	In general provisions are made in storage tanks to channel overflow of LNG into sumps. The types of fires that can be casued by such overflow are (i) pool fire in sump, (ii) vapor emanation, dispersion within the dike and, if the vapor cloud is ignited, vapor fire.	Sump pool fire radiant heat hazard Vapor cloud fire radiant heat hazard
11	LNG roll over in the tank	LNG rollover could lead to the release of vapors through the relief valve over an extended period of time. These vapors may partially disperse from the top of the tank. In the event ov very low wind speeds, the vapors can descend due to higher-than-air density, disperse within the dike and outside the dike. If the vapor cloud is ignited at ground level, a flash vapor fire will result.	Vapor cloud fire radiant heat hazard
12	Extended release of vapor from process equipment	Either liquid from the vaporizer equipment or high pressure gas in the sendoff pipeline may be released. If a liquid release occurs without immediate ignition, then there will be flash vaporization of a fraction of the liquid, a continuous vopr cloud formation (for the duration of release). Should this vapor cloud get ignited at a down wind distance , a flash vapor fire can form. If the jet of LNG liquid is still issuing at the time the fire flashes back to the source, a liquid jet fire will result. In the case of high pressure gas release and its ignition, a high pressure gas jet fire will result. Otherwise, the high pressure gas jet mixes with air and disperses. Again, depending upon the time of ignition, either a vapor fire will result followed by a jet fire or passive dispersion of vapors if no ignition occurs	Liquid jet fire Flash vapor fire High pressure gas jet fire

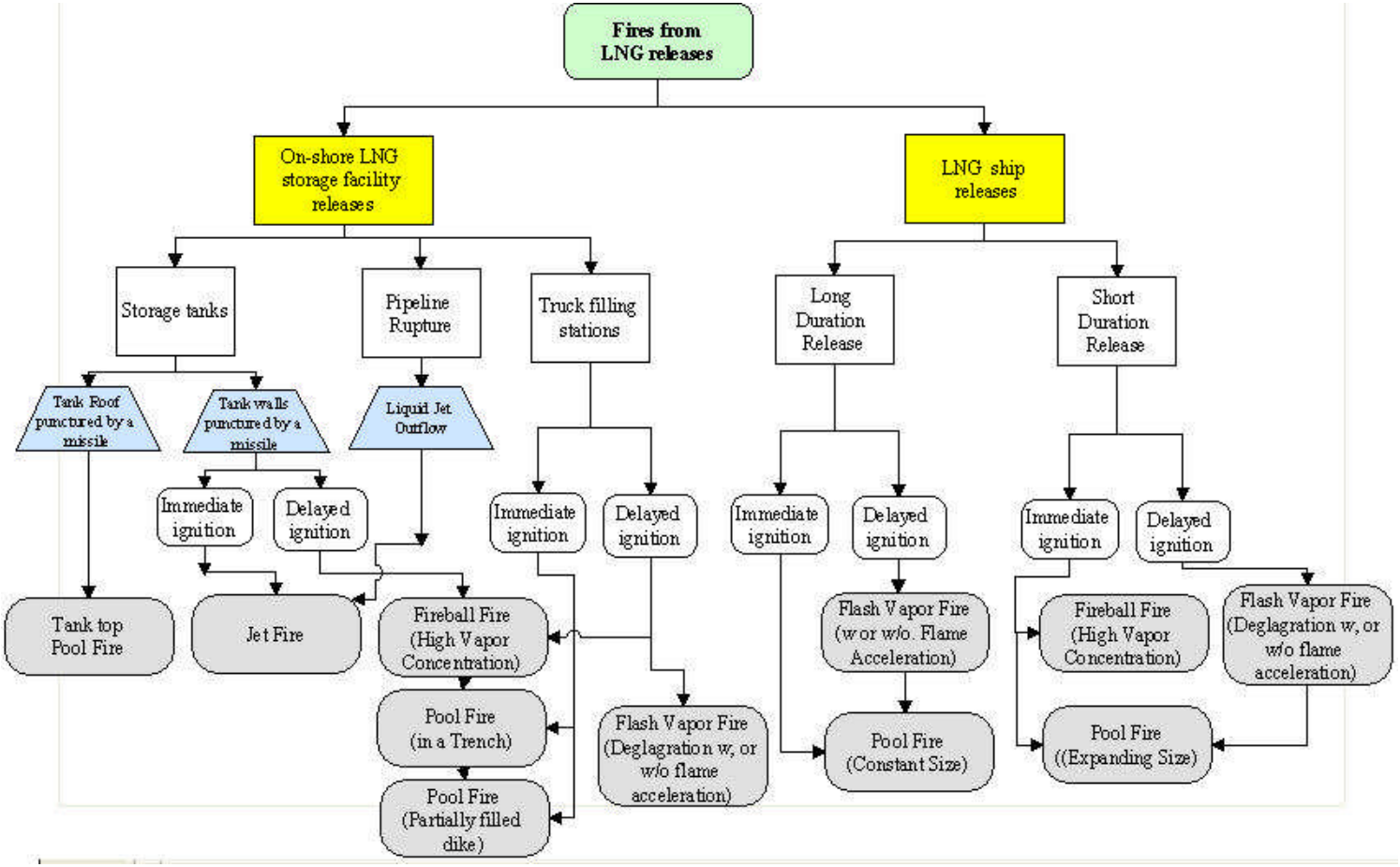

Figure 1-1: Spectrum of possible fires from LNG releases in on-shore storage facilities and from LNG ships

1.5 LNG fire effects assessment in LNG Regulations, Codes and Standards

In the US the requirements related to the design, location, safety exclusion distances, operations and maintenance of an LNG facility are stipulated in the Federal Regulations 49CFR, Part 193 and in NFPA 59A, "Standard for the Production, Storage, and Handling of Liquefied Natural Gas (LNG)." Both these documents stipulate the requirements for on-shore LNG facilities only. Specifically, the requirements include evaluation of the hazard distances for different size LNG fires; however, the fires to be considered are the pool fires in the impoundments.

1.5.1 US DOT regulations in 49 CFR, Part 193

Section 193.2051 of 49 CFR stipulates that each LNG container and LNG transfer system must have a thermal exclusion zone in accordance with section 2.2.3.2 of NFPA 59A (2001 edition). Three exceptions to the specifications in NFPA 59A are indicated. These relate to the required use of (i) LNGFIRE3 model[2] to calculate the exclusion distances, (ii) 95th percentile wind speed, and (iii) ambient temperature and relative humidity that produce the maximum exclusion distances, except for values that occur less than 5 % of the time based on recorded data.

The Federal Regulation does not specifically identify the types of fires to be considered in the evaluation of the exclusion distances. It is implied that the "Thermal radiation protection" under § 193.2057 is for spills in the facility that are directed to impounding areas and pool fires that may occur on these impoundments.

The Regulation also requires, in § 193.2059, the assessment of "Flammable vapor-gas dispersion protection" and the calculation of the dispersion exclusion zone. Implicit in this requirement is the consideration of the vapor cloud fire arising from the dispersion of the flammable vapor; however, no specific "hazard area" calculation is specified for the thermal radiation hazard zone next to a propagating vapor cloud fire that may result if the vapor cloud is ignited.

1.5.2 NFPA 59A Standard[3] for the production, storage, and handling of LNG

NFPA 59A Standard requires that the "Thermal radiation flux from a fire shall not exceed the limits" specified in Table 1-2, under atmospheric conditions of 21 ^{o}C (70 ^{o}F) and 50 % relative humidity. In addition, the Standard stipulates that the thermal radiation distances are to be calculated using any one of the specified models, namely, (i) The LNGFIRE3 model, (ii) An alternative model that takes into account the same physical factors as the LNGFIRE3 and which has been validated by experimental data, and (iii) A point source model specified in the Standard which is based only on the base size of the fire.

---

2 This model is reviewed in detail in Chapter 2 on literature review

3 Refers to the 2006 edition. However the calculation requirements for thermal radiation exclusion distances are the same in both 2003 and 2006 editions.

Table 1-2
Thermal hazard criteria in NFPA 59A Standard

Table 5.2.3.2: Thermal Radiation Flux Limits to Property Lines and Occupancies		
Thermal Radiation Flux		**Exposure**
Btu/hr ft^2	**KW/m^2**	
1,600	5	A property line that can be built upon for ignition of a design spill[a]
1,600	5	The nearest point located outside the owner's property line that, at the time of plant siting, is used for outdoor assembly by groups of 50 or more persons for a fire in an impounding area[b]
3,000	9	The nearest point of the building or structure outside the owner's property line that is in existence at the time of plant siting and used for assembly, educational, health care, detention and correction, or residential occupancies for a fire in an impounding area[b,c]
10,000	30	A property line that can be built upon for a fire over an impounding area[b]
[a] See 5.2.3.5 for design spill. [b] The requirements for impounding areas are located in 5.2.2.1. [c] See NFPA *101*, *Life Safety Code*, or *NFPA 5000*, *Building Construction and Safety Code*, for definitions of occupancies.		

Note: The above table is extracted from the 2006 Edition of NFPA 59A.

A formula is specified in the point source model indicated in NFPA 59A Standard for calculating the distance to radiative thermal hazard to the different heat flux criteria. The hazard distance from the edge of the impoundment is specified by the formula:

$$d = F\sqrt{A} \tag{1.1a}$$

where:

d = distance from the edge of impounded LNG [m or ft]
F = flux correlation factor equal to the following:
= 3.0 for thermal radiation heat flux = 5 kW/m^2 or 1,600 Btu/hr ft^2
= 2.0 for thermal radiation heat flux = 9 kW/m^2 or 3,000 Btu/hr ft^2
= 0.8 for thermal radiation heat flux = 30 kW/m^2 or 10,000 Btu/hr ft^2
A = surface area of impounded LNG [m^2 or ft^2]

Equation 1.1a can be written as,

$$\frac{S}{R_{eq}} = 1 + \sqrt{\pi}\ F \tag{1.1b}$$

where:

S = distance from the center of impounded LNG [m or ft]
R_{eq} = Radius of a circle of area equal to A [m or ft]

While NFPA 59A requires the calculation of the hazard distance to indicated thermal hazard heat flux values specified in Table 1-2, the Standard does not explicitly indicate the type of LNG fire that is to be considered. However, it is implicit from the descriptions that the hazard distances from impoundment pool fires are to be evaluated. There is no specification of other

types of fires that could occur within a LNG facility or the criteria for assessing the hazards and hazard distances from such fire.

NFPA 59A also requires the calculation of the vapor dispersion hazard distances based on specified scenarios of LNG releases from "design spill." The quantity of LNG released and its rate of release in these design spills depend upon the details of design of the storage tank, location of the fill and withdrawal piping, and the fill and withdrawal rates. The spacing of an LNG tank impoundment to the property line that can be built upon is to be such that the mean concentration of the dispersing vapors generated by the "design spills" will not be greater than 50 percent of the lower flammability limit (LFL) at the property line. Again, NFPA 59A does not require the consideration of the potential vapor fire propagation due to the ignition of a dispersed vapor cloud or the thermal radiation hazard distances next to such (traveling) flash fire or associated phenomena (vapor fire acceleration).

Both the 49 CFR, Part 193 Regulations and the NFPA 59A specify only a set of thermal heat flux criteria for the hazard. The true hazard will depend not only on the heat flux, but also on the duration of exposure, the properties of the irradiated object (or the person), the spectral characteristics of the incident radiation (after its alteration due to significant absorption of the energy in the water vapor and CO_2 bands). Neither the Federal Regulation nor the NFPA 59A Standard consider or allow credits to be taken for the effects of any mitigating phenomena or conditions that may affect the thermal radiation hazard distances.. Potentially beneficial items such as clothing worn by people or the movement of people into shelters or buildings (which reduce the thermal flux to people), effects of obstructions (structures, trees, buildings, etc) in the line of propagation or path of thermal radiation, the thermal inertia of objects and structures, cooling effects by windy conditions, and the anatomical characteristics of human skin, which reflects heat energy and absorbs heat only in certain specific wavelength bands are mitigating factors that reduce the potential radiant heat hazard to people and structures. These "natural" mitigating factors have not been considered in the regulations or the NFPA standard. Other approaches include active, engineered techniques (that absorb radiant heat) such as water curtains and water addition to the fire plume to reduce combustion efficiency (thereby increasing smoke production and reducing the radiant thermal emission from the fire). It should be noted, however, that unless maintained properly and are ready to perform their functions in an emergency, the usefulness of active engineered mitigation systems may be questionable, because they generally degrade with time.

1.5.3 LNG fire hazard assessment in European regulations, EN 1473

The European regulations, EN 1473 [2005], stipulate the requirements for the design, construction and operation of on-shore LNG facilities. Unlike the US Regulations and Standards, which are prescriptive, the European EN 1473 Regulations are based on a different philosophy, namely, a risk based evaluation of safety. These regulations require that "*LNG installations shall be designed to provide generally accepted levels of risk (refer to annex L) for life and property outside and inside the plant boundaries.*" Furthermore these regulations stipulate that, in order to ensure this high level of safety in the LNG facilities and its surroundings, safety should be considered throughout the development phases of a LNG facility construction and startup. Hazard assessment is required to be performed. One key feature of these regulations, as opposed

to those in the US, is the allowance and required considerations of mitigation strategies (engineering and/or procedures based) to reduce the magnitude of potential hazards and the implementation of the required safety measures to ensure acceptable risk levels.

The assessment of hazards requires the development of credible LNG release scenarios and consideration of both the probability of a selected scenario (and its sub–effects) occurrence and the evaluation of the magnitude of its consequences. In the case of LNG fires assessments include the (i) Jet fire from both gas release and liquid release, (ii) Dispersion of vapors and vapor fire, (iii) Liquid pool fire and, (iv) Explosions arising from the full or partial confinement of LNG vapors during dispersion and subsequent ignition. Scenarios of potential LNG release to be considered is not limited to storage facility spills but include releases from the LNG carrier and highway trucks as well as in associated pipelines. Guidance for the probabilistic assessment of minimum acceptance criteria of site location is presented in these regulations.

In the assessment of the hazards from LNG pool fires, the above regulation allows the consideration of the topography, size and elevation of dike and its walls, other obstructions, atmospheric absorption of thermal radiation, etc., in the calculation of the exclusion distance to specified thermal flux levels. These specified levels are indicated in Table 1-3. While the EN 1473 Regulations stipulate the (specified) heat flux levels as the criteria for hazard assessment, the regulations allow for the use of other "local" governmental criteria, which could be more stringent than the one in EN-1473.

Table 1-3
Thermal hazard criteria in EN 1473 (European) standard

Object Exposed to Radiation	Maximum Allowable Thermal Radiation Heat Flux (kW/m^2)
Inside the Boundary of the Facility	
Concrete outer surface of adjacent storage tanks	32
Metal outer surface of adjacent storage tanks	15
The outer surfaces of adjacent pressure storage vessels and process facilities	15
Control rooms, Maintenance workshops, laboratories, warehouses, etc	8
Administrative buildings	5
Outside the Plant Boundary	
Remote area **a)**	8
Critical area **b)**	1.5
Other areas **c)**	5

a) An area infrequently occupied by small numbers of persons, e.g. moor land, farmland, and desert.

b) This is an unshielded area of critical importance where people without protective clothing can be required at all times including during emergencies, or urban area (defined as an area with more than 20 persons per square kilometre) or a place difficult or dangerous to evacuate at short notice (e.g. hospital, retirement house, sports stadium, school, outdoor theatre).

c) Other areas typically include industrial areas not under control of the operator/occupier of the LNG facilities.

Note: Allowable maximum radiation heat flux is exclusive of the local maximum solar flux. The heat flux level can be reduced to the required limit by means of separation distance, water sprays, fire-proofing, radiation screens or similar systems.

The British Health and Safety Executive (HSE) has stipulated thermal radiation criteria based on the consideration of modified dosage. The modified total dosage unit (MTDU) is the product of the intensity of heat flux raised to $(4/3)^{th}$ power multiplied by the time of exposure ($MDU = I^{4/3} t$). The HSE criteria are indicated in Table 1-4. It is seen that this requirement takes into account the effect of both the intensity of radiant heat flux and the duration of exposure of a person for causing burn injuries or fatalities. The HSE criteria also provide a means of determining the average exposure duration by specifying the mean ambulation speeds for different types of populations and indicating the average distance to travel before one can get shelter (within buildings or from building shadows), in urban and rural settings.

Table 1-4
Criteria in British Health and Safety Executive (HSE) guidelines for fire thermal hazard assessment

Type of Hazard	Hazard level* (mtdu)
Dangerous dose of thermal radiation for vulnerable people	500
Dangerous dose of thermal radiation for average members of society	1,000
Significant likelihood of death	1,800
Death from exposure to thermal radiation	3,000
Conditions to be considered in thermal exposure	
The exposure period for fireballs	Fireball duration
Ambulation speed of average members of the public to seek shelter from heat radiation	2.5 m/s
The ambulation (escape) speed for the old and very young	1.0 m/s
The distance to shelter in suburban areas	50 m
The distance in rural areas	75 m
*** mtdu = $I^{4/3} t$, where I = heat flux intensity in kW/m^2, and t = time in seconds**	

Source: HSE (2006)

There are disadvantages in the use of both the exposure type criterion for hazard assessment as well as the risk-based assessment. The exposure type criteria fial to take into account (at least, at present) the modifications of the "character" of radiant heat from the time it leaves the fire to the time it impinges on the object, the details of the object, per se, in either absorbing or reflecting the heat incident, the response of the object (including human beings) to the absorbed radiant heat (that is, the damage to skin being a function of both the intensity, spectral quality and the dosage over time). Last but not the least, the current criteria for exposure are not based on real life, large fire exposure data but on very small, laboratory size tests. Also, the variation in the susceptibility of different populations (children, elderly, etc) have not been considered.

In the case of risk based assessments the principal question always is what is a "tolerable risk?" Also, what should the criterion of risk be based on? That is, should burn injury, (and if so what level of injury) or fatality be the criterion for the "consequence" and what level of details of the local topography, population density and diversity should be considered. In addition, since

risk assessments are based on both consequence of LNG releases and the probability of occurrence of different type of releases, quantity of releases and methods of release (liquid, vapor, dispersed vapor, jet fire, etc), one needs to have reasonable value for the occurrence probability of each possible scenario of events. For example, a simple question as to the probability of ignition of a released LNG (either immediately or over a duration of time) is not known, let alone its dependence on the release conditions, release phase, location of release or other environmental and release initiating factors. However, not withstanding all of the handicap that a risk based assessment has it, perhaps, will provide a more rational basis on which to make informed decisions rather than based on single large event scenarios, as are now in regulations and standards.

Chapter 2 provides a review of the technical literature on LNG fire experiments conducted to date and their results. Chapter 3 discusses the various modeling approaches to characterize the different types of fires and calculating thermal radiation heat flux variation with distance from different types of fires.

1.6 Definitions and Acronyms

AGA	American Gas association
ALARP	As Low As Reasonably Practicable (for risks)
CFR	Code of Federal Regulations
DOT	Department of Transportation
EN	European National
HAZOP	Hazard Operability (study) - A systematic study identifying potential hazards and operability problems arising from the failure of one or more process elements.
HSE	Health and Safety Executive
IR	Infra Red
IRR	Infra Red Radiation
LFL	Lower Flammability Limit
LNG	Liquefied Natural Gas
MDU	Modified Dosage Unit $[(kW/m^2)^{(4/3)}\ t]$
MSEP	Mean Surface Emissive Power over the entire fire, when it is described by a specific geometrical shape (say, a circular cylinder)
MIT	Massachusetts Institute of Technology
NAR	Narrow-Angle Radiometer
NFPA	National Fire Protection Association
PHMSA	Pipeline and Hazardous Materials Safety Administration
RPT	Rapid phase transition
SEP	Surface Emissive Power (Average) at a specified height within the fire plume
STP	Standard Temperature and Pressure (20 ^{o}C and 1 bar pressure)
SpEP	Spot (Surface) Emissive Power (such as the one inferred from a NAR measurement) – Emission per unit area from a particular location on the fire
TMS	Technology & Management Systems, Inc.
UFL	Upper Flammability Limit
WAR	Wide-Angle Radiometer

Chapter 2
LNG Fires
Review of Experiments and Findings

Over the past 30^{+} years several LNG fire tests have been conducted both in the US and abroad to understand the fire characteristics and the thermal radiation emission from these fires [Raj, 1982;]. Broadly, two types of fire tests have been conducted, namely, pool fires and vapor fires. Tests included LNG spills on land and on water with ignition of the spill. Spills on land were into dikes; hence, the fire base size was constant in time. In water spills, expanding pool fires resulted. Vapor fires involved ignition of vapor clouds both on land and on water. Table 2-1 lists some of the important fire tests of the past 3 decades. Significantly more tests have been conducted with dike fires on land than with LNG-on-water pool fires. The fire sizes have ranged from about 2 m to 35 m in diameter on land. In the only one set of pool fire tests on water, the maximum diameter achieved was about 15 m. A summary of the sizes of fires used in different experiments and the values of important parameters measured in these tests are indicated in Table 2-1.

A workshop was held in 1982 at the Massachusetts Institute of Technology (MIT) to discuss the state of LNG fire research (up to that time) and debate the knowledge available for LNG fire hazard predictions [Raj, 1982]. LNG Spill experiments to date have been reviewed in a recent paper by Luketa-Hanlin [2006]. Some of the issues related to LNG fire models are presented in a recent paper [Raj, 2005]. A detailed review of the LNG fire experiments and associated models is in the process of being published [Raj, 2006]. Additional information on models applicable to evaluating the LNG fire hazards are also available in the TNO publications [TNO-1, 1992 and TNO-2, 1997] and in Loss Prevention Handbook [Lees, 1996]. Only salient issues related to and principal findings from the tests with LNG pool fires and vapor cloud fires are reviewed in this chapter. The various fire models and their applicability, difficulties and shortcomings (if any) in using in LNG fire hazard evaluations are then discussed

2.1 LNG pool fire tests on land

In the late 1960's and early 1970's several test series of LNG fires on land were conducted, involving primarily the spill of LNG into a dike formed on virgin soil and its ignition forming pool fires on land. These tests and their findings have been reported by Burgess and Zabetakis [1962], May & McQueen [1973], AGA [1974], and Raj & Atallah [1974]. In these tests the diameters of LNG pool fires ranged from 1.8 m to 6 m. Results of field tests involving 20 m diameter pool fires of LNG, LPG and kerosene have been reported by Mizner and Eyre [1982] of Shell oil company. The largest size LNG pool fire conducted to date has been in a 35 m diameter, insulated concrete dike. The details of the tests and their results have been reported by Nedelka [1989] and Malvos & Raj [2006).

The principal results from the tests with LNG fires on land with diameters less than or equal to 20 m are summarized below:

Table 2-1
Summary of LNG fire experiments

#	Details of Field Tests			Type of Tests	# of Tests	Fire Dimensions	Principal Results			Technical Reference(s)
	Year	Sponsored by	Conducted in				Liquid Regression Rate (m/s)	Wide-angle Radiometer based, Mean Emissive Power {1} (kW/m^2)	Fraction of combustion energy radiated (%)	
1	1969	Esso	Libya	LNG fire in a land diked area (trench): Continuous LNG feed	6	70 m long x 25 m widest x 5 m depth (avg). Eq diam = 18 m	1.6×10^{-4}	92	12 - 16	May and McQueen [1973]
2	1962	US Bureau of Mines	Lake Charles, LA	LNG spill on ground surrounded by a dike	NA		--	--	----	Burgess, and Zabetakis [1974]
3	1973	AGA	San Clemente, CA	LNG spill on ground surrounded by a dike	7	Diameter = 1.8 m	1.5×10^{-4}	100	20	AGA[5]
					8	Diameter = 6.1 m	2.2×10^{-4}	160 ± 17	25	Raj & Atallah [1974]
4	1974 - 76	USCG	China Lake, CA	Unconfined pool on water: Continuous spill	5	Steady state fire diameters 8.5 m - 15 m	4×10^{-4} to 6×10^{-4}	185 - 224(1) 220 ± 47(2)	12 to 32 (depending on spill rate)	Raj, et al. [1979]
5	1976	JGA	Japan	LNG spill on ground surrounded by a dike	3	2 m x 2 m square	NA	58	13	JGA [1976]
6	1980	British Gas		LNG spill on ground surrounded by a dike	29	Square and rectangular (2.5:1) dikes. Equivalent diameters 6.9 m to 15.4 m	NA	NA	NA	Moorhouse [1982]
7	1980	Shell Research	Thornton Research Ctr.	LNG spill into insulated concrete dike	1	Diameter = 20 m	2.37×10^{-4}	153 ± 16	NA	Mizner and Eyre [1982]
			Maplin Sands, England	Unconfined pool on water	?	Mostly vapor fires resulting from delayed ignition	NA	203 ± 35	NA	Mizner and Eyre [1983]
8	1981	Tokyo Gas	Japan	Diked pool on land	8	Square pools of 2.5 m x 2.5 m	NA	NA	NA	Kataoka [1982]
9	1984	USCG	China Lake "Coyote Test Series"	Spill on water in a pond and ignition of vapor cloud on land	6	NA	NA	NA	NA	Rodean, et al [1984]
10	1987	Gaz de France	Montoir, France	LNG spill into insulated concrete dike	3	35 m diameter shallow dikes	3.11×10^{-4}	257 – 273(3) 165 ± 10(4)	NA	Nedelka, Moorhouse & Tucker [1989]

(1) Based on the average of Narrow-angle radiometer data (corrected for atmospheric transmissivity) from 7 tests
(2) Based on the data from a single working Wide-angle radiometer in only one test (# 12)
(3) Surface emissive power based on actual radiating surfaces from the fire as measured from video films
(4) Mean surface emissive power based on the assumption of flame surface being that of a tilted circular cylinder of length given by Thomas' correlation.

1 The pool fires (of less than 20 m diameter) burn with a bright yellow flame. However, as methane in LNG is consumed and other higher hydrocarbon fractions such as ethane, propane, etc., start to burn the fire becomes more and more red and begins to produce black smoke. In these tests (with fire size < 20 m) no data are available that correlates the "color of the fire" with LNG hydrocarbon fraction that is burning.

2 The fire plumes show relatively steady sizes (except for pulsation in the height of the burning zone – or visible fire plume, due to turbulence effects) in the form of columnar fires. No significant puffing type of burning[4] has been reported.

3 Only mean surface emissive power (MSEP) values have been reported for these fires. The MSEP values were obtained from wide-angle radiometer data and are based on the assumption that the fire can be represented by a "solid cylinder" of height and tilt given by Thomas' correlations (see discussions in section 3.2.2.1) and accounting for the atmospheric absorption of radiant heat. The MSEP values calculated vary from 100 kW/m^2 for the 1.8 m fires, to about 153 kW/m^2 for the 20 m fires. These are indicated in Table 2-1. Graphical representation of the MSEP variation with fire diameter is shown in Figure 2-1.

4 The liquid regression rates were measured indirectly by noting the duration of burn and the volume of LNG spilled. The steady state liquid burning rate increases with increase in fire diameter; it varies from about 1.5×10^{-4} m/s for 1.8 m diameter fire to 2.37×10^{-4} m/s for the 20 m diameter fire.

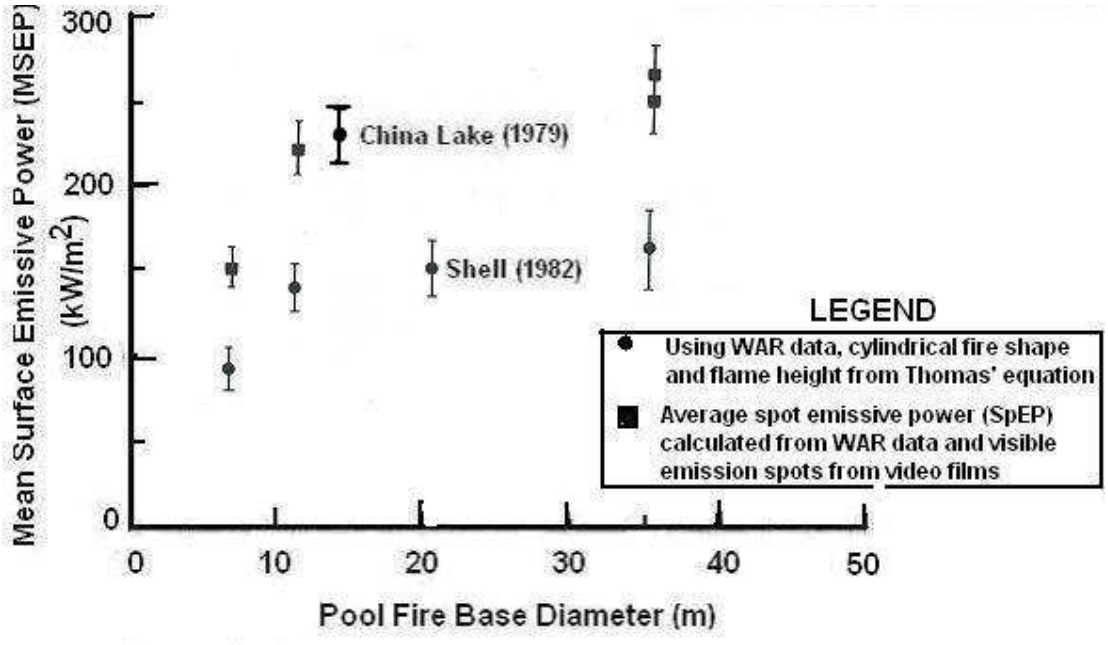

Figure 2-1: Experimental data on mean surface emissive power (MSEP) variation with fire size

[4] Large fires burn by releasing balls of fire (combustion eddies) at regular frequencies, which are dependent upon the fire base diameter and properties of the flammable vapor. This frequent releases of burning fire balls is termed "puffing"type of burning.

The tests conducted in Montoir, France in 1987 with 35 m diameter LNG pool fires [Nedelka, et al., 1989; Malvos & Raj, 2006] indicate considerable differences in both the physical characteristics of and magnitude and distribution of radiant heat emission from this size fires compared to those measured in the smaller diameter fire tests discussed above. Therefore, the results from these tests (which form the basis of a large fire turbulent model discussed in Chapter 3) are discussed in greater detail below.

Gaz de France: [Nedelka, et al., 1989]. In 1987 a consortium of companies including Gaz de France conducted a series of 35 m diameter LNG pool fire tests on an insulated concrete dike, in the field test facility of Gaz de France (GdF) at the Montoir de Bretagne methane terminal in France . The size of fire used in this series of three tests remains the largest fire test to date. The objective of the test program was to understand the burning characteristics of and quantify the radiant thermal emission from large LNG pool fires, in which the dominant heat for the vaporization of the liquid pool comes from the fire. The test series was instrumented with over 40 wide-angle radiometers, six narrow-angle radiometers, two spectrometers, gages to measure the liquid depth in the dike for obtaining the liquid evaporation rate during the fire, calorimeters located within the dike and just above the liquid surface to measure the heat flux from the fire to the liquid, and gas sampling devices within the dike. More details of the instrumentation, quantity of LNG in the pool at the time of ignition, wind and weather data and a discussion on the measured data have been published [Nedelka, et al., 1989; Malvos and Raj, 2006]. The quantity of LNG in the pool was measured to be, respectively, 80 m^3, 90 m^3 and 110 m^3 in tests 1, 2 and 3, before ignition. As was found in the 20 m diameter Shell tests, the burning rate was quite steady (at a mean burning rate of 0.146, 142 and 134 kg/m^2 s, respectively in the three tests) and methane preferentially burned for over one half of the duration of the fire. The mean duration of burning of the fires in the 3 tests was about 450 s. Also noticed was the copious amount of black smoke produced by the burning of the LNG even during the period when only methane was burning. Significant (black) smoke in the higher elevations of the fire plume and the "reddening" of the fire in the lower portions were also seen.

The variation in the SEP from the base of the fire to the top of the visible fire was considerable. Figure 2-2 shows the data from a narrow-angle radiometer (NAR) located 155 m from the edge of the dike, in test 1. The data presented have not been corrected for atmospheric absorption of radiant heat between the fire "surface" and the NAR. Figure 2-3 shows the data from two spectrometers that were located 20 m from the edge of the dike. One spectrometer was sensitive in the 0.5 μm – 1.2 μm and the other was sensitive to the 2 μm – 7.8 μm wavelength ranges. The findings from the 35 m diameter LNG fire tests can be summarized as follows:

1 The mean liquid evaporation rate due entirely to the heat feed back from the fire is 0.14 kg/m^2 s. This value obtained from the measurement of the actual liquid depth variation with time is considerably lower (by about a factor of 2.5) than the value that can be calculated using the data on the heat flux (from the fire) into the liquid pool measured inside the dike and close to the liquid surface. The discrepancy may be explained as due to (i) methane vapor absorption of heat radiation at the lower levels of the fire, (ii) absorption and scattering by any liquid droplets thrown up due to the violent boiling inside the pool, and (iii) absorption by low temperature soot present close to the liquid surface. Note that the

heat input into the pool from the dike floor during the fire test is very small because of the insulated concrete as well as the fact that the floor was pre-cooled[5].

2 The NAR readings at the bottom of the fires, time averaged over 5 s, are generally in the range 180 kW/m^2 - 200 kW/m^2. The maximum values recorded differed in the different tests but were in the range 201 kW/m^2 - 210 kW/m^2. Using the calculated atmospheric transmissivity values (0.65 to 0.665), consistent with the atmospheric conditions and the location distance to the NAR, the maximum spot emissive power (SpEP) was found to be in the range 308 kW/m^2 - 316 kW/m^2. Nedelka, et al., [1989] report that occasionally, over a 5 s to 10 s averaging period, a SpEP value (after correcting for atmospheric absorption) of 350 W/m^2 was obtained. It should be noted that because of the "narrow view" of the NARs these SpEP values are for a very small region of the fire and do not represent the overall SpEPs even in the lower regions of the fire.

3 The fire burned as a puffing fire, releasing connected fireballs through the fire column with a fireball release period varying between 3 s and 3.5 s. The estimated upward velocity of upward motion of the fireballs through the fire column is about 20 m/s.

4 The fires exhibited a bright, intense burning region close to the bottom of the fire followed (upwards) by a region in which the interior of the fire was exposed intermittently by otherwise smoke blanketed regions. The fraction of the "surface area" of the fire that contained exposed burning, and therefore heat radiating, regions decreased continuously and substantially with the height of the flame. The axial length of the bottom intense fire region seems to increase in a windy condition.

5 The fires in all three tests were very smoky, beyond a certain height (or length along the tilted axis). The narrow angle radiometer readings confirm that the time averaged apparent emissive power of the fire decreases with height (or length along the axis). The mean emissive power calculated from actually visible burning area spots over the entire length of the fire plume was about 265 kW/m^2. The mean emissive power value, based on idealized fire geometry (tilted circular cylinder with axial length given by Thomas' correlation), is reported to be 165 kW/m^2.

[5] In the three tests conducted in Montoir, durations of pre-cooling of the dike were, (1) 4 hours in test #1, (2) 2 hours in test #2 and (3) 1 hour in test #3, before the pool was ignited in each test. It is calculated that even in the last test, the duration of cooling is sufficient as to reduce the heat transfer from the ground to be negligible. The fire characteristics in all three tests are, therefore, not affected by the heat transfer from the ground. Hence, the evaluation of the thermal radiative characteristics of large LNG fires is on a consistent basis.

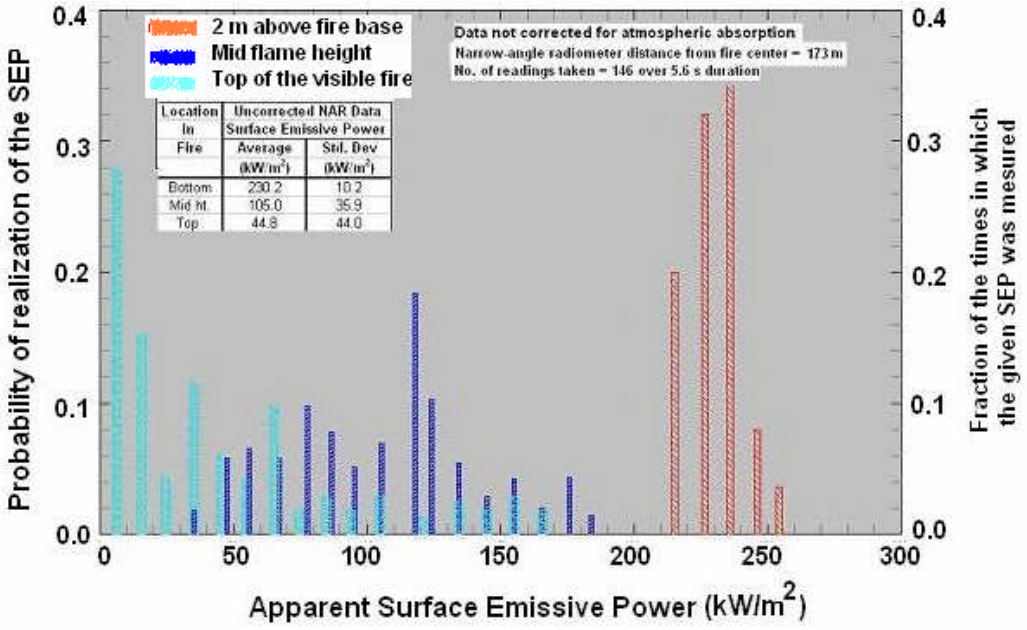

Figure 2-2: Statistics of apparent SEP (NAR data) – for different locations along the fire plume axis

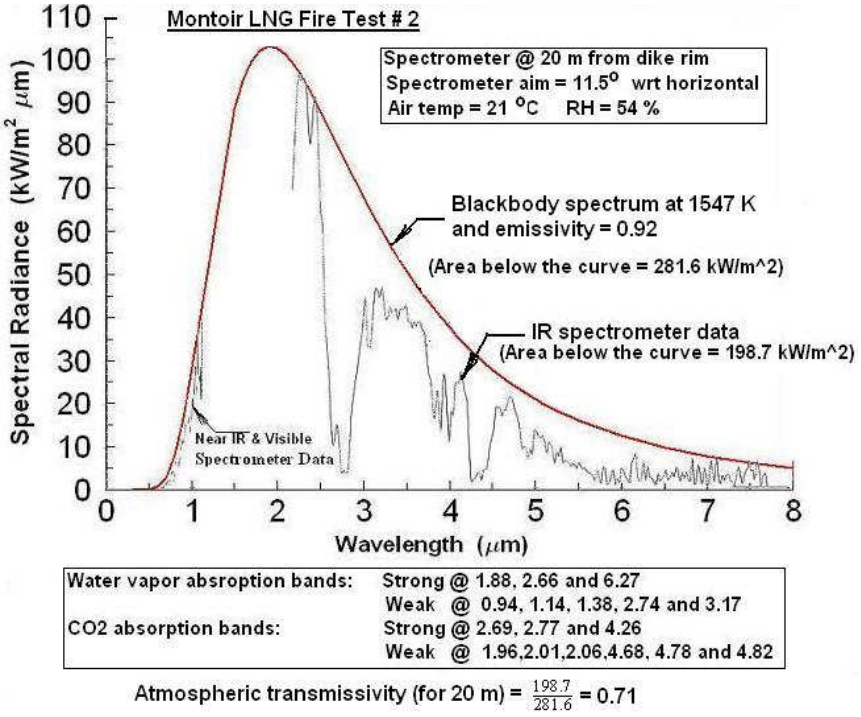

Figure 2-3: Measured 35 m diameter fire emission spectrum and comparison with blackbody emission spectrum

6 The spectral data (shown in Figure 2-3) obtained from the lower parts of the fire indicate that the 35 m LNG fire is almost optically thick, with a mean emissivity of 0.93. The equivalent blackbody temperature for radiation is estimated to be 1547 K. [Spectral data were gathered only for a short duration during the steady burning period – no data were gathered during later time periods when higher hydrocarbons were burning)]. This emission applies only to those parts of the fire that are luminous. However, considerable smoke at higher regions masks the high radiant heat emission associated with the above temperature, thereby lowering the apparent emissive power, averaged over time and fire size.

7 The absorption of the IR emission by water vapor in the atmosphere is significant. From the data shown in Figure 2-3, almost 30% of the total energy emitted from the base of the fire is absorbed in a distance of about 20 m. The relative humidity during the tests was 54% and air temperature was 21 ^{o}C.

Experimental investigation of **LNG pool fires in trenches** is reported by Croce, et al., [1984] who conducted a series of 13 field scale fire tests with trench sizes varying from 0.82 m (W) x 4.4 m (L) to 3.9 m (W) x 52.1 m (L), covering a range of length to width (aspect) ratios from a minimum of 4.97 to a maximum of 30. The wind speeds during the different tests varied, from a minimum of about 1 m/s to a high of 8.36 m/s. The principal findings from trench fire tests are summarized as follows:

1 In a previously reported laboratory scale tests the flame sheet was not coherent for length to width aspect ratios greater than 4. For larger aspect ratios the flame sheet broke up into distinct columns of flame ("flamelets") with the overall heights of the fire being lower compared to the case of coherent flame sheet.

2 The heat flux data on the perpendicular bisector to the trench length show an inverse square relationship with the dimensionless ratio of distance from fire center to the equivalent diameter based on the trench area (S/D_{eq}), in both the laboratory and field tests for values of $S/W > 2$.

3 The flame height to trench width ratio, in the laboratory tests, reaches a constant value after the flame sheet loses coherency. In the tests by Croce, et al., the flame height to width ratio decreases linearly with wind speed based Froude number[6] ($Fr' = \frac{U_W}{2\sqrt{gW}}$) up to $Fr' = 0.25$ and then becomes essentially a constant at about 2.5 and independent of Fr'. This implies that at lower wind speeds, increase in wind speed resulted in a decrease in the burning fire plume length; above a critical wind speed flame length is independent of the wind speed.

4 The burning rate in a small aspect ratio trench fire is much smaller than the fire induced burning rate in a circular pool of equivalent diameter. The steady state burning rate measured in the field tests ranged from 4.3 x 10^{-2} kg/m^2 s to 8.0 x 10^{-2} kg/m^2 s. The burning rate does

[6] Croce, at al., [1984] define the trench Froude number (Fr') as indicated in which, W= width of the trench, U_W = wind speed, and g = acceleration due to gravity.

not seem to correlate with wind speed implying that the bending of the fire has limited effect on the heat feed back to the liquid.

5 Considerable ground overshoot of the flame in the downwind direction ("flame drag") was noticed in the field tests. The flame drag ratio (1 + downwind extension from the trench edge/trench width) was found to be dependent on both trench width and wind speed. For a given wind speed, the flame drag ratio was higher for smaller trench widths. While the flame drag increased with increased wind speed (zero at zero wind speed), it reached a constant value for all wind speeds above a critical wind speed. This critical wind speed was found to be dependent on the trench width. For trench widths equal to or greater than 1.8 m the flame drag was almost linear with wind speed up to about 3 m/s and thereafter remained constant at about a value of 3 (Flame drag = 1.21 at 1 m/s wind). The flame drag ratio was higher (at a value of 4) for smaller trench widths (0.8 m) and remained at this high value for wind speeds greater than 2 m/s.n

6 The flame plume is tilted by the wind - the higher the wind speed the more the tilt from the vertical.

7 Fire (mean) surface emissive power (MSEP) values, calculated using the radiometer data from the field tests, measured mean flame lengths and tilts, range from 50 kW/m^2 to 200 kW/m^2, the latter from wider trenches. Croce, et al., conclude that based on these results it can be postulated that a LNG fire on 6 m width trench would exhibit a MSEP of 220 kW/m^2.

The thermal radiation hazard distances can be predicted by using the standard models by considering the fire geometry as rectangular, optical length (in width direction) as 4 m and the maximum MSEP of 220 kW/m^2 and using the flame tilt correlations available in the literature by using the trench width as the characteristic dimension of the fire

2.2 LNG pool fire tests on water

Very limited data are available on the burning characteristics of and radiant heat emission from LNG fires on water. The only series of tests[7] to understand the pool burning of an unconfined pool of LNG on a large body of water was conducted in 1976-78 in China Lake, CA. Details of the design of the tests, data measured and the findings are reported by Raj, et al., [1979].

China Lake tests were conducted by spilling LNG at rapid but controlled rates on to the water surface in the middle of a 50 m x 50 m x 1 m depth pond. A series of 8 pool fire tests was conducted, with a majority of tests conducted under essentially calm conditions so that the fire plume was vertical. The volumes of LNG released ranged from 3 m^3 to 5 m^3. In the "pool fire" tests, an igniter was activated near the spill point as soon as the LNG hit the water surface. This produced an immediate ignition and resulted in an initially expanding, burning, pool of LNG

[7] In 1980 Shell Research Ltd., UK conducted tests at Maplin Sands to understand the characteristics of burning of flammable vapor clouds generated by LNG spills on water and dispersed without ignition at the source. In one of these tests, the flashing vapor fire ignited the still boiling pool at the source resulting in a relatively short-lived LNG pool fire (Mizner and Eyre [1983]).

with a generally tall and columnar fire plume. The steady state pool fire diameter varied between the tests and was a function of the spill rate. The steady state diameters ranged from 12 m to 15 m. The resulting fire was columnar, tall and yellow in color signifying high radiant emission.

The principal findings from China Lake pool fire tests on water are as follows:

1 The apparent burning rate increases with an increase in spill rate. This phenomenon is attributed to the deeper penetration of the spilled LNG into water, its break up and vaporization over a large number of LNG droplet surface area that is considerably larger than is presented by the horizontal (water – LNG) contact area defined by the mean pool diameter.

2 The burn rate increases with an increase in the spill rate. This result is correlated by a dimensional, linear least square fit equation:

$$\text{Apparent burn rate } \dot{y}\,(\text{m/s}) = 10^{-4} \times [2.73 + 58 \times \text{Spill rate } (\text{m}^3/\text{s})] \qquad (2.1)$$

The above correlation contains the heat flux contributions from water and fire. It is likely that the heat flux from fire-to-pool in fires of diameters larger than the ones in these tests will be different. Hence, it is uncertain whether the above correlation will be applicable to the burn rates of LNG on water with very large pool fires.

3 The time averaged height to diameter ratio of the visible flame is slightly less than that predicted by Thomas's correlation in the range of the measured burn rates. The height to diameter ratio data is correlated by the following least square linear fit equation on the log – log plot.

$$\frac{L_F}{D} = 46.5 \left\{ \frac{\rho_L}{\rho_a} \frac{\dot{y}}{\sqrt{gD}} \right\}^{\frac{2}{3}} \qquad (2.2)$$

4 The energy emitted by the fire as radiant heat, expressed as a fraction of combustion energy generated by burning, decreases with increase in spill rate. This implies that in high rates of release a part of the released vapor does not burn at all; that is, the faster the vapors are generated, the less the chance for combustion. In much smaller scale tests (0.38 m diameter) involving the spill of LNG on to a warm tray, Burgess and Zabetakis [1962] also found that about 70% of the vapor generated initially did not participate in combustion.

5 The flame emissive power values obtained from the narrow angle radiometer (NAR) and that inferred from wide angle radiometer (WAR) data by assuming a cylindrical shape for the fire and the measured mean height of the fire, agree very closely in their mean values. The mean emissive power of the 14 m diameter fire is found to be 220 kW/m^2 ± 47 kW/m^2. However, if the NAR data from all tests are considered (see Figure 3 in Raj [2006b]), the mean and standard deviation of the NAR data are represented by 205 kW/m^2 ± 20 kW/m^2. The scatter in the WAR data is about twice the scatter in the NAR data. The large variation in the computed emissive power from the WAR data is due to the fact that in reality the fire is not a cylindrical columnar fire of constant height but tends to pulsate both in diameter (as

the large turbulent eddies rise up through the fire) and in height, whereas the emissive power calculating procedure uses only a constant height and diameter fire. Had the exact shape of the fire at every instant been used to calculate the mean emissive power, the data scatter would have been much less.

6 The fire emissivity, temperature and the optical depth were obtained from a single set of spectral data that were taken at 236 m from the fire. The data showed the fire to be a band emitter (rather than a blackbody emitter) consisting primarily of band emissions from water vapor and CO_2 and a continuous emission due to luminous soot. The emissivities of luminous soot, water vapor and CO_2 were found to be, respectively, 0.14, 0.19 and 0.35. Also, the flame temperature for the China Lake fire (13 m diameter) was calculated to be close to 1500 K.

As described in the sections above, the experiments with LNG pool fires have consisted of fires of diameters varying from 1.8 m to 35 m. Not all fires are considered to be optically thick (for a discussion of optical thickness see section 3.2.2.2). The reported values for the extinction coefficient (and the corresponding optical thickness values) are indicated in Table 2-2.

Table 2-2
Experiments results on LNG fire extinction coefficient

Experiment	Nominal fire diameter (m)	Extinction coefficient (m^{-1})	Optical depth (m)	Literature Reference
AGA Test series	1.8	0.492	2.03	Raj & Atallah [1974]
	6.1	0.18	5.54	AGA [1974]
China Lake LNG fires on water	15	0.072	13.89	Raj, et al. [1979]
Montoir tests	35	0.05	20.0	Malvos & Raj [2006]

2.3 Vapor fire tests

Vapor fire tests involving the ignition of dispersed LNG vapor clouds have been performed both on land and on water. During the China Lake series of LNG fire tests a few vapor fire tests were also conducted. These tests involved the ignition on land, with a flare igniter, at the downwind edge of a dispersing cloud. The cloud burned back to the source of the vapor, with a deflagration fire. No pressure increases in the atmosphere were noticed. Raj and Emmons (1976) have reviewed the results of these tests and have developed a model for the burning of a vapor cloud in the form of a deflagration fire in the absence of obstructions. This model is discussed in Chapter 3.

Another series of tests, called the “Coyote Series” was conducted, also in China Lake, in early 1980s [Rodean, et al., 1984]. A further objective of these series of tests was to determine if non-energetic ignition of the vapor cloud would result in explosive burning of the vapor cloud when the cloud is ignited at the downwind edge or at the center of the cloud.

The tests involved the spill of LNG on to the water surface in the middle of a pond 58 m in diameter and igniting the vapor cloud formed at a selected downwind location on land. Three tests with LNG (of methane concentrations varying from 75% to 81.5%) and one test with liquid methane (LCH_4) are reported. The spill quantities varied from 14.6 m^3 to 28.6 m^3 (LNG) and 26 m^3 (LCH_4) and the spill rates from 13.5 m^3/min to 17.1 m^3/min. Mean wind speeds varied between 4.6 m/s to 9.7 m/s over the series and wind speeds were variable both in speed and direction within the duration of a test. This series of test forms a set of well instrumented vapor fire tests; instruments measured such items as the heat flux to objects within the "burn zone," radiant heat flux at several locations outside the vapor fire zone, flame velocity, ground heat input to the cloud, vapor concentrations in the cloud, etc. In addition there was extensive photographic data taken with both IR and visible video instruments both from the sides and from the top ("bird's eye view"). Ignition of the vapor cloud was initiated only after the cloud had been fully established so that the lower flammability limit (LFL) distance downwind was a maximum, as measured by the concentration sensors.

Important findings from the Coyote series related to the ignition within the center of the cloud are:

1 The fires on the lower concentration cloud burning regions were very blue in color

2 The cloud burning phenomenon and the production of hot combustion gases, seem to result in a "pushing" and expansion of the area enclosed within the pre-ignition 5% (LFL) contour at the time of cloud ignition. The maximum downwind burn distances were 85 % - 90 % of the non-ignition, dispersion model based estimates.

3 Burn areas were not in the same location as the pre-burn 5% contour areas but considerable movement in cross wind and down wind direction (relative to the 5% contour area before ignition) was noticed. However, the propagating flames did not go beyond the 5% gas concentration locations.

4 The relationship of the total burn area to the pre-ignition 5% contour area is not clear from the data. In one test the burn area was smaller than in the 5% contour area whereas in another test it was about 150 % of pre-ignition, 2 m level, and flammable area. However, in the one test there was a rapid phase transition (RPT) explosion. In addition, there was significant instantaneous generation of gas, which then moved downwind as a unit. The burn area in this test was almost 2 times the measured pre-ignition flammable area.

5 Flames were hardly visible in the lean concentration parts of the cloud whereas the burning vapor cloud, upwind and closer to the vapor source had a yellow (and visible plume) flame. This is attributed to higher concentration (and higher hydrocarbon content) of vapor in the cloud. Ratio of visible flame height to pre-ignition visible cloud height was in the 5 – 10 range.

6 By and large the flame speeds measured with respect to the ground had similar magnitudes both in the downwind and upwind direction. The initial velocities, immediately in the vicinity of the igniter were greater than at farther distances. Upwind flame propagation

velocities were slightly higher than those of downwind propagation. However, the turbulent flame speed relative to unburnt gas does not seem to correlate well with wind speed.

7 No flame acceleration was noticed; on the contrary all fires seem to have higher flame velocities (relative to the ground) near the ignition sources. The flame speeds with respect to ground were close to 30 m/s near weak ignition source tests and about 40 m/s - 50 m/s in the jet ignition test. However, the flame speeds rapidly decreased to essentially constant speeds of 10 m/s -15 m/s within about 50 m

8 Pressure increase measured in the atmosphere due to the propagation of fire was in millibars and hence inconsequential.

9 The heat fluxes measured inside the fire were in the 150 kW/m^2 to 340 kW/m^2 range. The surface emissive power of the yellow flame (seen when the cloud near the vapor source was burning) is calculated to be in the 220 kW/m^2 - 280 kW/m^2 range.

A series of tests performed by Shell Research Ltd., UK in1980 involving the spill of LNG (and LPG) on to the sea and ignition on water of the vapor cloud dispersing on water is reported by Mizner and Eyre [1983]. A total of 7 LNG spill tests and 4 LPG tests were conducted. The objective of the tests was to understand the thermal radiation from a vapor cloud fire formed by the ignition of a cloud generated by spill of a cryogenic flammable liquid on to water and the dispersion of the cloud on water. All LNG tests resulted in the ignition and complete combustion of the spilled LNG after it had been dispersed in the form of a vapor cloud. The vapor fire in all cases flashed back to the source in the form of a deflagration fire. Radiometers were provided (on a number of pontoons stationed on water over several concentric semi circles with the spill point as the center) to measure the radiant heat flux from vapor cloud fires. The farthest semi circle containing the radiometers was of radius 650 m.

The measured flame heights of the vapor fires were in the 10 m to 20 m range and the flame height-to-width ratios during he cloud fires stages were in the 0.2 to 0.5 with wide scatter. The mean surface emissive power (MSEP) of the vapor fires ranged between 138 kW/m^2 and 226 kW/m^2 with standard deviations in the 7 % to 15% range. It should be noted that in this test series the fire was well ventilated and the vapors were well mixed with air; therefore, the fires behaved more like pre-mixed flames than diffusion fires.

Summary: Vapor fire test findings: The principal findings from the field experiments reported in the literature on dispersed LNG cloud vapor fires in the open can be summarized as follows:

1 When the vapor cloud is ignited at downwind locations, a turbulent fire propagates to the vapor source (against the wind). No downwind propagation of the fire was observed in any tests involving the ignition of the cloud at the leading edge. Downwind propagation was, however, seen when a cloud was ignited at the center (of the dispersed cloud). This indicates that propagation downwind will occur when the vapor concentrations downwind of the ignition point is still above the lower flammable limit (LFL) and that vapor cloud with concentrations below LFL will not sustain a propagating fire.

2 Flames were hardly visible in the lean (5% to 15%) concentration parts of the cloud. The flame in the regions of higher vapor concentrations (closer to the source) burned with a yellow plume. This can be attributed to a change in the "mode of burning" from a premixed fire to a diffusion fire at higher concentrations. In addition, closer to the source of vapor the vapor contains higher concentrations of higher hydrocarbons (ethane, propane, etc).

3 The velocity of the flame front (moving into the unburnt vapor) with respect to the unburnt gases ("flame speed" U_F) was more or less constant in a given test. Considerable turbulence is noticed in the movement of the flame front. The experimental data can be correlated by a linear square fit equation of the type $U_F = 0.8 + 1.6 \times U_{wind}$. It is noted that the laminar burning velocity of the stoichiometric concentration of methane in air is 0.4 m/s. Because of natural turbulence in the atmosphere, even at zero wind speed, it can be argued that the burning velocity of stoichiometric mixture of methane and air will be higher than the laminar burning velocity. It should also be noted that the above correlation represents a mean burning velocity over all concentrations in the vapor cloud (and not just the stoichiometric concentration), especially, the higher than upper flammability limit (UFL) concentrations.

4 No flame acceleration was noticed; on the contrary all fires seem to have higher flame velocities (relative to the ground) near the ignition sources.

5 A burning zone supporting a fire plume follows the flame front. The height of the fire plume is dependent on the concentration of the unburnt gas. The higher the concentration, the greater is the fire plume height (diffusion fire). In regions of vapor cloud where the concentrations were in the LFL to UFL the flame height was essentially equal to the vertical depth of the cloud and the flame was hardly visible. Also, the width of the burning zone (in the direction of propagation of the fire) was dependent on the longitudinal concentration gradient (prior to the flame propagation). In high vapor concentration regions the ratio of visible flame height to pre-ignition visible cloud height was in the 5 – 10 range.

6 Heat fluxes measured inside the fire were in the 150 kW/m^2 to 340 kW/m^2 range. The surface emissive power of the yellow flame (seen when the cloud near the vapor source was burning) is calculated to be in the 220 kW/m^2 - 280 kW/m^2 range.

7 Objects or even undulations in the ground, which acted as flame holders, could arrest the flash back of the fire to the source. This phenomenon has not been fully investigated but seems to indicate that flame holder effect would occur only in high concentration parts of the cloud.

8 None of the vapor tests conducted with a weak ignition source or a jet flare ignition in the open have lead to flame acceleration or explosive ("detonation") burning of a LNG vapor cloud, not withstanding the presence of high concentrations of higher hydrocarbons (ethane and propane) in the LNG.

9 Pressure increase measured in the atmosphere due to the propagation of fire was in millibars and hence inconsequential. All of these tests were conducted in the open atmosphere (out door) with the propagation of flames not impeded by any natural or man-made obstructions.

It is well known that flame shape gets wrinkled due to obstructions in the flame front path and consequently the flame speed increases. No systematic assessment of this phenomenon has been investigated in any of the field experiments.

2.4 Fireball type vapor burning

There have been some concerns in the literature on the potential burning of a LNG vapor cloud in the form of a fireball. The concern is whether such a burning would lead to higher heat release rates and the consequent larger hazard distances. Until recently there were no controlled tests to understand this phenomenon or the conditions under which such fireball type of burning could occur. Also, the characteristics of the fireball had not been investigated. Tests conducted in 2000 by Gaz de France and reported by Daish, et al. [2001] provide the first experimental data on such fires.

In the above a series medium-scale tests were carried out with LNG vapor clouds being produced with controlled emission of LNG vapor with high gas concentrations in order to study fireball formation. High-concentration vapor clouds with low momentum were generated by spilling LNG into a pit (1.8 m diameter and 1.7 m deep) consisting of pebbles to simulate a very large LNG spill due to an accident and significant vapor generation. Ten experiments were performed in total. In each test the objective was to generate a cloud with a substantial volume above the UFL and then to ignite the cloud at various locations relative to the flammable volume to determine the effect of placement of igniter relative to the high concentration parts of the cloud. Radiometers, gas concentration sensors, igniters, thermocouples were placed at several radial positions at the intersections of 10^o sectors with the radial lines. Video and photographic records were also made of the tests. Seven tests were conducted with electric spark igniters and the others with flares. In the seven spark ignition tests the igniters that were fired were located at 10.8 m (radially from the center of spill) except in one test where it was at 20.9 m. Fuel release rates ranged from 2.6 kg/s to 5.6 kg/s. The estimated UFL and LFL radial distances were 5 m – 7.5 m and 15 m – 30 m, respectively. That is, the ignition was within the cloud concentrations of LFL and UFL. The mass of LNG vapor within the LFL zone was estimated to be in the range 8.2 kg – 19.2 kg.

The fire produced varied between the trials. The fire was characterized by a high and wide flames, propagating over the entire cloud area and generating fireballs, or the fire was observed to be traveling from the middle to the borders of the cloud without the generation of a fireball. The most significant finding from these tests was that some form of identifiable fireball event was observed in at least 6 of the 10 trials. It appeared that ignition of a cloud with a large vapor-rich volume led to strong combustion and heat generation over a sufficiently localized area that a self-sustaining motion entraining fuel and air was generated and continued until most of the fuel was exhausted. This burning mode had a distinctive "starting thermal[8]" type of characteristic that distinguished it from other burning modes. The diameter of the observed fireballs ranged from 5 m to 30 m and the height to which the fireballs rose ranged from 17 m to 26 m. Measurements at 20 m distance indicated a very rapidly varying heat flux with a duration corresponding to the lifetime of the fireball and reaching, in one test, as high as 50 kW/m^2 lasting only for a few

[8] A "starting thermal" occurs when a buoyant fluid is released over a short duration. The released fluid together with entrained air has the shape of a mushroom while rising in the atmosphere.

seconds. The temperatures measured within the fire ranged from 928 K to 1243 K. No surface emissive power data or the rise time of the fireballs has been provided in the data sets.

While there are no other controlled tests to determine the conditions under which fireballs occur from the ignition of LNG vapor clouds, it is reported by Brown, et al., [1990] that a fireball type of fire was observed due to an accidental ignition of a high concentration LNG vapor cloud in the Falcon series of tests (conducted by Lawrence Livermore National Laboratories -LLNL). In Falcon test # 5 a RPT occurred and high concentration cloud of vapor formed was ignited by an unknown ignition source (speculated to be a piece of pipe insulation saturated with oxygen condensed from the air). No quantitative data on this fireball are available.

In summary, it can be stated that the Gaz de France's vapor fire ball tests do not provide any definitive set of criteria by which one can postulate the conditions under which a fireball will occur in a dispersed, flammable vapor cloud. The qualitative conclusion seems to be that if a LNG vapor cloud is ignited at a location between the LFL and UFL concentrations, and a substantial mass of the cloud is still in regions above UFL concentration, then vapor burning in a fireball is possible. No mathematical criteria have been developed relating the physical size of the cloud, the mass of vapor above UFL and the type of igniter that will lead to a fireball type burning. It is also not clear from the data whether the fireball would result in a larger total thermal burn hazard area compared to that from a dispersed cloud which when ignited results in a flash fire (and burns almost everything within the fire area) and poses radiant heat hazard to near field distances from the edge of the burn zone. A rising fireball only poses the hazard due to the transient thermal radiation field and not much by its physical size (compared to a dispersed cloud). Therefore, the question of the comparative extent of potential hazards from vapor burning in a fireball and from the flash fire burning of a LNG vapor cloud is at present not completely answered.

Chapter 3
LNG Fire Models – A Review

3.1 Jet fires

A LNG jet fire results when the liquid is released from under pressure through an orifice (or a small opening or crack) and it is ignited. Jet fires of this type are diffusion fires since, the oxygen/air for combustion is ingested into the jet by turbulent entrainment. Many models used for assessing the thermal radiative field surrounding jet fires are based on or are extensions of the models developed for single-phase gas flares. Lees [1996] has reviewed experimental data on flares and jet fires and discusses a number of mathematical models. In this section, only those models that are applicable to describing the physical size of a jet flame and those used for evaluating the general safety of liquefied gas releases are indicated.

The model due to Cook, Bahrami and Whitehouse [Ref §16.19.9, Lees, 1990], improves the flare model indicated in API-RP 521 Jet Flame Model. The modified model describes the jet flame by its length and the radius of the flame as a function of the distance from the origin as follows

$$L = 0.00326\left[\dot{m}\ \Delta H_c\right]^{0.478} \tag{3.1}$$

and

$$\left\{\frac{R}{L}\right\}^2 = 0.037\left(x/L\right)^2\ \ell n\left(L/x\right) \tag{3.2}$$

where,

L	=	Length of the jet flame	(m)
$\dot{m}$	=	Mass flow rate of the fuel at the base of the jet	(kg/s)
R	=	Radius of the jet fire at any axial location x	(m)
x	=	Distance along the axis/centerline of the jet fire	(m)
ΔH_C	=	Lower heat of combustion of fuel	(J/kg)

It is noted from equation 3.2 that at $x/L = e^{-0.5} = 0.607$, the value of R is a maximum with $R_{max}/L = 0.082$.

The model due to Clay, et al., [1988] referenced by Lees [Ref §16.19.13, 1996] is indicated by the Health and Safety Executive (HSE) to be applicable for jet fire thermal radiation hazard assessment, and in particular, for LPG fires. It is assumed that the same model is applicable to LNG fires also, provided that certain parameters are adjusted (see below). The Clay, et al., model gives the following correlations:

$$L = 0.006\left[\dot{m}\ \Delta H_c\right]^{0.444} \tag{3.3}$$

The flame is modeled as a point source radiator with heat radiated from a point located 4/5 of the flame length from the origin.

$$\dot{q}''(s) = \chi_R\ \frac{\dot{m}\ \Delta H_c\ \tau(s)}{4\pi s^2} \tag{3.4a}$$

where,

$\dot{q}''(s)$ = Radiant heat flux to an object at distance "s" from the fire (kW/m^2)

χ_R = Fraction of combustion energy that is radiated ($0.19 \leqslant \chi_R \leqslant 0.23$, for natural gas fires [Lees, 1996])

s = Distance from the jet fire to the object (m)

$\tau(s)$ = Atmospheric transmissivity over distance s

with,

$$\tau(s) = 1 - 0.0565\, \ell n(s) \qquad (3.5)$$

The rate of heat transfer to an object by an impinging jet fire depends on the jet fire temperature (which itself is a function of the fuel burning), location of the object with respect to the length of the jet, size of the object relative to the jet fire diameter at the location of the object and, the thermal characteristics of the object. No simple formula can be indicated for the transfer rate; each situation has to be evaluated considering all of the above parameters and using standard heat transfer equations. For methane/natural gas jet fires the peak radiative temperature inside the fire can be as high as 1525 K [Ref § 16.20.2, Lees (1996)], with an equivalent blackbody emissive power of 307 kW/m^2.

Under normal conditions of potential jet fires that may occur in a LNG facility the use of the point source model (equation 3.4) together with the jet physical description given in equation 3.3 (or 3.1) may suffice to determine the radiative hazard distance because the diameter of the LNG jet is expected to be small (a few centimeters to at most a meter); similarly, the jet length will be smaller than 50 m. On the other hand, if in a LNG plant, a critical component is found to be impacted by a jet fire scenario (identified by a "HAZOP" study), then more detailed heat transfer calculations need to be undertaken to determine the time-temperature profile of the equipment subject to the jet fire heat. Such an analysis is very specific and is beyond the scope of this study.

3.2 Pool fires

A diffusion fire sustained on a boiling/evaporating liquid fuel is termed a "pool fire." Two types of mathematical models are reported in the literature to assess the effective (radiant heat) hazard distance from a LNG pool fire, namely, (i) point source model and (ii) the solid flame model. The mathematical representations of these two models and their hazard distance prediction accuracies are discussed below.

In the solid flame model the visible and radiative part of the fire plume is represented by an enclosing cylinder of base diameter equal to that of the firebase and of axial length equal to the mean visible plume length of the fire. Furthermore, in the solid flame model there are certain geometrical variations depending upon the wind and other conditions. The details of each of these two models, the values of the parameters used and the modifications/enhancements needed in the models, in the light of data from large-scale LNG fire experiments, are discussed below.

3.2.1 Point source LNG fire model

The essential features of this model are indicated, schematically, in Figure 3-1. The fire is considered to be point source of heat emission and the heat flux at any radial distance follows the "*inverse square law*" and is represented by[9]

$$\dot{q}''(s) = \chi_R \frac{(\pi/4)\, D^2\, \dot{m}''\, \Delta H_c\, \tau(s)}{4\pi s^2} \qquad (3.4b)$$

where,

D	=	Fire base diameter	(m)
$\dot{m}''$	=	Mass evaporation rate of fuel	(kg/m^2 s)

Other parameters have been defined following equation 3.4a. Implicit in the above equation are the following assumptions.

1 The ground is a perfect absorber of heat (i.e., there is no reflection of heat at ground level).
2 The observer is oriented normal to the ground.
3 The observer is far from the fire (i.e., s/D >> 1, at least 5 or larger).
4 All of the fuel injected (by evaporation of the liquid fuel) into the fire is burned.
5 The fraction of combustion energy released as radiant heat is independent of the size of the fire.

Based on radiation measurements (discussed in Chapter 2) in a limited number of field experiments with LNG fires of diameters less than 15 m, the fraction of combustion energy radiated (χ_R) is shown to vary between 0.12 and 0.32 (see Table 2-1) and does not show any systematic variation with the fire size. It can be argued that for larger diameter fires the fraction radiated will decrease due to smoke obscuration effects and simple geometry effects (see discussions below, in the section on "Solid Flame Model"). McGrattan, et al (2000) present the data from heavier hydrocarbon fuel fires (other than LNG), and show a correlation for the fraction radiated with fire diameter as

$$\chi_R = 0.35\, e^{-(D/20)}; \quad \text{D = fire diameter in meters}$$

Applying the above correlation to a 35 m diameter fire used in the Montoir LNG fire tests discussed in Chapter 2 yields $\chi_R = 0.06$, which is not supported by the measured radiant heat flux values at different distances from the fire. Application to a 100 m diameter fire results in $\chi_R = 2.36 \times 10^{-3}$, which would make such size LNG pool fire almost non-radiative. Such a result is highly questionable. Hence, the above correlation for the fraction of combustion energy radiated cannot be correct for LNG fires of all diameters of interest to the US DOT. Also presented in Appendix A is an assessment of the LNG fire point source model allowed in NFPA 59A Standard and the difficulties associated with its results. Therefore, it is recommended that the

[9] In the point source model the atmospheric absorption is not strictly used. The version indicated above should therefore be considered as a modified point source model.

point source model not be used for calculating the hazard distances to people exposure from large LNG fires. Also, in large LNG fires the actual hazard distance can be significant (tens to hundreds of meters); over this distance the absorption of radiant heat by the water vapor in the atmosphere becomes significant, a phenomenon not considered in the point source model.

The "point source" model provides reasonably good estimate of the human exposure hazard distance provided the radiant heat emission characteristics of the fire (in terms of the fraction of combustion energy emitted as radiant heat) is known *a priori*, and the magnitude of the hazard heat flux of interest is low (of the order of 1-5 kW/m^2) and the fire size is small (less than 5 m in diameter). However, calculation of the fraction of combustion energy released using only the properties of the fuel, the dimensions of the fire and the laws of physics cannot be performed with information available. at present. Because of this difficulty and the fact that experimental results have not provided reasonable correlation of this factor to the experimental variables, this model is not generally used (or recommended for use) where relatively accurate determination of the hazard distance is needed.

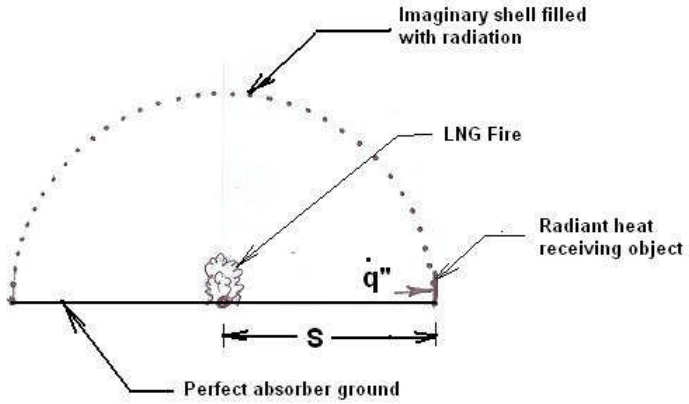

Figure 3-1: Schematic representation of the point source model

3.2.2 Solid flame model

This model is based on semi empirical correlations and represents a fire as a surface emitter of radiant heat energy. The model represents the fire by a geometrical shape (and its orientation due to wind effects), assigns either uniform or variable surface irradiance (also termed "Surface Emissive Power" – MSEP), and includes the transmissivity of radiant heat in the atmosphere, and the relative distance and orientation of the radiant heat-receiving object. The mathematical representation of the model is given by:

$$\dot{q}'' = \sum_{i=1}^{N} F_{dA \to A_{obj}} \int_{\lambda} \left(E_{\lambda,i}\, d\lambda \right) \tau_{\lambda,dA} \qquad (3.6)$$

where,

$\dot{q}''$ = Radiant heat flux received by an object located at a specified distance from and orientated in a specified angle to the fire

λ = Wavelength of radiation

$E_{\lambda,i}$ = Wavelength dependent spectral radiance (Emissive power per unit wavelength) at an elemental surface on the fire (represented by position "i") at wavelength λ

$F_{dA \to A_{obj}}$ = Contribution to the overall geometric view factor from the elemental area on the fire (at position "i") calculated by methods published in the literature, for example by Hottel & Sarofim [1967]

τ_{λ, dA_i} = Wavelength dependent spectral transmissivity of the atmosphere between the elemental surface on the fire and the object, λ is the wavelength of the radiation.

The schematic representation of the various phenomena implied in the above model is shown in Figure 3-2. Simplified versions of the above model are used in most circumstances (including for regulatory purposes) by assuming a constant, and wavelength independent, emissive power over the entire visible surface of the fire, atmospheric transmissivity independent of the wavelength and assuming the fire shape to be that of a cylinder of base diameter equal to that of the burning liquid pool. The descriptions of the simplified model are described in previous publications (Raj [1974], Raj [1982], Moorhouse and Prichard [1982], Considine [1984], SFPE [1995]).

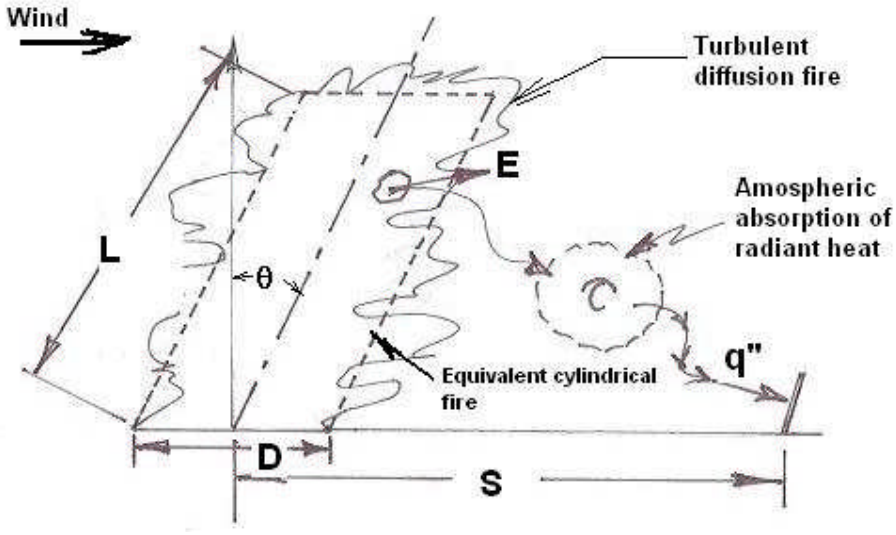

Figure 3-2: Schematic representation of the solid fire

The simplified "Solid Flame" model is represented by

$$\dot{q}'' = E\ F\ \tau \qquad (3.7)$$

where,

E = Average emissive power over the entire surface of the selected shape of the equivalent fire.

F = Mean view factor between the geometry that represents the fire and the heat receiving object located at a specified distance from and orientated in a specified angle to the fire.

τ = Wavelength independent radiant heat transmissivity of the atmosphere between the object and the fire.

The determination of the distance to a specified level of hazard radiant heat flux ($\dot{q}''_{haz}$) requires the specification of both the "solid shape" of the fire and the corresponding average emissive power (E). The known correlations for the relevant parameters for use in equation 3.7 are discussed below.

3.2.2.1 Fire shape

In most "solid flame" models the shape of the fire is chosen to be a circular cylinder of diameter equal to the base diameter of the fire and axial length representing the visible plume of the fire. The axis of this cylinder is assumed to be vertical in low wind speeds (wind velocity below a critical value) and tilted in the wind-direction by an angle with the vertical, which depends on the wind speed, the diameter of the fire and the burning rate. In some models, the drag of the base of the fire at ground level due to the wind is also considered. Other modifications include considering the horizontal cross section of the tilted cylinder to be elliptical rather than circular.

Fire plume length (L): In general, the length of the solid shape representation of the fire is set equal to the time-averaged fire plume length (or height) of the visible fire. Correlations of the following type due originally to Thomas (1963, 1965) have been used in the models to calculate the visible fire plume length (L) for a fire of diameter D.

$$\frac{L}{D} = A\,Fr_C^{p}\,(U^*)^{q} \qquad (3.8)$$

with A, p and q being correlation constants determined empirically from test data and

$$Fr = \frac{\dot{m}''}{\rho_a \sqrt{g\ D}} = Froude\ \ Number = Dimensionless\ burning\ rate \qquad (3.9)$$

$$U^* = \frac{U_{wind}}{\left\{\frac{\dot{m}''}{\rho_a}\ gD\right\}^{\frac{1}{3}}} = Dimensionless\ wind\ speed \qquad (3.10)$$

Thomas (1963) proposed a value A = 42, p = 0.61 and q = 0, which was modified in a later report (Thomas, 1965) to A = 55, p = 2/3 and q = − 0.21. The same p = 2/3 correlation has also

been indicated in a book by Murgai (1976) based on analysis of forest fire data. Moorhouse (1982) has proposed a correlation with p = 0.254 and q = -0.044 for cylindrical shape representation. Many models, including the models required by regulations such as LNGFIRE3 [2004] use the following values for the parameters: A = 42, p = 0.61, q = 0, with a wind induced tilt angle that depends upon U*, but the plume length being independent of the wind speed.

It is not correct to use a single value for the exponent on the Froude number (Fr) to determine the fire plume length over all values of F that is normally associated with liquid pool diffusion fires. For large LNG fires (D>30 m) the correlation used in such models as LNGFIRE3 tends to over predict the length of flame and, hence, the radiation hazard distance. In fact, Thomas (1963) has provided data that indicate different values for the exponent (p) in different value ranges of Fr; p = 0.4 for $Fr>10^{-1}$; p = 0.61 for $10^{-2}<Fr<10^{-1}$ and p = 2/3 for $Fr<10^{-2}$. Heskestad (1983) shows data for a large span of Fr ($10^{-3}<Fr<10^{0}$) indicating varying values for the exponent (p). The experimental results of Cox and Chitty (1985) indicate that p = 1 for $10^{-4}<Fr<10^{-3}$ and p = 2 for $10^{-5}<Fr<10^{-4}$.

Appendix B contains the derivation of the equation for the visible plume height of a turbulent diffusion fire (under calm conditions). The model presented in Appendix B is based on the assumption that the visible fire height/length is the location at which all fuel injected into the fire plume at its base is consumed. In addition a simple analysis of air entrainment and combustion of fuel in the fire are assumed. It is seen from this model (presented in Appendix B) that, in fact, the value of the exponent on the Froude number (Fr) is 2/3.

Figure 3-3 shows the plot of measured visible flame length to diameter ratios from a number of LNG experiments. The Moorhouse correlation is unacceptable because, (i) the physical and scientific basis for the correlation is unknown and has not been published (ii) the correlation seems to be based on only one size LNG test data and therefore cannot provide a trend for different diameter fires, and (iii) does not predict the measured L/D rations in other tests both LNG and other fuels. The size of a typical low earthen dike surrounding single tank LNG storage in on-shore facilities can be as large as 100 m equivalent diameter; hence, a full dike fire can be as large as 100 m diameter. Other impoundment sizes can vary from 10 to 30 m in size. Postulated spills from ships and the formation of pool fires range in size from about 330 m to 512 m diameter [Sandia, 2004] with Froude number (Fr) in the range 1.98×10^{-3} and 1.59×10^{-3}. The values for the flame height-to-diameter ratios (L/D) used by Sandia, based on Moorhouse correlation, for the above range of Froude numbers are 1.21 and 1.28, respectively. These are considerably higher than L/D = 0.71 and L/D = 0.822, which are predicted by Thomas' correlation, respectively, for the above Froude numbers. All other things being equal the radiation hazard distances from large LNG fires predicted by using Moorhouse correlation will be significantly higher than that obtained by using Thomas' correlation for flame heights. Thomas' correlation is based on physical principles and experimental measurements and is therefore used for large LNG fire scenarios. The Cox & Chitty correlation is not applicable in the range of Froude numbers encountered in large LNG spill fires.

Flame drag on ground due to wind: In many experiments with shallow dikes and liquid pool levels coinciding with the top of dikes, it has been observed that a wind-induced downwind dragging of the fire plume very close to the ground occurs. The downwind distance in a circular

cylindrical fire to which the flame sheets at ground level are dragged has been correlated by Moorhouse (1982) as follows.

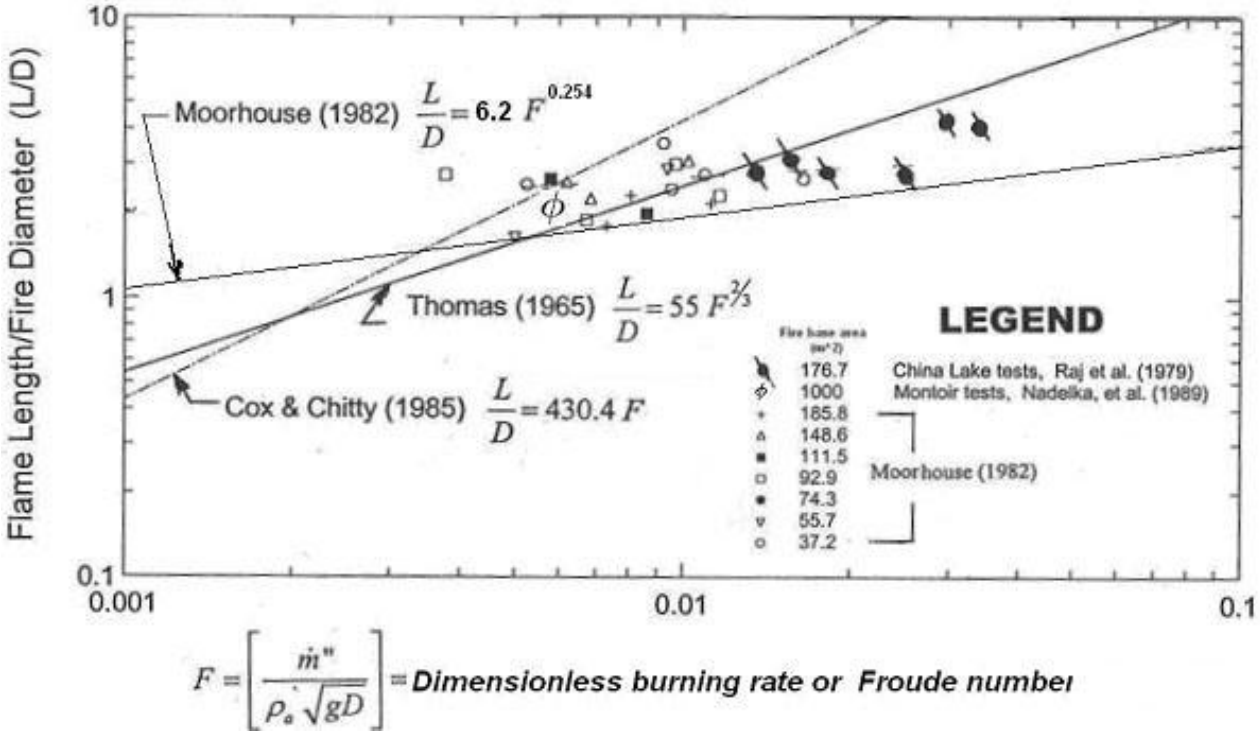

Figure 3-3: Fire height to diameter ratio data from LNG fire experiments

$$\frac{D'}{D} = 1.5\ F_{10}^{0.069} \qquad (3.11)$$

where,

D	=	Diameter of the circular base fire
D'	=	Elongated dimension of the fire base in downwind direction
Fr_{10}	=	Froude number based on wind speed at 10 m elevation

It is however, uncertain whether the above correlation holds good for the case when the liquid level relative to the dike wall is very low. Also uncertain is the application of the above correlation for LNG pool fires on water where the effect of wind will be to move the pool, *en masse,* in the downwind direction. However, the above correlation will be useful in determining the downwind hazard distance, which can still be calculated on the basis of assumption of a cylindrical fire of diameter D, but that the center of the fire is moved downwind from the actual center by a distance of (D'-D)/2.

Flame plume bending due to wind: The bending of the fire plume in the case of a pool fire on land has been found to correlate (Raj and Atallah [1974], Nedelka, et al.[1989]) by a correlation of the type,

$$\cos(\theta) = 1 \qquad for\ U^* \le 1 \tag{3.12a}$$

$$\cos(\theta) = 1/\sqrt{U^*} \qquad for\ U^* > 1 \tag{3.12b}$$

where,

θ = Angle of fire plume tilt with the vertical (mean value)
U* = Dimensionless wind speed defined in equation 3.10

On the basis of small size pool studies of liquid fuels, Welker & Sliepcevich [1966] proposed the following correlation for flame bending in a wind.

$$\frac{\tan(\theta)}{\cos(\theta)} = 3.3 F^{0.8}\ \mathrm{Re}^{0.07} \left(\frac{\rho_v}{\rho_a}\right)^{-0.6} \tag{3.13}$$

where,

Fr = Froude number defined in equation 3.9
Re = Reynolds number of flow over the fire = $\frac{U_{wind}\ D}{\nu_{air}}$
ρ_v = Density of vapor generated by the liquid pool evaporation
ρ_a = Density of air at ambient conditions

It is however seen that the differences in the actual value of the angle of tilt (θ) given by the correlations in equation 3.12 and 3.13 are small and therefore either correlation can be used to predict the plume tilt angle.

3.2.2.2 Surface emissive power

Mean values for the surface emissive power (E) measured in different experiments were indicated in Table 2-1 and in Figure 2-1. It is seen that the mean value of E depends upon the fire size and seems to increase with diameter up to a diameter of about 20 m and then decrease. It can be argued that, in general, the internal temperature in all hydrocarbon fires are about the same resulting in the black body emissive power of all fires to be the same (within the errors of measurement). However, what causes the effective emissive power (i.e., the energy emitted from the nominal fire surface per unit area) is the optical thickness of the fire. The optical thickness of the fire depends upon both the base diameter of the fire, the fuel properties (especially the carbon to hydrogen ratio in the molecule) and the combustion characteristics.

The effective emissive power (E) of an idealized fire is related to the fire temperature by the equation

$$E = E_B\,(1 - e^{-\kappa D}) \tag{3.13}$$

$$E_B = \sigma\, T_F^4 \tag{3.14}$$

where,

E	=	Effective emissive power of the fire	(kW/m^2)
E_B	=	Blackbody emissive power at fire temperature T_F	(kW/m^2)
κ	=	Extinction coefficient	(m^{-1})
σ	=	Stefan-Boltzmann constant = 56.697 x 10^{-12}	($kW/m^2\,K^4$)
T_F	=	Radiative temperature of the fire	(K)

It should be noted that MSEP is a derived quantity and its value depends upon the geometry of the fire used (especially the value used for the "height" of fire plume), assumptions made in calculating the atmospheric transmissivity and the general experimental errors. In fact, Nedelka, et al. (1989) have pointed out that in the Montoir tests (35 m diameter fire) when the photographically observed visible flame radiating areas and the wide angle radiometer data are used the value of E calculated is 275 kW/m^2, whereas the same radiometer data give a value of 175 kW/m^2 for MSEP when the Thomas' flame height correlation (equation 3.8 with A = 55 and p=2/3) is used for the radiating surface calculation. Therefore, the value of E and the flame geometry that should be used in equation 3.7 for calculating the hazard distances should be the same as those used in reporting the value of E from experimentally measured radiometer data.

The inverse of the extinction coefficient (κ) is defined as the "optical depth" (L_κ). The values for k deduced from radiant heat measurement data from various experiments are indicated in Table 2-2. It is seen that the extinction coefficient value varies considerably from test to test. This may be due to size effects, and the generation of high concentration of luminous soot as the size of the fire increases, and experimental errors. However, for very large fires (35 m diameter) the spectral data (Figure 2-3) clearly indicates that the fire is radiating nearly as a blackbody whereas similar spectral data from the 13 - 15 m diameter China Lake tests indicated that the fire of that size was far from being a blackbody emitter. In the latter fire the mean emissivity was estimated to be 0.61 for a 13 m diameter fire ([Raj, 2006b]. From this China Lake fire data it can be concluded that for LNG fires, burning in the open, the optical depth is 13.81 m (or $\kappa = 0.0725$ m^{-1}).

3.2.2.3 Atmospheric transmissivity of radiant heat

The atmosphere absorbs IR energy in specific bands due to the absorption characteristics of water vapor (principally) and carbon dioxide in the atmosphere. Based on the spectral absorption characteristics of water vapor and the relative amounts of water vapor in different relative humidity conditions, the transmissivity of the atmosphere as a function of the path length through the atmosphere for LNG fire radiation have been published by Raj [1977]. The calculated values are indicated in Figure 3-4 and are correlated by the equation,

$$\tau = 1.3989 - 0.0565\,\ell n\{s\; p_w^{sat}(T_a)\,RH\,/100\} \tag{3.15}$$

where,

τ	=	Atmospheric transmissivity	
s	=	Distance through atmosphere	(m)
$p_w^{sat}(T_a)$	=	Saturated water vapor pressure	(N/m^2)

$$p_w^{sat}(T_a) = e^{(11.5261+14.4114 - \frac{5328.1}{T_a})} \qquad (3.16)$$

T_a	=	Air temperature T_a	(K)
RH	=	Relative humidity	(%)

The above correlation is applicable to water vapor partial pressure over the temperature range of 240 K to 373 K (at the latter temperature the partial pressure of water vapor is exactly equal to one atmosphere or 101325 N/m^2). Lees [1996] has reviewed other correlations available in the literature for atmospheric transmissivity (including the one indicated in equation 3.5).

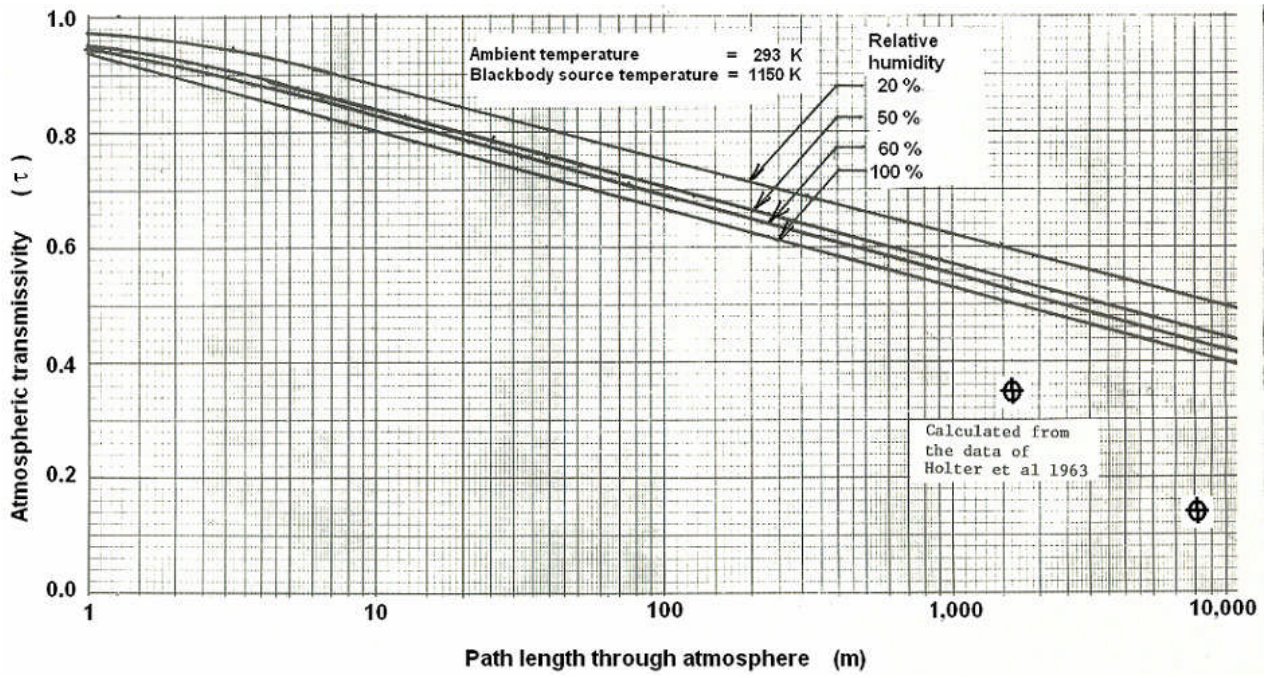

Source: Raj [1977]

Figure 3-4: Atmospheric transmissivity as a function of distance and relative humidity

3.2.3 LNGFIRE3 model assessment

LNGFIRE3 model described in the GRI report GRI-89/0176 [Atallah & Shah, 1989] is incorporated by reference in 49CFR, §193.2057. This regulation allows the use of LNGFIRE3 to determine the thermal radiation distances from LNG pool fires in on-shore facilities. Because of

the importance of this model and its use in most LNG related fire analysis it is reviewed in greater detail below. The principal features of this model and its limitations are discussed below.

The LNGFIRE3 model features as described by Atallah & Shah [1989] are:

1 Description of a circular pool fire by a cylindrical equivalent base diameter fire of constant emissive power over its surface of 190 kW/m^2.

2 The length of the fire plume is assumed to be independent of the wind speed and is given by Thomas' equation (of the type indicated in equation 3.8, with A = 42, p = 0.61, q = 0).

3 Wind induced base size increase in the windward direction due to flame drag and flame tilt with respect to vertical are assumed. (The model uses equations similar to those of equations 3.11 and 3.12, respectively).

4 The mass-burning rate for large fires (larger than 7 m in diameter) is assumed to be 0.11 kg/m^2 s.

5 The model also uses similar correlations for high aspect ratio trench fires.

6 Elevated base fires (such as fires on top of LNG storage tanks) are also considered, but no flame drag is used.

There are a number of limitations and shortcomings of the LNGFIRE3 model when compared with data from experiments involving large LNG pool fires on land. One of the serious shortcomings of the model is its use of a constant emissive power for the entire surface of an equivalent "idealized" fire and its application to sizes of fires of concern in a LNG plant. It is known that as the size of LNG fire increases, its characteristics, both physical and radiative, change significantly. Some of the limitations of the LNGFIRE3 model are indicated below.

1 The length of the visible (radiative) fire plume is dependent on both the wind speed and the vapor mass flux at the base. LNGFIRE3 uses 0.11 kg/m^2 s for the heat flux even though in the 35 m diameter Montoir test the value obtained for the LNG evaporation rate was, on the average, 0.14 kg/m^2 s. Atallah & Shah [1989] were aware of the Montoir data and actually had reviewed parts of the data in the GRI report. Also, while the effect of wind on the base drag and the tilt are considered, the more important effect on the length of the fire plume is not. The effect of increased wind speed is to reduce the effective fire plume length. LNGFIRE3 is more conservative in its calculation of fire plume length but is less conservative on the burning rate. Whether the two opposite effects cancel out for all diameters and wind speeds has not been investigated.

2 This model does not consider the fact that at the base of the fire the emissive power is significantly higher than the average over the entire fire plume. For example, the Montoir and other tests have indicated that the emissive power close to the base of the fire can be as high as 310 kW/m^2, whereas, LNGFIRE3 uses a constant value of 190 kW/m^2. Considering that for objects close to the ground, more than 50% of the heat flux received is from the bottom

portions of the fire, the hazard distances calculated using LNGFIRE3 will not be correct (i..e, LNGFIRE3 will calculate non conservative distances to objects on the ground, especially, for objects with higher heat flux damage criteria).

3 It is well known from Montoir experiments that the emissive power varies, almost by a factor of 5 from the base of the fire to the top of the fire. Also, other observations from accidental fires involving very large oil releases indicate that the ratio of the height of intense burning region near the base of the fire to the diameter deceases significantly as the fire size increases. The rest of the fire is obscured significantly by black smoke production, which reduces the radiant emission from layers above this "bottom" region. LNGFIRE3 model does not take any of these into consideration and therefore its application to fire sizes representative of large dike or sump fires in a LNG facility may be incorrect.

4 It is unclear how the calculated drag distance on the ground is used in LNGFIRE3 calculations. It is very likely that the entire size of the fire (i.e, the diameter) is increased by the extent of the drag. If this is the case, the model will overpredict the hazard distances because of the increased fire size. Also, such an assumption (that the entire size of the fire is increased by the ground level drag) is not supported by experimental observations. Experiments indicate that while the flame size close to the ground increases by about 10 % to 15%, the upward velocity of the gases is such that at very low heights this effect is almost absent and the fire shape resembles that of a no-drag case. That is, the effect of wind drag on the ground is to present a "boot" to the fire on the downwind side. This "boot" exists only for about 1 of 2 m above the ground surface and does not represent a general increase in the downwind dimension of the fire over its entire plume.

5 LNGFIRE3 literature indicates that the model is also applicable to determining the hazard distances from fires on top of storage tanks. However, the burning characteristics of LNG on top of a tank are considerably different from those on the ground because of several important phenomena, namely, (i) The steady state burning rate reduces considerably compared to that on the ground for liquid levels substantially lower than the lip top rim of the tank due to the radiation absorption effects of the intervening gas, (ii) The decrease in burning rate will be even more pronounced in a windy condition when the plume will be bent over and the view factor between the fire and the liquid inside the tank will be reduced compared to that in zero wind condition, (iii) The combustion of gases in the tank from above the liquid to the level of the tank rim will be anything but complete due to lack of air penetration (with the buoyant gases rising through the column below the tank rim), and lastly, (iv) The effect of wind in bringing down the fuel vapors on the lee side of the tank may result in a situation similar to the drag on the ground but with completely different relationship with wind speed, tank diameter and tank height. None of these have been considered in the LNGFIRE3 model.

3.3 Vapor fires

The principal hazard from the deflagration type burning ("vapor fire") of a dispersed LNG vapor cloud[10] is the physical impingement of the fast moving flames on objects and people who may be enveloped by the vapor cloud, before its ignition. The secondary hazard from the moving flame front is due to the radiant heat from the fire to objects and people outside the path of the propagating fire. The procedure for calculating the thermal radiation hazard distances outside the zone of a vapor fire is similar to that used in pool fire hazard estimation, with one singular exception. The vapor fire is generally a fast moving fire and, therefore, the radiant heat flux at any specific location changes with time both due to the changing distance from the fire as well as due to changing fire-to-object orientations. Raj & Emmons [1975] presented a model that describes the speed of the "burn back" flash fire under different wind conditions, the width (along the burn direction) of the burning zone and the height of the fire above the ground. The vapor fire experimental results were discussed in section 2.3. Also, Daish, et al., [2001] have reviewed the available experimental data and models applicable to characterizing vapor fires and concluded that the only model available is the Raj & Emmons model. This model is therefore described in greater detail below.

The principal elements of the Raj & Emmons' two-dimensional vapor fire model are shown, schematically, in Figure 3-5. A dispersed cloud of depth H_c with uniform concentration of vapor ϕ is ignited at the right hand edge (downwind edge) of the cloud. A propagating flame front FF moves (from right to left in Figure 3-5) into the unburned vapor cloud at a speed S, relative to the unburnt gas. S is termed the turbulent flame speed. A burning region of width W trails the propagating flame front. Also, a visible fire plume is established on top of the burning region of width W. The height of this visible flame is H.

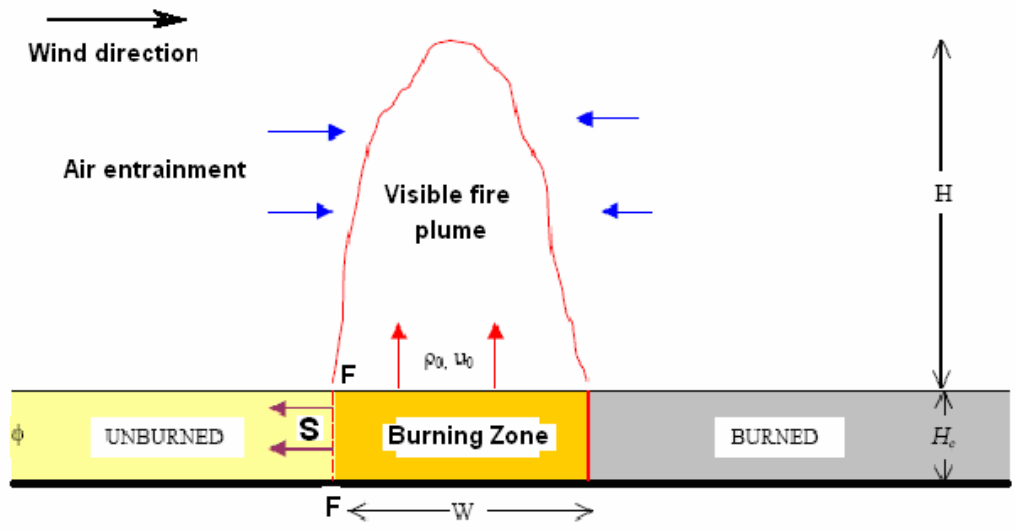

Figure 3-5: Schematic representation of the details of the model for the vapor fire propagating in a dispersed LNG vapor cloud

[10] Calculation of the extent of dispersion of LNG vapors under different weather and local topographical conditions are outside the scope of this investigation.

The model is applicable only if the mean vapor concentration in the cloud (ϕ) is above the stoichiometric value[11]. This condition is expressed mathematically as follows.

$$\phi = \frac{moles\ of\ \ fuel\ in\ unit\ volume}{moles\ of\ \ fuel\ in\ unit\ volume + moles\ of\ \ air\ in\ unit\ volume} \tag{3.17}$$

$$\phi \geq \frac{1}{(1+R)} \tag{3.18}$$

$$R = \left(\frac{1}{0.21}\right)\left\{\frac{1+3n}{2}\right\} \tag{3.19}$$

and

$$P = \{1+2n\} + \left(\frac{0.79}{0.21}\right)\left\{\frac{1+3n}{2}\right\} \tag{3.20}$$

where,

$C_nH_{(2n+2)}$ = Chemical formula for the saturated hydrocarbon fuel in the vapor cloud
R = Stoichiometric air to fuel molar ratio (for complete combustion of fuel)
P = Number of moles of products of combustion produced by the stoichiometric burning of a unit mole of pure fuel.

The model defines a parameter ω as follows:

$$\omega = \frac{Volume\ \ flow\ rate\ of\ \ entrained\ air\ at\ a\ specified\ \sec tion}{[Volume\ \ flow\ rate\ of\ \ gases\ at\ the\ \sec tion - Volume\ \ flow\ rate\ of\ \ gases\ at\ base]} \tag{3.21}$$

It is shown by Raj & Emmons [1975] that the value of ω is related to the physical conditions of cloud and air entrainment as follows.

$$\omega = \frac{1}{\left[\left(\frac{\mathcal{D}}{r} + \frac{P-1}{R}\right)\left\{1 + \frac{n_0}{n_a}(1-\phi)\right\} - \frac{n_0}{n_a}(1-\phi)\right]} \tag{3.22a}$$

where,

n_0 = number of moles of (premixed) fuel "burning"
n_a = number of moles of air burning with n_0 moles of the premixed fuel for stoichiometric combustion [Note: n_a =0 when $\phi = 1/(1+R)$]
$\mathcal{D}$ = Damkohler number = $\Delta H_c/(C_a\ T_a)$
r = Air to fuel mass ratio for stoichiometric combustion of pure fuel

$$r = \frac{\mu_a}{\mu_f} R = 34.4048\,\frac{1+3n}{1+7n} \qquad \text{for saturated hydrocarbons} \tag{3.23}$$

[11] The stoichiometric vapor concentration in air for methane vapor is 9.52 % whereas, the lower flammable limit (LFL) for methane vapor in air is 5%.

For the burning of a pure methane cloud (a LNG cloud can be approximated to a pure methane cloud) it can be shown from equations 3.19 and 3.20 that

$$(P-1)/R = 1 \tag{3.24}$$

with P = 10.5238 and R= 9.5238 for methane (CH_4). Applying the above result in equation 3.22a we get,

$$\omega_{CH4} = \frac{1}{\left[1+\frac{\mathcal{D}}{r}\left\{1+\frac{n_0}{n_a}(1-\phi)\right\}\right]} \tag{3.22b}$$

Where, ω_{CH4} is the value of ω (defined in equation 3.22a) for methane. It is noticed from the above equation that ω_{CH4} varies with the number of moles of air (n_a) entrained for complete combustion. A value for ω_{CH4} is defined below corresponding to a condition when the exact amount of air entrained is such that the total (unburnt) mixture of fuel and air constitute a stoichiometric value.

$$\omega^* = \omega^S_{CH4} = \frac{1}{\left[1+\frac{\mathcal{D}}{r}\left\{1+\frac{(1-\phi)}{\phi(1+R)-1}\right\}\right]} \tag{3.25}$$

where,

ω^* = Value of ω at stoichiometric conditions for methane vapor

The following result, for the steady state burning zone width, is obtained from the paper of Raj & Emmons [1975].

$$\frac{W_\infty}{\delta} = 40\left[F_f\,\hat{\rho}^2\,\frac{\omega^*\left\{r+\frac{\omega^*}{\hat{\rho}}\right\}^2}{(1-\omega^*)^3}\right]^{1/3} \tag{3.26}$$

$$\frac{H}{W_\infty} = 2 \tag{3.27}$$

$$\delta = \phi\, H_C \tag{3.28}$$

$$F_f = \frac{S^2}{g\delta} \tag{3.29}$$

$$U_F = (S + U_{wind}) \tag{3.30}$$

where,

W_∞ = Steady state (or asymptotic) width of the burning zone

δ = Depth of an equivalent pure vapor cloud for vapor at ambient temperature and pressure

Fr_f = Flame Froude number
S = Turbulent flame speed (with respect to unburnt gas)
$\hat{\rho}$ = Ratio of pure vapor density at ambient temperature and pressure to that of air at the same conditions.
H_C = Actual depth of the (uniform) concentration cloud
H = height of the visible fire above the equivalent pure vapor cloud depth (δ)
U_F = Upwind speed of the propagating fire with respect to the ground

Experiments involving the ignition of vapor clouds at the downwind edge have indicated a relationship between the turbulent flame speed and wind speed of the type (see discussion in section 2.3: "Summary: Vapor Cloud Fire Test Findings")

$$S = 0.8 + 1.6\,U_{wind} \qquad (m/s) \qquad (3.31)$$

Using the set of equations 3.25 through 3.31 the velocity of upwind propagation of the fire, the width of the burning zone, the total height of the visible fire and the depth of the equivalent pure vapor cloud depth can be calculated. For a, equivalent pure methane cloud of depth (δ) 1.8 m at 294 K (70 ^{o}F) the maximum wind-wise extent (width) of burning zone (W_{∞}) is estimated from the above equations to be 25 m.

For the purposes of calculating the radiant thermal hazard from such a traveling fire, it is generally assumed that the emissive power of the flame is between 220 kW/m^2 to 275 kW/m^2, the former value being used when the fire is in the low vapor concentration regions and the higher value for more concentrated parts of the cloud burning. It should be noted, however, that in the experiments where the concentration was low (i.e., concentration in air in the 5 % to 15% range within the vapor cloud) the fire was almost not visible due to the flames being thin wisps of blue flames. Also, the height of the burning region was equal to the depth of the visible cloud before ignition. The radiation from such a fire is minimal because the fire occurs in premixed regions and is optically thin. The above emissive power values should be therefore used only in regions where the vapor concentration in the cloud before ignition is above 15%.

3.4 Fireballs

The occurrence of large fireball type of fires, which pose thermal radiant hazard distances larger than from the liquid pool fires is, perhaps, rare in LNG spill caused fires. The ignition of a high concentration vapor cloud that forms initially on top of a boiling liquid pool, if ignited in its concentrated state, will form a fireball followed by a sustained liquid pool fire. Because of the importance of the fireball phenomenon, the models available in the literature are indicated below. Lees [§16.15, 1996] has reviewed many fireball models available in the literature. Most of these models are applicable to fireballs arising from the ignition of liquids flashing after being released from pressurized containers. One phenomenon that results in the formation of large fireballs is the sudden release of a pressurized, flammable liquid and its immediate ignition,. This phenomenon is generally referred to in the literature as the Boiling Liquid Expanding Vapor Explosion (BLEVE). Very few fire models are applicable to the description of a fireball type burning of a dispersed and partially mixed with air vapor cloud of the type encountered in LNG spills.

The model due to Fay and Lewis referenced in Lees [1996] gives the following correlations for a fireball from a "pure vapor" source.

$$g' = g\left(\frac{\rho_a}{\rho_p} - 1\right) = g\left(\frac{T_p}{T_a} - 1\right) \tag{3.32}$$

$$z = (\alpha / 2)\, D \tag{3.33}$$

$$t = \left(\frac{14}{\alpha g'}\right)^{\frac{1}{2}} \left\{\frac{3V}{4\pi}\right\}^{1/5} \tag{3.34}$$

$$\frac{V_p}{V_f} = \left\{\frac{T_p}{T_a}\right\} \Gamma \tag{3.35}$$

and

$$\Gamma = \left[\frac{m\varphi + 4.762(4n + m)}{4\varphi}\right] \tag{3.36}$$

where,

g	=	Acceleration due to gravity
g'	=	Buoyancy reduced gravitational acceleration
α	=	Air entrainment coefficient
V	=	Fireball volume at any instant of time t
V_f	=	Volume of the ambient pressure and ambient temperature, pure fuel vapor at the source
V_p	=	Volume of the fireball when all combustion is complete
t	=	Time (during the rise of the fireball) when the fireball volume is V
z	=	Location of the center of the rising fireball above ground at any t
m,n	=	Atoms of hydrogen and carbon, respectively, in a hydrocarbon molecule of formula C_nH_m
φ	=	Fuel to air equivalence ratio (volume of stoichiometric air/volume of actual air entrained for complete combustion)
T_a	=	Ambient air temperature
T_p	=	Final temperature of the products of combustion

Based on laboratory scale experiments Fay & Lewis report a value of α = 0.285 and φ = 0.271.

To calculate the rise rate and the maximum rise before complete combustion it is necessary to use the energy equation. Using the energy equation and the assumption that the gases are perfect with the same mass specific heat the following result can be obtained.

$$\frac{T_p}{T_a} = 1 + \frac{\rho_f}{\rho} \frac{\mathcal{D}}{\Gamma} \tag{3.37}$$

For the fireball type of combustion of a pure methane cloud at ambient temperature and ambient pressure, using the above values for the entrainment coefficient and the equivalence ratio we obtain the following dimensional results

$$t_p = 3.02\, M_f^{1/6} \quad (3.38a)$$

$$z_p = 1.05\, M_f^{1/3} \quad (3.38b)$$

$$D_p = 7.37\, M_f^{1/3} \quad (3.38c)$$

where, t_p is the time for complete combustion of the fireball in seconds, z_p the height to which the fireball rises in meters, D_p the final fireball diameter in meters and M_f the mass in kilograms of fuel from the cloud burning. Different investigators have obtained different values for the constants indicated in equations 3.38a through 3.38c. These values are indicated in Table 3-1.

Table 3-1
LNG vapor fireball correlations* from different models

Researcher	Parameter	Parameter values for t_p Rise time (s)	Parameter values for Z_p Rise Height (m)	Parameter values for D_p diameter (m)	Remarks
Fay & Lewis (Theoretical)	B	3.02	1.05	7.37	**Variable = B $(M_f)^N$** "Variable" is any of t_p, Z_p or D_p. The value of M_f is in kg
	N	1/6	1/3	1/3	
Fay & Lewis (Lab scale tests)	B			6.36	
	N			1/3	
Hardee, Lee & Benedick	B	2.57	N/A	6.24	
	N	1/6	1/3	1/3	
Roberts	B	0.45	N/A	5.8	
	N	1/3	N/A	1/3	
Pietersen	B	0.852	N/A	6.48	
	N	0.26	N/A	1/3	
Major Hazards Assessment Panel (MHAP)	B	0.45	N/A	N/A	For M_f < 30,000 kg
	N	1/3	N/A	N/A	
	B	2.6	N/A	N/A	For M_f > 30,000 kg
	N	1/6	N/A	N/A	
Moorhouse & Prichard [1982]	B	1.089	N/A	5.33	
	N	0.327	N/A	0.327	

* *Reported by Lees [1996]*

The models for calculating the **thermal radiation hazard distance from a fireball** include both the "point source" model and the "solid flame" model. In the point source model, the rate of heat emission (in W) is calculated by assuming (i) a value (15 % to 25%) for the fraction of combustion energy that is released as radiation, and (ii) constant rate of release of combustion

energy over the duration of the fireball "life." The latter value is determined by dividing the total heat release (fuel mass x fuel heating value) by the duration of the fireball, t_p. In the "solid flame" model a specific constant value is assumed for the emissive power (E) of the fireball (CCPS referenced by Lees [1966] assumes E= 350 kW/m^2). The time-wise variations of the diameter and rise height of the fireball are calculated using the equations presented earlier. The view factor from the rising fireball to an object on the ground is calculated as a function of time and thus the heat flux variation at the object as a function of time. Since these calculations are straightforward and have been discussed in the section on "pool fire models" no additional equations are indicated.

In the next chapter, the current regulatory model for determining the LNG pool fire hazard distance is reviewed in brief and its shortcomings are indicated. A more advanced model for characterizing a large LNG pool fire is developed and described.

Chapter 4
Large Size LNG Pool Fire Model

4.1 Background

Findings from the experimental data from the largest LNG fire test to date, namely, the 1987 Montoir tests, were reviewed in Chapter 2, § 2.1. The technical papers Nedelka [1989] and Malvos & Raj [2006] provide additional details of this test, the instruments used, data recorded and quantitative results from this series of tests. The principal findings that have a bearing on the model described below are indicated below for the sake of continuity.

1 The fire burned as a puffing fire, releasing connected fireballs through the fire column with a fireball release period varying between 3 s and 3.5 s. The estimated upward velocity of upward motion of the fireballs through the fire column is about 20 m/s.

2 The fires exhibited a bright, intense burning region close to the bottom of the fire followed (upwards) by a region in which the interior of the fire was exposed intermittently by otherwise smoke blanketed regions. The fraction of the "surface area" of the fire that contained exposed burning, and therefore heat radiating, regions decreased continuously and substantially with the height of the flame. The bottom intense fire region seemed to increase in a windy condition.

3 The fires in all three tests were very smoky, beyond a certain height (or length along the tilted axis). The narrow angle radiometer readings confirm that the time averaged apparent emissive power of the fire decreases with height (or length along the axis). The mean emissive power, calculated from actually visible burning area spots over the entire length of the fire plume, was about 265 kW/m^2. The mean emissive power value, based on idealized fire geometry (tilted circular cylinder with axial length given by Thomas' correlation), is reported to be 165 kW/m^2. The bottom regions of the fire exhibited mean surface emissive powers as high as 310 kW/m^2.

There are relatively few fire models in the literature that have considered the formation of black smoke in a hydrocarbon fire and its effects on the radiant heat output from fires. This is due to lack of quantitative data from experiments or theoretical predictions on the fraction of the carbon in the fuel that gets converted to "cold, " black soot and the dependence of this quantity on the combustion and turbulence processes in a fire. It is known, however, that in the burning of liquid fuels, the higher the number of atoms of carbon in the molecule, the greater is the production of black soot in the fire and the lower is the overall radiant heat emission from the fire. Considine [1984] in his review of pool fire radiation models alludes to a model by Smith (Reference number [11] in Considine's paper), which includes the effect of smoke obscuration in the upper regions of a fire. The radiation from the upper regions is modeled by defining a mean radiating edge together with an associated mean radiation temperature (T_R) for the upper parts of a fire. The temperature at the fire surface is assumed to vary as the square of the sine of time with an effective period of about 1 sec. The amplitude of temperature variation in the smoky region of the fire is assumed to be about a 30% of the "surface" temperature in the lower regions of the fire (without smoke effects). It is concluded in this model that the upper regions of the fire

(smoky regions) radiate with about 30% of the radiant heat flux emanating from the "lower region." Also, the lower region is assumed to extend to 30% of the average visible flame height. McGrattan, et al., [2000] have proposed a similar "two-zone" model for large hydrocarbon fires. The lower region, termed the "luminous region," is the only radiating surface and the top (rest of fire plume) is obscured by opaque smoke. Based on data measurements for up to 20 m diameter fires of gasoline, heptane, crude oil and kerosene fires, the authors conclude that the maximum height of the luminous region is a constant beyond a 20 m diameter fire and this maximum height being dependent only on the combustion heat release rate per unit area of the pool (for crude oil fire of 20 m diameter with a 2 MW/m^2 heat release rate the predicted height of bottom luminous zone is 12.8 m). In addition, in this model, the maximum emissive power of the "luminous" part of the fire does not exceed 100 kW/m^2.

The LNG fire thermal emission magnitude data and its variation with height obtained from the 35 m diameter LNG fire tests at Montoir indicate that neither the Considine model nor the McGrattan, et al., model predicts the fire physical characteristics and the radiation emission properly. The data indicate that the extent along the plume of the lower, "constant emissive power" region is about 6 to 7 % of the overall mean visible plume length (75 m). That is, the region is only about 5 m in height whereas the Considine model predicts this region to be 30% of 75 = 22.5 m in axial length, and the McGrattan, et al., model predicts this region to be 45 m in height. The experimental data also indicate that the radiation emission varies considerably with height, decreasing almost linearly with distance along the plume axis. Figure 2-2 presented in chapter 2 shows this variation in the measured narrow angle radiometer data together with its statistical variation (due to the effects of turbulence and intermittency of gas burning zone visibility). The Considine model assumes a constant 30% of base emissive power for this region whereas the McGrattan, et al. model assumes zero emission from this region. Obviously, there are difficulties in applying these two models to predict the overall emissions (and their variation with height) from large LNG fires and therefore the hazard distances calculated from such models will be incorrect. In addition, neither model takes into account the chemistry and the magnitude of soot production and their relationship with the properties of the fuel burning and fire size. A semi empirical model that considers smoke production rate, variation of the emissive power with height, dependence on fire size and the variation with size and fuel properties of the height of the bottom "luminous' zone is presented in this chapter.

4.1.1 Smoke production in fires.

Large diameter LNG fires seem to produce a significant amount of smoke (Nedelka, et al. [1989]). This smoke production phenomenon is similar to that observed in the burning of other liquid fuels of higher hydrocarbon content (propane, butane, gasoline, kerosene, JP4, etc). Two physical phenomena may contribute to the production of smoke, even in "clean burning" fuels such as LNG. The first is the lack of enough oxygen in the core of large diameter fires to burn the carbon produced by the pyrolysis of fuel vapor. This not only produces soot (carbon particles) but also lowers the overall heat release –and hence the temperature- resulting in the promotion of smoke production. The second phenomenon may be due to the lowering of the effective concentration of fuel and vapor in the core from the recirculation of burnt gases by the toroidal vortex that is prevalent in all large fires. The effect of smoke is to shield the emission of thermal radiation from the fire thereby reducing, significantly, the thermal radiation hazard

distance around large LNG or other fires. In addition, the formation (and recirculation) of smoke could result in less efficient combustion of the fuel and result in the lowering of the effective flame temperature. However, the reduction in the radiant emission out of the fire tends to increase the temperature of the gases; which one of the two effects dominates depends on the chemical properties of the fuel, chemistry of combustion, the physical dimensions and the hydrodynamics of gas flow within the fire. No model exists that considers all of these phenomena.

Soot is an agglomeration of fluffy carbon particles (with diameters in the range 3 nm to 30 nm) in a fire in which they are being oxidized and are "glowing"; in fact, the visibility of a fire is caused by the emission of radiation in the visible spectrum by the burning soot. When the carbon produced by the fuel vapor pyrolysis is either partially oxidized or is not oxidized at all because of lower local temperature, carbon particles agglomerate to form long chain molecules of carbon or "smoke."

Soot formation studies from small, laboratory-scale tests are reported extensively in the literature (Narasimhan & Foster [1965], Hura & Glassman [1988], Markstein [1988], Fowler [1988]). However, there is very little work on the measurement of smoke production rates in large turbulent diffusion fires and singularly absent for LNG fires. McCaffrey & Harkleroad [1988] have presented soot data from laboratory-scale experiments for a number of hydrocarbon fires in the form of specific extinction area (SEA) for soot; for propane SEA is found to be 124 m^2/kg and for crude oil fires it is 1000 m^2/kg.

No direct data for the smoke yield, as a function of fire diameter exists for large fires of different fuels. Notarianni, et al [1993] measured the smoke production in crude oil fires of diameters from 0.085 m to 17.2 m and found that smoke yield (mass % of burnt fuel that is emitted as smoke) increases as the diameter of the fire increases. Data on smoke yield from methane (or LNG) fires is singularly unavailable in the literature either for small scale or large scale turbulent diffusion fires! Also not available is the smoke extinction coefficient for soot formed in methane fires.

4.2 Pool fire model including smoke effects ("PoFMISE")

The model discussed this report is based on physical phenomena in a (circular geometry) turbulent diffusion fire represented, schematically, in Figure 4-1. The buoyant plume entrains ambient air and this air is "conveyed" to different interior parts of the fire by the self-generated turbulence augmented by wind turbulence. In the bottom region of the fire, below a height L_C, combustion of the vapor is very efficient. The flame sheet visible in this region is the outer layer of vapors burning and in a large diameter fire this part of the fire is practically optically thick and radiates at a high temperature. In the region designated as zone 2, the flame sheets are anchored to the base, but represent the less efficient combustion zone in a large fire because of the mixing internally of the unburnt and partially burnt gases (due to deficiency of oxygen in the central core region) from zone 1 and recirculation due to buoyant thermals. In this zone the intermittent formation of black smoke is observed which begins to partially obscure the hot interior flame. In the top region the gas burning is in clumps and generation/accumulation of significant amount of smoke is seen. Substantial to complete shrouding of interior burning regions occurs. The result of

such burning, noticed in all 'large' liquid hydrocarbon fuel fires is a reduction of the thermal radiative output to the surroundings. This does not, however, mean that the temperature inside the fire is lower in large fires[12]. The diameter of the fire at which it can be considered to be 'large' depends upon the fuel chemical composition (especially on the carbon to hydrogen mass ratio), burning rate (dictated by feed back energy from the fire as well as heat input from the substrate) and environmental conditions (wind turbulence). The above physical description of the fire is captured in the model elaborated below.

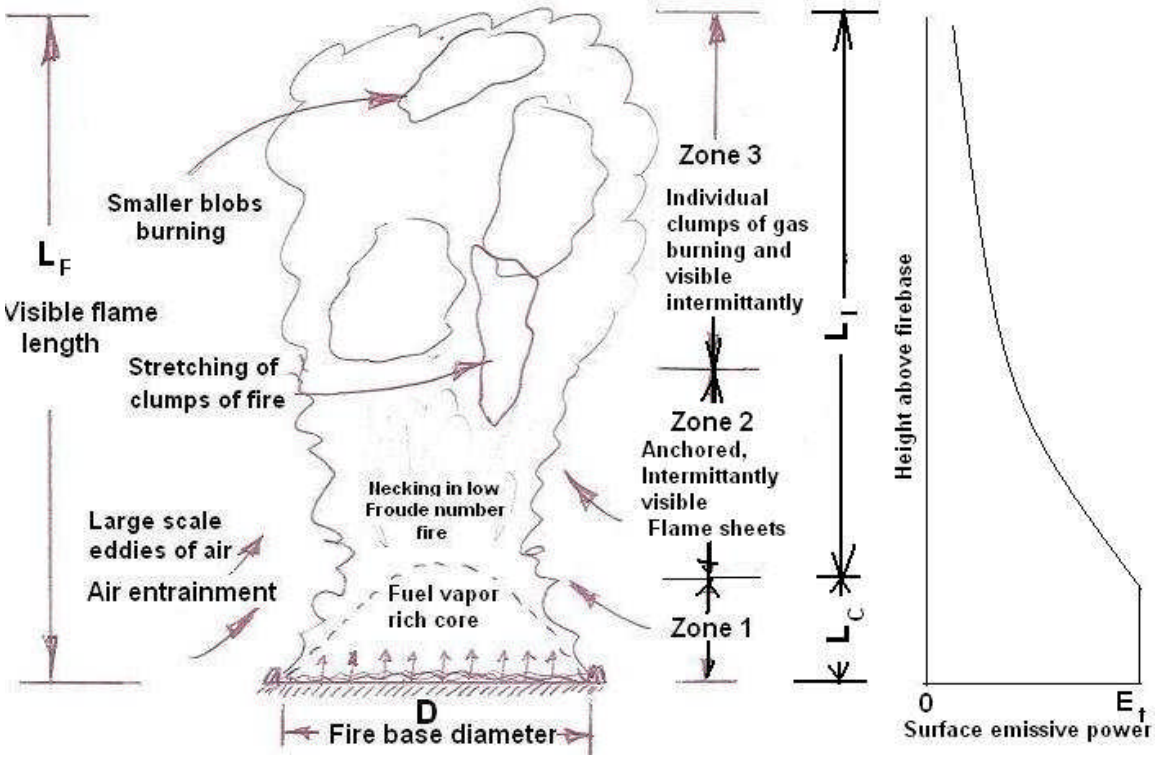

Figure 4-1: Schematic representation of different regions of combustion and intermittency in a buoyant diffusion fire

[12] It is noted that all liquid hydrocarbon fuels have about the same heating value per unit mass (within 10%). Also in all turbulent diffusion fires, the total mass of air entrained by the time the combustion is complete is about the same (about 10 to 15 times the stoichiometric mass value). If the radiative output to the outside is reduced due to smoke shrouding, it stands to reason to expect that the fire temperature in all fuel fires to be about the same, within about 10%.

4.2.1 Assumptions

The following assumptions are made in the formulation of the model:

1 The time averaged mean geometry of the pulsating, turbulent diffusion fire can be represented by an enveloping cylinder of circular cross section, tilted downwind, at winds above a critical wind speed (dependent on the diameter and burning rate).

2 The axial fire plume length (or height) over which all vapors generated by the evaporating liquid pool are burnt is represented by a "mean visible plume length" and is calculated using the correlation by Thomas [1965]. This correlation results in the plume length to diameter ratio varying as $D^{-1/3}$. In Appendix A it is shown that this is the correct representation (various fire height correlations in the literature and their incorrectness have been discussed by Raj[2005]).

3 The air entrainment rate is independent of the wind speed and depends only on the internal updraft velocity of gases inside the fire. Also, only a fraction of the mass of air entrained at any section is burned with its corresponding stoichiometric mass of fuel at that section.

4 The fire emits uniformly in all directions at the same surface emissive power (SEP) at a given axial length from the base. The SEP, however, varies axially.

5 Thermal radiation emission is uniform (i.e., the surface emissive power – SEP - is constant) near the base of the fire, over an axial length of fire equal to the clean burning zone length (L_C). This lower zone SEP represents the maximum value for the fire SEP. In zone 2 and zone 3 it is assumed that the inner core "hot flame" will be visible for a fraction of the time and for the other part of the time the flame core is shrouded by black smoke. However, since the smoke transmissivity is dependent upon the smoke concentration a part of the inner flame radiation will pass through the smoke layer. The fraction of the time the inner flame is visible is represented by a probability and this probability value decreases with increase in height (or axial distance from base). In the intermittency zones the overall surface emissive power is a linear, weighted sum of the maximum SEP and the smoke transmitted SEP. The weighting factor is the probability that at any time a given fraction of the cylindrical surface area is "open" so that the inner burning core of the fire can be "seen."

4.2.2 Details of the model

4.2.2.1 Fire plume length (L_F)

The following correlation due to Thomas [1965] is used to calculate the average visible plume length for a fire of diameter D (see foot note below[13]).

[13] That the L/D ratio is proportional to the 2/3 power of the Froude number (F), or proportional to $(D)^{-1/3}$ in windless condition is derived, in detail, in Appendix B. Other correlations have been published in the literature based solely on curve fit to experimental data, with no basis in physics of entrainment or combustion.

$$\frac{L_F}{D} = 55\ F^{\frac{2}{3}}\ (U^*)^{-0.21} \qquad (4.1)$$

where,

$$F = \frac{\dot{m}''}{\rho_a \sqrt{g\ D}} = Froude\ \ Number = Dimensionless\ burning\ rate \qquad (4.2)$$

and,

$$U^* = \frac{U_{wind}}{\left[\frac{\dot{m}''}{\rho_a} gD\right]^{\frac{1}{3}}} = Dimensionless\ wind\ speed \qquad (4.3)$$

4.2.2.2 Axial length of the lower clean burning zone (L_C)

Heskestad [1983] indicates a correlation for the length of the intermittent zone (L_I) with the Froude number Fr (for $7.5 \times 10^{-4} < Fr < 2.5 \times 10^{-1}$) as follows:

$$\frac{L_I}{L_F} = 0.167 - 0.25 \log_{10}(F) \qquad (4.4)$$

We assume a form similar to the one in the above correlation for the intermittency zone but with a slight modification to conform to the data from 35 m diameter Montoir LNG fire test results (Nedelka, et al., [1989]). It is seen in Montoir tests that the height of the bottom, clean burning zone (L_C), near the base of fire is very small and can be represented by the following equation.

$$\psi = \frac{L_C}{L_F} = (1 - \frac{L_I}{L_F}) = 0.70 + \log_{10}(F^{\frac{1}{4}})\} \qquad (4.5)$$

The above formula will make the bottom clean burning zone length (L_C) to be zero for F = 1.585×10^{-3} (which will represent a LNG fire on water of about 2,000 m in diameter!).

4.2.2.3 Absorption of radiation by smoke

The presence of smoke in a fire results in the absorption of thermal radiation emission and a reduction in the effective emissive power. It is assumed that in the inner regions the fuel is burning at the same mean temperature, irrespective of the axial location within the visible plume. That is, the radiation emission internally within the fire is the same at all axial distances. Smoke is generated in the interior sections of the fire from the incomplete combustion of fuel due to reduced oxygen concentration. The smoke produced transmits only a fraction of the radiation produced inside the fire body to the nominal flame surface. We define an effective emissive power for smoke (i.e., the emission from the cylinder surface shrouded by smoke layer) as:

$$E_S = E_b \tau_s \qquad (4.6)$$

where,

E_S	=	Effective surface emissive power in the smoke	(kW/m^2)
E_b	=	Surface emissive power at the lower regions.	(kW/m^2)
τ_s	=	Transmissivity of smoke	

The transmissivity of smoke is related to the density of smoke and its optical characteristics by the equation:

$$\tau_s = e^{-(k_m C_s L_b)} \qquad (4.7)$$

where,

k_m	=	Specific soot extinction area	(m^2/kg)
C_s	=	Mass concentration of smoke in the flame gases	(kg smoke/m^3)
L_b	=	Beam length = 0.63 D, for cylindrical fires	(m)

In general, the extinction coefficient and the beam length are functions of the wavelength and, hence, the transmissivity is also a function of the wavelength. Because of the paucity of data (for the wavelength dependent extinction coefficient and beam length) we use wavelength independent representation in the above equation.

It can be shown that the soot concentration C_S (kg/m^3) is related to the burning efficiency of the fuel (β), the heat of combustion of the fuel (ΔH_C), the stoichiometric air to fuel mass ratio (r) and the soot mass yield per unit mass of fuel burned (Y) by the formula

$$C_S = \rho_a Y \frac{1}{\left[1 + \frac{r}{\beta} + \frac{\Delta H_c}{C_a T_a}\right]} \qquad (4.8)$$

Notarianni, et al. [1993] measured the smoke production in crude oil fires of diameters from 0.085 m to 17.2 m and found that smoke yield, Y (mass fraction of burnt fuel that is emitted as smoke) increases as the diameter of the fire increases. The data for the mass fraction smoke yield (Y in %) vs. fire diameter (D in meters) presented by these researchers can be correlated (for crude oil fires) by the following equation:

$$Y = 9.412 + 2.758 * \log_{10}(D); \quad [D \text{ in meters}] \qquad (4.9)$$

There are no experimental data for the soot yield in large methane (or LNG) fires. However, as will be shown later based on the test results of 35 m diameter Montoir LNG fire tests, and the model proposed for the variation of the emissive power along the axis length of the fire, it is seen that the above correlation may be appropriate for large methane fires also. Of course, this assumption has to be verified experimentally.

4.2.2.4 Emissive power variation through the fire axial length

In the intermittency zone (zone 2 and zone 3 in Figure 4-1), the surface emissive power varies because of smoke shrouding. We assume that the rate of intermittency varies between zero (i.e., there is no smoke obscuration) just at the top of "clean burning zone" to 100% (i.e., full smoke obscuration) at the top of the intermittency zone. In other words the probability of realizing the maximum SEP (recorded at the bottom region of the fire) changes from 1 to zero, respectively, from the bottom of the intermittency zone to the top of the intermittency zone. This probability can also be interpreted as the fraction of the time that the outer layers of the cylindrical fire show the "inner core" thus radiating at the maximum SEP; the remainder of the time the emission is from the smoke layers. The above concept is mathematically expressed as follows:

The probability of observing the maximum SEP value (E_b) at any axial position along the flame plume is p. In the intermittency region "p" is assumed to have the following cubic parabolic variation with axial length:

$$p(\xi) = \left[\frac{(1-\xi)}{(1-\psi)}\right]^3 \qquad for \quad \psi \le \xi \le 1 \tag{4.10}$$

$$\xi = \frac{Z}{L_F} = \frac{Length\ from\ the\ liquid\ surface\ along\ the\ fire\ axis}{Visible\ fire\ plume\ length} \tag{4.11}$$

$\psi = L_C/L_F =$ Ratio of "clean burn zone" axial length to the visible plume length (4.12)

Also from the assumed correlation for ψ (from 35 m diameter fire test data) we have from equation 4.5 above

$$\psi = \frac{L_c}{L_F} = 0.70 + 0.25 \log_{10}(F) \tag{4.5}$$

For LNG fires on water of diameters in the 15 < D< 350 meters it can be shown that the value of ψ is in the range $0.3 > \psi > 0.1$, respectively.

The axial variation of the surface emissive power (SEP) over the entire visible plume length of the fire can then be represented as follows:

$$E(Z) = E_b \qquad for \quad 0 \le \frac{Z}{L_F} \le \psi \tag{4.13a}$$

$$E(Z) = p\,E_b + (1-p)\,E_S(Z) \qquad for \quad \psi \le \frac{Z}{L_F} \le 1 \tag{4.13b}$$

where,

E_b = Emissive power of the brightest part of the fire (near the base)
$E_S(Z)$ = Emissive power of the smoke layer (from equation 4.6)
p(Z) = Probability that at any give time the inner fire is visible at height Z (see equation 4.10).

The overall mean surface emissive power (MSEP) is then obtained by integrating E in equation 4.13a and 4.13b from Z = 0 to Z = L_F. That is,

$$\bar{E} = \int_{\xi=0}^{\xi=1} E(\xi)\, d\xi \qquad (4.14)$$

Substituting equations 4.13a and 4.13b in 4.14 and using the definition of p from equation 4.10 it can be shown that

$$\frac{\bar{E}}{E_b} = \psi + (\tfrac{1}{3} + \tfrac{2}{3}\tau_s)(1-\psi) \qquad (4.15)$$

The fire base emissive power will depend on the size of the fire. This base emissive power in the "clean burning region" of the fire can be represented by the equation

$$E_b = E_{\max}\left(1 - e^{-\frac{D}{D_{Opt}}}\right) \qquad (4.16)$$

where,

E_{max} = Maximum emissive power of a black body consistent with the equivalent black body temperature of an LNG fire
D = Base diameter of the fire
D_{opt} = Optical depth

The China Lake experiments indicated that the 13 m diameter LNG fire on water was not radiating like a blackbody at the hot gas temperature. Based on the analysis of the spectral data from these tests the fire base emissivity was calculated to be 0.61 (Raj, et al [1979], Raj [2005]). This leads to a calculated optical length[14] for a LNG fire to be 13.81 m. Therefore, it can be assumed that any fire of diameter less than the optical depth radiates at its bottom at an emissive power lower than the maximum consistent with the gas temperature. The equivalent blackbody temperature of the 35 m diameter fire was estimated by Malvos & Raj [2006] to be 1547 K with an emissivity of 0.92 based on the measured spectrum (Figure 2-2) in the Montoir tests.

The emissivity of the 35 m diameter fire was calculated based on the optical path length (13.81 m) obtained from the China Lake tests. The equivalent black body temperature was

[14] The optical path length (L_{opt}) is calculated using the following relationship between emissivity (ε) and L_{Opt}

$$\varepsilon = [1-\exp(-D/L_{Opt})]$$

obtained by assuming that the fire was a grey body with an emissivity of 0.92 and matching the spectral radiance at 2.25 μ wavelength (with the assumption that at that wavelength there was no absorption in the atmosphere). However, the latter assumption may lead to some errors in the estimated blackbody temperature of about 10 K. If the above value of optical depth (of 13.81 m) obtained from the China Lake tests is used together with the measured value of 300 kW/m^2 for E_b from the Montoir tests, it can be shown that the maximum base emissive power (E_{Max}) is equal to 325 kW/m^2. This maximum emissive power corresponds to an equivalent blackbody temperature of 1547 K.

4.2.3 Results

Calculations are performed to evaluate the mean surface emissive power of different diameter LNG pool fires. These results are presented in Table 4-1. The values assumed for some of the parameters are also indicated in the Table. Also shown in the table are the experimental values for the mean emissive power as calculated from the wide-angle radiometer measured heat flux values in field tests corrected for atmospheric absorption and the visible fire height calculated using Thomas' correlation (equation 4.1).

The variation of the emissive power with axial distance through the length of the visible plume of a 35 m diameter fire for the conditions of test # 2 in the Montoir series is shown in Figure 4-2. The statistical distribution of the narrow angle radiometer (NAR) data from one fire test, uncorrected for atmospheric absorption, was indicated in Figure 2-2. In Figure 4-2 the same data are plotted after correcting for the atmospheric absorption of radiation over the distance to the NAR. The atmospheric transmissivity factors for the test conditions are calculated to be 0.67 to the bottom of the fire, 0.668 to the mid height and 0.661 to the top (for a detailed discussion of the various atmospheric transmissivity models and their accuracies see Lees [1996]). Also plotted for comparison in Figure 4-2 are the model-predicted results for a 35 m LNG fire on land.

Using the above model calculations have been made to obtain the values of the "mean" emissive power over the entire visible fire plume, when the fire is described by a circular enveloping cylinder of diameter equal to the base diameter of the fire and the fire plume length being predicted by the Thomas' equation (4-1). These "mean" emissive power values deduced from test data for various diameters of LNG fires was shown in Figure 2-1. The model indicated in this chapter is used to extrapolate to potentially larger LNG fires on land and on water. The results from such calculations are indicated in Table 4-1.

4.2.4 Uncertainty analysis

The results above indicate that the mean surface emissive power (MSEP) calculated by the model using the assumption of an idealized cylindrical geometry for the fire corresponds quite closely with the MSEP calculated using the wide angle radiometer data of the Montoir tests and the assumption of an idealized fire geometry. The current model results are dependant upon several physical parameters for which no data exist for methane burning in air. The model uses values for these parameters obtained with other fuels. These parameters include the soot extinction specific area (κ_m), and the height of the lower "clean burning" zone. In addition, the

model has another unknown, namely, the exponent (or index "n") in the vertical distribution of the core visibility probability (p). There exist no experimental data for this latter parameter.

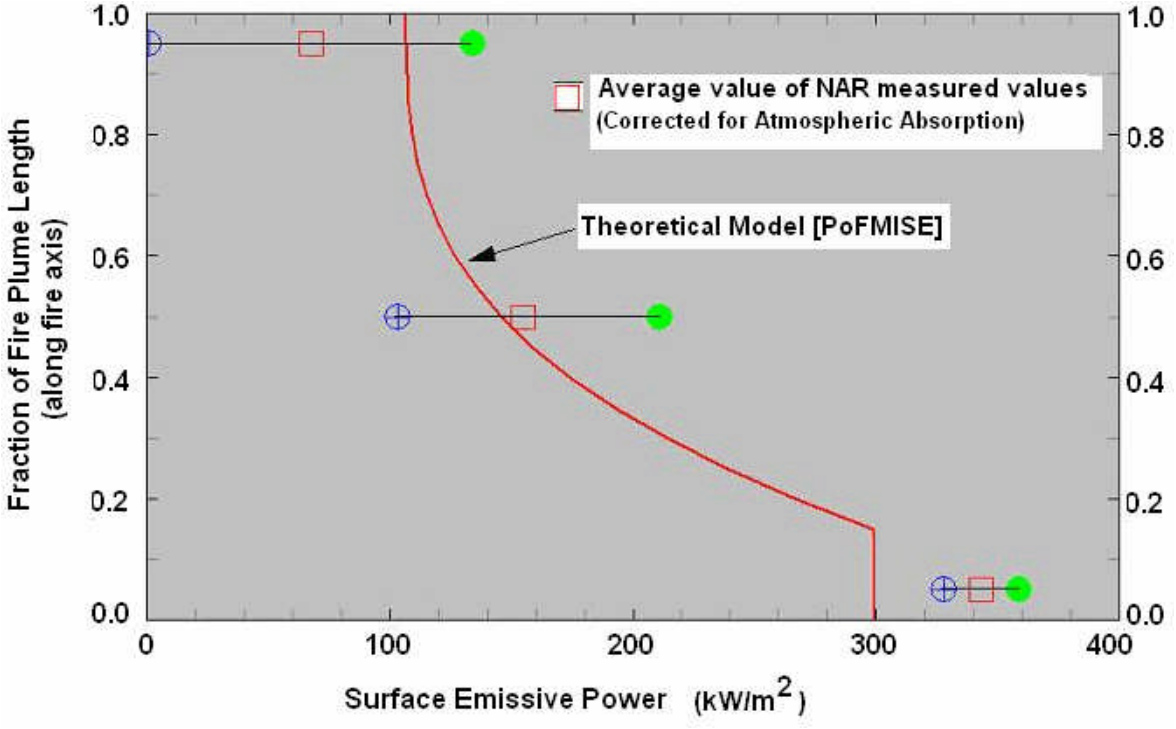

Figure 4-2: Mean emissive power variation with height above firebase - Comparison of the model result and 35 m Fire NAR data

An analysis was conducted to determine the uncertainty in the model-predicted MSEP value with variation in the magnitudes of the soot extinction area and the probability distribution exponent. No changes were made to the height of the lower burning zone since there are no documented values of the size of this zone for field size fires of different diameters and fuels.

Nedelka, et al (1989) indicate that the MSEP calculated from the Montoir tests is 175 ± 20 kW/m^2 with WAR data and the assumption of an idealized circular geometry for the fire (with visible plume length given by Thomas' correlation). Table 4-2 shows the model calculated MSEP for the 35m diameter land-based pool fire[15]. The value of the soot extinction area ($\square_m$) is not known for methane fires; however, it could be argued that it should be lower than that for propane (130 m^2/kg). This parameter is varied from 100 m^2/kg to 1000 m^2/kg (a value for crude oil fires). The exponent ("n") of the vertical distribution of the probability (or the fraction of the time that the hot core is visible) is varied from 1 to 4. The distribution shown in Figure 4-2 is with a value of n=3.

[15] This diameter (35 m) is chosen for uncertainty analysis since field test data exist for this size fire.

Table 4-1
Comparison of model predicted MSEP with experimental data

Fire Diameter (m)	Substrate on which LNG boils	Soot mass yield **(Y)*** **(%)**	Soot Concentration **(C_S)** **(kg/m^3)**	Fractional length of the "Clean burning zone" **(ψ)**	Soot Transmissivity **(τ_S)** **$= 10^{-2}$ x**	MSEP over the visible fire plume height **(E_{avg})**		Remarks
						PoFMISE model result **(kW/m^2)**	From field tests **(kW/m^2)**	
15	Water	12.7	3.328×10^{-4}	0.196	66.40	172	185-224	China Lake tests Raj, et al [1979]
20	Land	13.0	3.419×10^{-4}	0.180	57.12	183	140-180	Mizner & Eyre [1983]
35	Land	13.7	3.595×10^{-4}	0.150	35.70	177	175±30	Montoir tests GDF [1987]
100	Land	14.9	3.926×10^{-4}	0.093	4.00	113	-----	Potential size of future pool fire tests
300	Water	16.2	4.272×10^{-4}	0.033	0.00277	90	-----	Estimated pool size from one tank content spill from LNG ship

Assumed parameter values; **$r = 17.17$ for CH_4 ;** **$\beta = 0.06$;** **$k_m = 130\ m^2/kg$;** **$E_{max} = 325\ kW/m^2$;** **$T_a = 293$ K**

*** Notarianni correlation for smoke yield;** **Optical path scale length at bottom of LNG fire = 13.5 m**

Table 4-2
Variability in model predicted MSEP with uncertainty in the magnitude of model parameter values (for a 35 m diameter LNG fire on insulated concrete)

"n" ➔	1	1.5	2	2.5	3	4
Soot specific extinction area (κ_m) [m^2/kg] ⬇	**Model Predicted Mean Surface Emissive Power (kW/m^2)**					
100	229.6	215.7	206.4	199.7	**194.8**	**187.8**
130	217.4	201.0	**190.0**	**182.3**	**176.5**	**168.3**
200	198.1	**177.8**	**164.3**	**154.7**	147.5	137.4
500	**174.4**	**149.5**	132.8	120.9	112.0	99.5
1000	**172.0**	146.6	129.7	117.5	108.5	95.7

Notes: (1) Diameter of the diked land based pool fire considered = 35 m (Montoir test)
(2) Length of bottom bright zone as a fraction of fire length (ψ) = 0.15
(3) MSEP obtained with idealized flame shape = 165 kW/m^2 [Nedelka, et al (1989)]
(4) Experimental variation on MSEP = 10%, i.e., $157.5 \leq MSEP \leq 192.5$ kW/m^2

In Figure 4-3 are plotted the distribution of SEP with position along the fire plume axis. Also shown are the experimentally measured SEP data from (atmospheric corrected) NAR values. It is seen that the distribution for value of n=1 does not fit the experimental data at all.

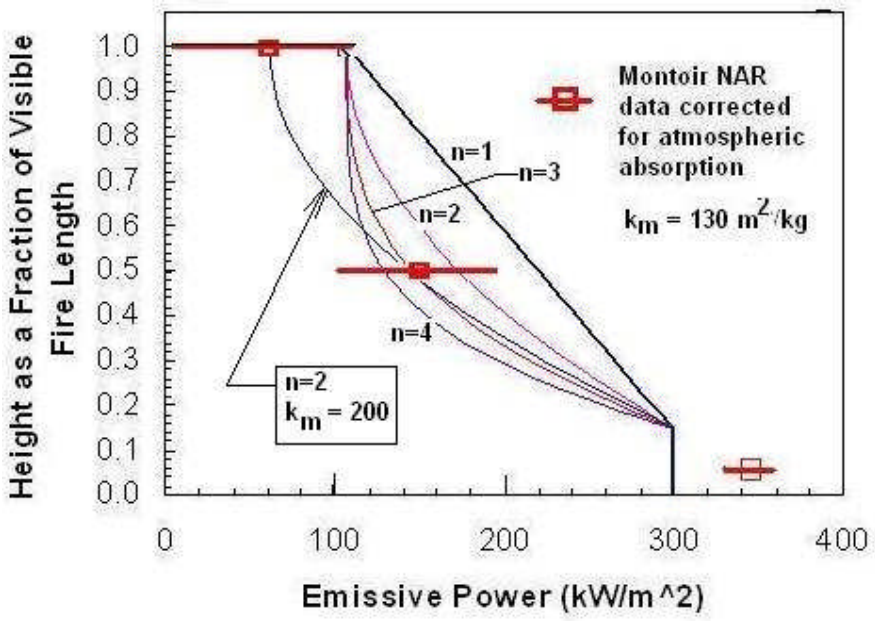

Figure 4-3: Mean emissive power variation with height above firebase - Comparison of the model result and 35 m Fire NAR data

The best fit for the case with κ_m = 130 m^2/kg is represented by n=3. However, it is noted that at the top of the fire the model predicts much higher SEP than has been observed in the test data. This is because of the assumption of a particular value for the soot extinction coefficient (k_m = 130 m^2/kg), which value was taken from propane data. A recalculation of the model with k_m = 200 m^2/kg and n=2 shows a better fit to the data for most of the fire plume. The fact that the model predicts lower than observed NAR value at the bottom can be attributed to the fact that the NAR was looking at only one position whereas the model result at the bottom of the fire is the mean of all SEP around the bottom of the fire.

The results indicated in Table 4-2 show that only a certain combination of n and κ_m result in the prediction of MSEP within the experimental range of values obtained in the Montoir test series (namely, 157.5≤MSEP≤192.5). These parameter combinations that are acceptable in comparison with test data are, n=2, κ_m = 130 to 200, n=3, κ_m = 100 to 130, and n=4, κ_m = 100 to 130. The reasonable fit is n= 2 or 3 and κ_m = 200 m^2/kg. It is again emphasized that we have only one set of data from any fire experiment on the variation of the NAR measured SEP value with height (or length along the plume axis) of a fire. Unless more data of this type are obtained from future tests, the distribution of "probability of visible fire" with height has to be guessed. Also, the fact that the good fit for measured data occurs only when the value of κ_m is about 200 m2/kg implies that may be in a large diffusion fire the size of soot particles formed are larger therefore presenting a higher cross sectional area for IR attenuation by smoke within the fire than that resulting from a propane diffusion fire of laboratory scale. This again needs to be determined from carefully controlled laboratory and field scale tests with methane and other fuels. However, use of n=3 and κ_m = 130 m^2/kg results in a conservative estimate of the overall emissive power.

4.2.5 Discussions

This paper has attempted to describe a semi-empirical model for predicting the thermal radiation output from large turbulent diffusion fires on flammable liquid pools. Observations from large tests with LNG (at 35 m diameter), field tests with other higher hydrocarbon fuels (JP-5 at 15 m diameter) and large oil spill fires on the ocean have indicated clearly that large fires, irrespective of the fuel involved, burn with the production of copious amount of smoke. The "density" of smoke generated seems to be a function of the fuel characteristics and the fire size. It is theorized that the production of smoke in large turbulent diffusion fires is the direct effect of reduced oxygen concentration in the inner (radial) regions of the fire. Unfortunately, there are no data from field experiments on the values of concentrations of oxygen, fuel vapor, combustion product gases, smoke density and their variation axially and radially. The lack of data is especially true for large LNG fires.

The motion picture records from the largest LNG fire tests that have been conducted to date (in Monotoir, France, 1987) clearly indicate that this fire burns with production of very large amount of soot. Also observed is that the dynamics and visual characteristics of this (LNG) fire are not much different from that of an oil fuel fire (see photographs comparing 35 m LNG fire and a pool fire of refined crude oil released from the rupture of a pipeline, Raj [2005]). One of the important observations from large fire behavior is that the burning is pulsed with rising

thermals of burning gas (in the form of large eddies). In addition the smoke at heights greater than a critical level envelops the entire inner burning region, thereby curtailing the radiant heat output from those sections of the fire to the outside. Also noticeable both in the film of 35 m LNG fire tests and in narrow-angle radiometer readings taken at three different heights is that the fraction of the time the "inner burning fire" is visible through the shrouding smoke layer decreases with increasing height. Unfortunately, there are no published data in the literature on the fraction of the time of the inner burning region is visible through the smoke layer (intermittent visibility) and the variation of this fraction with the fire height and other characteristics of the fire including its size (diameter), properties of the fuel, etc. The available experimental observations, albeit from a limited number of tests, are included in the model, with several simplifications.

The rate of smoke production, expressed as a constant mass fraction (Y) of the fuel burned, used in the model is based on a dimensional data correlation from one set of tests with crude oil fires of varying diameter up to a maximum of 17.2 m (Notarianni, et al [1993]). No such data (i.e., fraction of the mass of fuel converted into unburnt smoke or carbon particles) are available for methane, propane or any other fuel fires and certainly not for large liquid pool fires in the open. Not available also are the black smoke extinction coefficients for the smoke generated from a methane fire. It is, however, assumed that the IR spectral average extinction coefficient value depends on the characteristics of the fire. In view of the above gaps in knowledge, the model uses the best available value for each of the physical parameters such as the smoke yield mass fraction (Y, as a function of the diameter), the extinction coefficient for absorption of thermal radiation by smoke particles (k_m), and the excess air entrained in large fires (β). It is noteworthy that the correlation for the smoke yield does not explicitly indicate its dependence on the burning rate. It is argued that the values used for the different parameters (even though they were obtained from tests involving fires of other-than-methane hydrocarbon fuels) are conservative. This is because, even though the smoke production rate used in the model is obtained from crude oil fire (which is, in general, more smoky than an LNG fire, when the diameter of the fire is small < 20 m), the LNG-fire-measured radiant heat flux data can be reconciled only if a high rate of production of smoke is assumed in LNG fires.

The second important parameter that has influence on the radiative emissive power at different locations is the "soot extinction area," (see equation 4.7). The value of extinction area used was taken from premixed propane jet fire data. It is anticipated that the size of soot particles (which contribute to radiant heat scattering and absorption) will be smaller than in a premixed propane fire, thereby presenting a smaller extinction area. Therefore, the use of propane extinction area factor is conservative (in that in a LNG diffusion fire the particles will be bigger and scatter/reflect IR radiation more; but we are accounting in the model a less absorption). It should be noted that the only parameter in the model that is adjusted (to conform to the vertical radiant emissive power data from the 35 m diameter tests) is the vertical distribution trend of the probability of finding an "open" flame among the smoky layers. The observation that the physical and radiative behavior of large LNG fires could be "predicted" by the use of one parameter obtained from the data indicates the model's robustness in including the essential physics of LNG fires. The observation from the field experiments, the concurrence between the model and the measured data from the tests even with the use of crude oil smoke production

correlation, leads to the conclusion that the dominant effect in large diffusion fires is the anoxia suffered by the fire rather than the carbon to hydrogen ratio in the fuel.

The diameter dependence of the fraction of fuel converted to smoke (see equation 4.9) reveals that the diameter can be used as a proxy for air mixing inefficiencies and starvation in the central parts of the fire of oxygen for combustion. It can be argued that for a given diameter, if the rate of vapor flow into the fire is increased, a higher percent of the fuel should be converted to smoke. This is due to the reduced oxygen concentration and corresponding increased concentration of fuel. Thus a higher vapor evolution rate should lead to further inefficient combustion and, hence, the production of a greater fraction of the fuel mass into unburnt carbon (smoke). This argument, if true, will lead to a more smoky LNG fire on water compared to a fire on land of the same diameter. Such a fire behavior leads to the conclusion that hazard distance from LNG fires on water will be less than that from a land fire of the same diameter. Therefore, it will be necessary to evaluate, by experiments, the dependence of the values of "constants" in equation 4.9 on burning rate and fuel type (and ensure that for large diameters that fuel type does not have a significant effect).

The parameter β represents the combustion efficiency at any layer of burning; that is, efficiency (or probability) with which the air entrained at the particular layer burns with its stoichiometric equivalent mass of fuel vapor. (The expression $1/\beta-1$ represents the mass of excess air required for the complete combustion of the fuel vapor emanating from the pool; for more details of this see Raj [1981]).

The results presented in Figure 2-2 are the 'as measured' narrow-angle radiometer (NAR) readings taken at the bottom, mid height and the top of a 35 m diameter LNG pool fire on insulated concreted dike in test # 2 of the Montoir series. The x-axis represents the uncorrected (for atmospheric absorption) emissive power of the fire measured by the NAR. The y-axis indicates the fraction of the time during the measurement in which the particular value of the emissive power was recorded. The data presented represent, for each location on the fire, a recording duration of 5.8 s during which a total of 145 measurements were made. Two important features are noticeable from the data presented. First, the mean value of the emissive power varies drastically from the bottom of the fire to the top (by a factor of about 5). Second, the statistical distribution of the measurements shows very narrow dispersion (low ratio of standard deviation to mean) at the bottom of the fire and high dispersion at the top of the fire. This can be interpreted as due to the fact that at the bottom of the fire radiant heat is being emitted un-obscured by smoke layers. That is, the bottom layers burn "clean." However, as one goes up in height, the dispersion in NAR readings is higher with considerable scatter in the measured emissive power, although the mean value is reduced significantly. That is, the higher one goes up along the fire axis, the larger is the shrouding effect by the smoke of the inner burning regions and the greater is the variation in the smoke layer aperture that "opens" and "closes." One can attribute this to a higher level of the intensity of turbulence in higher layers.

The experimental NAR data shown in Figure 4-2 are the same as in Figure 2-2 except that the in the former plot the data in Figure 2-2 have been corrected for the IR radiation absorption by the atmosphere at the conditions prevailing during the test (54 % relative humidity and 21 ^{o}C, with the NAR being located 155 m from the edge of the dike). Only the corrected

mean and standard deviation values as a function of the height are plotted. Also plotted in Figure 4-2 is the variation of the emissive power with height predicted by the model.

The model results are based on the assumption that the black body emissive power of the "clean burning" region (at the base of the fire) is 325 kW/m^2 (equivalent blackbody temperature of 1547 K). The actual emissive power at the base of the fire is calculated to be 299 kW/m^2. This value is in keeping with the mean value from other NAR data focusing on the bottom of the fire. The model further assumes that the height of the lower clean burning zone is given by equation 4.12b in which the properties of methane and 35 m diameter values are used. The correlation results in a height of the bottom, "clean and bright burning" region to be 11.3 m. No data have been published on the actual variation of the NAR readings close to the bottom of the fire; however, based on known information (GDF [2005]) it appears that the bottom "bright region" is about 10 m in test #2, which was conducted under 7 to 10 m/s wind speed conditions. The correlation indicated in equation 4.5 was some what modified from that in the literature (equation 4.4) to coincide with the Montoir LNG test #2. It should be noted however, that this correlation predicts reasonably well the lower bright region of a 15 m diameter LNG fire (on water tested in China Lake) – this region is predicted as 25% of visible plume height (of 50 m).

The values of other parameters used in the model (β, k_m, r) are indicated in Table 4-1. The results of the model agree reasonably well with the experimental NAR data. It should be noted that the NAR data provides information on only a specific spot (of about 1.5 m diameter) on the nominal surface of the fire, whereas the model predicted value should be considered as a mean value over all radiating fire surfaces at a given height. There are uncertainties in specifying which exact part of the fire the NARs were pointing to. Also, there is uncertainty as to the exact height at which the NARs were looking and because of slight wind the line of sight to the spot "seen" by the NAR may not have intersected the fire axis; thus the NAR readings may, in fact, represent a slightly off center value of the emissive power (with the effect of the cosine of the angle of the spot area with respect to the line of sight being important). The model predicts slightly lower values for the emissive power at the base compared to measured values. Again it is emphasized that the model provides a "mean" value for the emissive power over a horizontal section at any height where as the NARs 'look' at a single spot. The model predicts higher values with height than is indicated by the data, in spite of the fact that the crude oil values for smoke yield and propane values for the smoke extinction coefficient were used (One expects that using crude oil smoke yield correlation one would get a lower emissive power at the top parts of the fire). It is not certain why this slight discrepancy between the model and the LNG fire NAR data occurs. It may be due to the recipe assumed for the distribution of the probability of "inner core view" assumed in equation 4.10; may be a faster rate of decrease of this probability with height is appropriate. However, any such assumption at this time will only be a theoretical exercise without any other data to compare with.. There is, therefore an important need to obtain such intermittency data from large, outdoor fires.

The distribution along the fire axis of the average value (over the visible plume length) of the calculated emissive power has been obtained for four different size fires, both on land and on water. These include hypothetical LNG fires of a 100m diameter on land and a 300 m diameter fire on water. It is seen from the results in Table 4-1 that the model-predicted mean emissive power for the 15 m fire is slightly lower than measured values, whereas for the 35 m diameter

fire it is within the range of measured values. Considering the uncertainties in the values of parameters used in the model and their applicability to a methane (or LNG) fire, the small differences in the predicted and measured values are within the acceptable range. Table 4-1 results illustrate that as the fire diameter increases, the mean emissive power over the entire visible fire plume length becomes smaller and smaller. As can be seen, the mean emissive power for a 300 m fire is only about 60% of that of a 15 m diameter fire!

The result of this model clearly indicates that as the fire size increases the mean emissive power decreases. Also, as the fire diameter increases, the fire plume length to diameter ratio decreases. Therefore, the hazard distance, as a fraction of the fire diameter, for any specified hazard heat flux decreases as the diameter increases. The current models specified in US Government regulations and those in NFPA standard 59A for LNG do not consider the issue of reduction in the total energy out put (as a fraction of the fire size) due to smoke effects. The result of using the current regulatory model for LNG or other large fire hazard evaluation is the prediction of significantly larger distances for people hazards compared what they may be due a real large LNG fire. Secondly, as seen from the above model and the results of large scale tests with LNG the bottom part of the fire radiates at a much higher level than the parts at the top. This phenomenon is extremely important to note in the calculation of hazard distances from dike fires in LNG or other fuel storage facilities (surrounded by a high enough dike wall). The presence of a dike wall of even relatively small height (say, 10 m) cuts a very significant level of radiation from the fire to the surrounding. The hazard distance calculated using the emission from the parts of the fire visible above the dike wall is likely to be a factor of 1.5 to 2 less than that obtained from currently used models.

4.2.6 Summary of findings

The model development effort indicated in this report was initiated after a review of the current fire radiant heat flux prediction models indicated that they did not take into account several effects that are seen in large LNG fire experiments. Specifically, these phenomena observed in large fires, including in LNG fires, are the production of large quantity of black, thermal radiation absorbing smoke, which reduces the effective fire emission intensity and the fact that the magnitude of effective emission intensity varies from bottom to top of the fire. The model indicated in this report utilizes some of the data from the 35 m diameter ("Montoir") LNG fire tests on land. However, the data from the Montoir tests alone are insufficient to describe, in a mathematical model, the characteristics of the fire, For example, not only is the fraction of fuel converted into black smoke is needed for calculating the effective screening by smoke but also needed is the variation of this fraction with fuel burning rate and fuel characteristics. Such data are not available in the literature for most fuels including LNG.

The model presented in this report utilizes smoke production rate and smoke optical property data, respectively, from crude oil and propane test. It is remarkable that even with these data the fire emission characteristics for different size LNG fires are predicted by the model. While the model has been some what calibrated using the radiant emission data from the Montoir tests and is capable of providing the variation of emissive power along the fire axis, no such data exits for other LNG or other hydrocarbon fires. Therefore, the model predictions are compared with the only other available LNG fire data, namely, the fire mean emissive power. The comparisons with other fire data indicates that the model predicts, within 10% error, not only the

observed mean surface emissive power (measured in smaller than 35 m diameter LNG fire tests) but also the size or axial extent of the lower part of the fire over which the emissive power is considered to be constant. Since the model captures the essential physical characteristics of observed large LNG (and other hydrocarbon fires), and predicts the measured radiation, fire height and the bottom “high emissive power” region extent of smaller fires, it is considered to be superior to currently used fire radiant heat prediction models such as LNGFIRE3.

The model presented has, however, a number of following limitations.

1 First, it is a semi-empirical model based the consideration of the overall fire dynamics and radiation from a fire using an “integral” type of approach. Therefore, the accurate description of the internal variations of important fire properties, such as turbulence, distribution of temperature, velocity and combustion rates, are sacrificed. These are, of course, the kinds of parameters considered in detail in computational fluid dynamics based models. The currently proposed model (PoFMISE) does not “predict” the fire core temperature but assumes its value based on the measured spectral data of the largest fire to date. This assumption may not be a serious limitation of the model, considering that the spectral data from both smaller and larger fires agree on fire temperature.

2 Second, the model assumes the characteristics of large fires and uses fire diameter dependent correlations for smoke production rate and optical properties of smoke. There exist no data for methane (or LNG) even in small scale fires let alone large fires. Until some laboratory data are obtained for these parameters under controlled conditions which can then be confirmed by actual measurements in field scale experiments, the applicability of smoke production correlations to LNG fires and to larger than 35 m fires is unproved.

3 The model assumes a similarity profile for the distribution, with scaled axial non dimensional distance, of the probability or the fraction of the time that the inner hot burning layer would be visible. This similarity profile is independent of the fire size and varies as the cube of the non dimensional distance. Neither the hypothesis that this scaled distribution is independent of the fire size or that it follows a cubic law has been confirmed with any data but is based on engineering judgment. Data from large fire experiments conducted with specific instruments to measure this parameter only can confirm or refute the assumption made in the PoMISE model.

The correctness of the model predictions for larger than 35 m diameter LNG diffusion fires can be confirmed only with additional large scale tests (that the model predicts the published data for smaller scale fires has already been discussed). The data to be obtained from such large scale tests should include all of the measurements made in the 35 m Montoir fire test series as well as (i) smoke production rate data, (ii) variation of the height of the bottom “constant emissive power” region, (iii) the distribution of the spot emissive power with distance along the fire axis, (iv) Spectral emission characteristics from different parts of the fire plume, etc.

The PoFMISE model can be used in much the same way and with the same ease as has been the case with LNGFIRE3. It can be easily executed with the computer model available as an adjunct to this report.

4.2.7 Conclusions

The following conclusions are drawn from the model reported in this chapter.

1 A semi empirical model to predict the thermal radiation output from large hydrocarbon liquid fuel pool fires has been developed, which takes into consideration the formation of smoke, its effect (by shrouding the inner burning region) in reducing the thermal output into the surroundings.

2 The model assumes a constant emissive power zone at the bottom of the fire. The height of this zone varies with the properties of the fuel, the size of the fire and the evaporation rate. The variation of the emissive power with height above this zone has been modeled by assuming a probability distribution for the fraction of the time the inner core of burning fire is visible through the smoke shroud.

3 The results of the model have been compared with the only available (narrow angle radiometer) data for the measured variation of the emissive power with height. The model results track this variation reasonably well, given the uncertainties in the model assumptions and in the data.

4 The model also predicts the measured mean emissive power from 15 m and 35 m LNG fire tests within the accuracy that can be ascribed to the model.

5 The model is more realistic in its treatment of the actual dynamics and phenomena observed in all large hydrocarbon fuel fires, including the very important one relating to smoke production and obscuration of the burning regions of the fire. In this regard it is, perhaps, superior to any of the existing single-mean-emissive-power models.

The use of the model developed has significant implications for the calculation of realistic hazard distances as opposed to the significantly large hazard distance predictions of the currently used LNG fire models.

4.3 Risk analysis protocol

The use of fire hazard evaluation models in a risk analysis to determine the risk pose by different size fires with different probabilities of occurrence is discussed in Appendix C. The protocol for developing the risk estimates is described. This involves first categorizing the scenarios of events that can lead to a LNG fire in a facility, determining the types of fires that may occur, the sequence of different types of fires occurring if such a possibility exists, the magnitude and duration of each fire event and the determination of the area of hazard using the above described models. Also shown in Appendix C is the approach to classifying and recording the various probabilities of fire events, including the primary event probability and the subsequent sub-event occurrence probabilities. An example is provided (without numerical values) illustrating the procedure by which the burn-injury risk to a population can be calculated for the occurrence of pool fires of various sizes.

Chapter 5
Recommendations

Based on the assessments performed in this project and the large fire model developed, the following recommendations are put forth.

1 Laboratory studies should be performed to obtain certain key parameter values for LNG vapor burning in air. These include the fraction of the fuel mass that gets converted to smoke particles as a function of combustion temperature and fuel-air (or oxygen) concentration ratio. Similarly, laboratory studies should be performed to obtain the optical properties of smoke produced in diffusion fires of methane in air.

2 Additional field tests with LNG fires of sizes larger than 35 m diameter should be conducted to determine the large diameter effects and to verify whether large fires have reduced heat emission compared to smaller size (< 35 m) LNG fires. Dike fires on land and unconfined spill fires on water should be conducted.

3 The PoFMISE model developed in this project should be included in any revisions to the 49 CFR, part 193 regulations, since the model represents the best data available for large LNG fires and includes many of the phenomena seen in large fires. Current model recommended for use in the regulations does not include these important phenomena.

4 Effects of passive and active mitigation techniques (such as dike walls, sub surface sumps, water curtains, water application directly to the fire plume to reduce temperature and affect combustion processes) in reducing fire thermal hazard effects should be evaluated both theoretically and experimentally. This effort should be initiated with a detailed review of the available techniques, their effects and their incorporation into a fire radiant heat flux model.

5 An integrated fire hazard model should be developed which includes the characteristics of large LNG fires (and radiant heat from such fires with due consideration to the variation of emissive power with height), the spectral characteristics of emission from various parts of the fire, the absorption in the atmosphere of the intensity of fire emission in different wavelengths, the characteristics of the intervening objects between the fire and the heat receiving object, the thermal characteristics of the receiver and the proper consideration of the hazard to the object based on its susceptibility to heat input and duration of exposure.

6 A data base of probabilities of different types of releases of LNG from both fixed plant equipment and from shipping and transportation incident should be developed.

7 A realistic risk assessment procedure that considers the probabilities of occurrence of different types and sizes of LNG fires, many of the phenomena, parameters and models identified in this report and other considerations (such as the effects of mitigation technology) should be developed. The application to a generic plant or transportation condition should be demonstrated with an example calculation.

8 A set of criteria should be developed for the acceptability of risk results in evaluating the safety of a LNG plant or LNG transportation, relative to public safety.

References

- AGA, "LNG Safety Program, Interim Report on Phase II Work," IS-3-1, American Gas Association, Arlington, VA, 1974.
- Atallah, S. and J.N. Shah, "LNGFIRE3 – A Thermal Radiation Model for LNG Fire," Report # GRI-89/0176, Gas Research Institute, Chicago, IL, June 1990.
- Brown, T. C., R. T. Cederwall, S. T. Chan, D. L. Ermak, R. P. Koopman, K. C. Lamson, J. W. McClure, and L. K. Morris, "Falcon Series Data Report: 1987 LNG Vapor Barrier Verification Field Trials," GRI-89/0138, June 1990.
- Burgess, D., and M.G. Zabetakis, "Fire and Explosion Hazards of LNG," US Bureau of Mines Investigation Report # 6099, 1962.
- China Lake Tests, 1976; See Raj, et al., [1979].
- Clay, G.A., Fitzpatrik, R.R.D., Hurst, N.W., Carter, D.A. and Crossthwaite, P.J., "Risk assessment for installation where liquefied petroleum gas (LPG) is stored in bulk vessels above ground," J. Haz. Materials, 20, 357, (1988).
- Considine, M., "Thermal Radiation Hazard Ranges from Large Hydrocarbon Pool Fires," Report # SRD R297, Safety & Reliability Directorate, UK Atomic Energy Authority, Wigshaw Lane, Culcheth, Warrington, WA3 4NE, UK, Oct 1984.
- Cox, G. and R. Chitty, "Some Source-Dependent Effects of Unbounded Fires," Combustion & Flame, v 60, p 219-232, 1985.
- Croce, P.A., K.S. Mudan and J. Moorhouse, "Thermal Radiation from LNG Trench Fires – Volume I," Report # GRI 84/0151.1, Gas Research Institute, Chicago, IL, September 1984.
- Daish, N.C., Linden, P.F., Vieillard, V., Nedelka, D., Roberts, T.A. & Butler, C.J., "A new unified investigation into vapour cloud fires," Proc. LNG13, 13th International Conf. and Exhibition on Liquefied Natural Gas, Seoul, Korea, 2001
- EN 1473, " Installation and equipment for liquefied natural gas – Design of onshore installations," prEN 1473:2005 (E), CEN/TC 282, STD Version 2.1c2 meeting of 1st September 2005, AFNOR Secretariat, Brussels, Belgium, 2005.
- Fowler, W.L., An Investigation of Soot formation in Axisymmetric Turbulent Diffusion Flames at Elevated Pressure, Twenty-Second Symp. (Int'l) on Combustion, The Combustion Institute, p 425-435, 1988.
- GDF (Gaz de France), Narrow angle radiometer data from the Montoir 35 m diameter LNG Fire Test # 2, personal communication to P.K. Raj, November 2005
- HSE (2006), "Safety Report Assessment Guide: LPG – Criteria," **http://www.major-hazards.gov.uk/comah/sraglpg/index.htm,** Published as a part of the guidance documents to comply with the requirements of the COMAH (Control of Major Accident Hazards) Regulations of 1999**,** May 2006.

- JGA, “A Study of Dispersion of Evaporated Gas and Ignition of LNG Pool Resulting from Continuous Spillage of LNG,” Journal of Japan Gas Assoc., July 1976.
- Heskestad. G., “Luminous Heights of Turbulent Diffusion Flames,” Fire Safety Journal, v 5, p 103-108, 1983.
- Hightower, M, L. Gritzo, A. Luketa-Hanlin, J. Covan, S.Tieszen, G. Wellman, M. Irwin, M. Kaneshige, B. Melof, C.Morrow, and D. Ragland, “Guidance on Risk Analysis and Safety Implications of a Large Liquefied Natural Gas (LNG) Spill Over Water,” Sandia National Laboratory Rep.# SAND2004-6258, U.S. Department of Energy, Washington, DC, Dec 2004.
- Hottel, H.C., and A.F. Sarofim, “Radiative Transfer,” McGraw-Hill Book Company, New York, 1967.
- Hura, H.S. and I. Glassman, Soot Formation in Diffusion Flames of Fuel/Oxygen Mixtures, Twenty-Second Symp. (Int’l) on Combustion, The Combustion Institute, p 371-388, 1988.
- Kataoka, H., “Report on LNG Anti-disaster Experimental Test,” Report by Tokyo Gas Co., Ltd. Japan, 1981.
- Lees, F.P., “Loss Prevention in the Process Industries, Hazard Identification, Assessment and Control,” v 2, Second Edition, Butterworth-Hinemann, Oxford, England, 1996.
- LNGFIRE3, “A Thermal Radiation Model for LNG Fires,” Version 3 Computer file available from the Gas Technology Institute, Des Plains, IL, March 2004.
- Luketa-Hanlin, A., “A review of large-scale LNG spills: Experiments and modeling,” Journal of Hazardous Materials A132 (2006) 119–140, 2006.
- Malvos, H., and P.K. Raj, “Details of 35 m Diameter LNG Fire Tests Conducted in Montoir, France in 1987, and Analysis of Fire Spectral and other Data,” paper presented in session LNG VI - Risk & Safety, AIChE Winter Conference, Orlando, FL, April- 2006.
- Markstein, G.H., Correlations for Smoke Points and Radiant Emission of Laminar Hydrocarbon Diffusion Flames, Twenty-Second Symp. (Int’l) on Combustion, The Combustion Institute, p 363-370, 1988.
- May, H.G., and W. McQueen, “Radiation from Large Liquefied Natural Fires,” Comb. Sci. Tech., V 7, p 51-66, 1973.
- McCaffrey, B.J. and M. Harkleroad, Combustion Efficiency, radiation, CO and Soot Yield from a variety of Gaseous, Liquid and Solid Fueled Buoyant Diffusion Flames, Twenty-Second Symp. (Int’l) on Combustion, The Combustion Institute, p 1251-1261, 1988.
- McGrattan, K.B, H.R. Baum and A. Hamins, “Thermal Radiation from Large Pool Fires,” NISTIR 6546, National Institute of Standards & Technology, U.S. Department of Commerce, Washington, DC, Nov 2000.
- Mizner, G.A., and J.A. Eyre, “Large Scale LNG and LPG Pool Fires,” Inst. Chem. Eng. Symp., Ser 71, Manchester, April 1982.

- Mizner, G.A., and J.A. Eyre, “Radiation from Liquefied Gas Fires on Water,” Combustion Science and Technology, v35, pp. 33-57, 1983.
- Montoir tests, 1987. See Nedelka, et al [1989] and or Malvos & Raj [2006].
- Moorhouse, D.J., “Scaling Criteria Derived from Large Scale Experiments – The Assessment of Major Hazards,” Inst. Chem. Eng., Manchester, 1982.
- Moorhouse, D.J., and M.J. Pritchard, “Thermal Radiation Hazards from Large Pool Fires and Fireballs – A Literature Review,” Inst. Chem. Eng. Symp. Ser No. 71, p 397-428, 1982.
- Murgai, M.P., “Natural Convection from Combustion Sources,” Oxford & IBH Publishing, New Delhi, 1976.
- Narasimhan, K.S. and P.J. Foster, The rate of Growth of Soot in Turbulent Flow with Combustion Products and Methane, Tenth Symp. (Int’l) on Combustion, The Combustion Institute, p 253-257, 1965.
- Nedelka, D.J., J. Moorhouse and R.F. Tucker, “The Montoir 35 m Diameter LNG Pool Fire Experiments,” TRCP.3148R, 9th Intl. Conf & Expo on LNG, “LNG9,” Nice, France, 1989.
- NFPA, 59A, “Standard for the Production, Storage, and Handling of Liquefied Natural Gas (LNG),” 2006 Edition, National Fire Protection Association, 1 Batterymarch Park, Quincy, MA 02169, 2006.
- Notarianni, K.A., D.D. Evans, W.D. Walton, D. Madrzykowski and J.R. Lawson, “Smoke Production from Large Oil Pool Fires,” Interflam ’93, Fire Safety, Int’l Fire Conference, 6th, Oxford, England; Interscience Communications Ltd., London, England (Ed: Franks, C.A.), p 111-119, March 1993.
- Raj, P.K. and S. Atallah, “Thermal Radiation from LNG Fires,” Advances in Cryogenic Engineering, v 20, p 143, 1974.
- Raj, P.K. and H.W. Emmons, “On the Burning of a Large Flammable Vapor Cloud,” paper presented at the meeting of the Western & Central States Section of the Combustion Institute, San Antonio, TX, April 1975.
- Raj, P.K. “Calculations of Thermal Radiation Hazards from LNG Fires - A Review of the State-of-the-Art," Paper presented at the AGA Transmission Conference, ST. Louis, Missouri, Paper number 2, Session 18, May 18, 1977.
- Raj, P.K., N.A. Moussa, and K.S. Aravamudan, “Experiments Involving Pool and Vapor Fires from Spills of LNG on Water,” NTIS # AD-A077073, USCG Report, Washington, DC 20590, 1979.
- Raj, P.K., Analysis of JP-4 Fire Test Data and Development of a Simple Fire Model, ASME Paper 81-HT-17, 20th Joint ASME-AICHE National Heat Transfer Conference, Milwaukee, August 1981.

- Raj, P.K., (Editor) "Volume III – Combustion and Radiation," Proceedings of MIT-GRI LNG Safety Workshop (March 22-24, 1982) held at MIT, Cambridge, MA 02139. Published by the Gas Research Institute, Chicago, July 1982.
- Raj, P.K., "Large LNG Fire Thermal Radiation – Modeling Issues and Hazard Criteria Revisited," (AIChE) Process Safety Progress, v 24, n3, Sept 2005.
- Raj, P.K.,"LNG Fire Spectral Data and Calculation of Emissive Power," Paper presented at the International Symposium on Process Safety, October 25 & 26, 2005, Texas A& M University, College Station, TX. (Paper accepted for publication in the Journal of Hazardous Materials, June 2006a)
- Raj, P.K., "LNG Fires - A Review of Experimental Results, Models and Hazard Prediction Challenges," paper accepted for publication in the Journal of Hazardous Materials, October 2006b.
- Rodean, H.C., Hogan, W.J., Urtiew, P.A., Goldwire, H.C., Jr., McRae, T.G. & Morgan, D.L., Jr**.,** **"**Vapor burn analysis for the Coyote series LNG spill experiments," Lawrence Livermore National Laboratory, Rep # UCRL-53530, 1984.
- Sandia; See Hightower, et al, 2004.
- SFPE, *The SFPE Handbook of Fire Protection Engineering (Second Edition)*, ISBN 0-87765-354-2 (NFPA No. HFPE-95), 1995.
- Thomas, P.H., "The Size of Flames from Natural Fires," 9th Symp (int'l) Combustion, Academic Press, New York, p 844-859, 1963.
- Thomas, P.H., "Fire spread in wooden cribs: Part III, The effect of wind," Fire Research Note Nr. 600, Fire Research Station, Boreham Woods, England, June 1965.
- TNO-1, Van den Bosch, et al., "Damage caused by heat radiation," published in the report "Methods for the determination of possible damage – Green Book," CPR 16E, Report developed by TNO Environment, Energy and Process Innovation, Ltd., for the Committee for the Prevention of Disasters caused by Dangerous Substances, Director-General of Labour, The Netherlands, First Edition, 1992.
- TNO-2, Englehard, W.F.J.M, "Heat flux from fires," published in the report "Methods for the calculation of physical effects – Yellow Book," CPR 14E, Report developed by TNO Environment, Energy and Process Innovation, Ltd., for the Committee for the Prevention of Disasters caused by Dangerous Substances, Director-General of Labour, The Netherlands, Third Edition, 1997.
- Welker, J.R., and C.M. Sliepcevich, "Bending of wind-blown flames from liquid pool fires," Fire Technology, v 2, p127, 1966.
- 49 CFR, Part 193, "Liquefied natural gas facilities: Federal safety standards," Code of Federal Regulations, 1 October 2005. **http://www.access.gpo.gov/nara/cfr/waisidx_05/49cfr193_05.html.**

List of Symbols

C_a	=	Specific heat of air	(J/kg K)
C_S	=	Concentration of smoke particles in the fire	(kg/m^3)
D	=	Diameter of the base of the fire (or liquid pool diameter)	(m)
D_{Opt}	=	Optical path length consistent with the type of fuel burning	(m)
$\mathcal{D}$	=	Damkohler number = $\Delta H_c/(C_a T_a)$	
E(Z)	=	Emissive power of the fire nominal surface at axial position Z	(Wm^2)
E_b	=	Emissive power of the fire nominal surface near the base	(W/m^2)
E_{max}	=	Blackbody emissive power at the base flame temperature	(W/m^2)
E_S	=	Emissive power of the fire nominal surface covered by smoke	(W/m^2)
$\bar{E}$	=	Average emissive power over the entire length of the visible fire	(W/m^2)
$E_{\lambda,i}$	=	Wavelength dependent spectral radiance from the i^{th} elemental fire surface	($W/\mu m\ m^2$)
F	=	View factor between fire and object	
Fr	=	Froude Number = $\left(\frac{\dot{m}''_f}{\rho_a\sqrt{gD}}\right)$; Also called Combustion Froude number	
g	=	Acceleration due to gravity	(m/s^2)
H_C	=	Cloud depth	(m)
ΔH_c	=	Lower heat of combustion of the fuel	(J/kg)
k	=	Extinction coefficient	(m^{-1})
k_m	=	Specific soot extinction area	(m^2/kg)
L_C	=	Length (height) of the bottom "clean burning zone	(m)
L_F	=	Mean length (height) of the visible fire plume	(m)
L_I	=	Length (height) of the intermittency zone	(m)
L_{Opt}	=	Optical length	(m)
$\dot{m}$	=	Mass flow rate of fuel at the jet exit or over the pool	(kg/s)
$\dot{m}''_f$	=	Mass flux of fuel vapor at the base of fire	($kg/s\ m^2$)
M_f	=	Mass of fuel burned	(kg)
p	=	probability at height Z of finding, at any time, on the surface of the nominal cylinder the emission from the inner core flame on obscured by smoke	
$p_w^{sat}(T_a)$	=	Saturated water vapor pressure	(N/m^2)
$\dot{q}''$	=	Radiant heat flux impinging an object	(W/m^2)
r	=	Air to fuel mass ratio for stoichiometric combustion	
R	=	Radius of flame	(m)
Re	=	Reynolds number of flow over the fire = $\frac{U_{wind}\ D}{\nu_{air}}$	
R_{eq}	=	Radius of a circle of area equal to the pool or the impoundment	(m)
RH	=	Atmospheric relative humidity	(%)
S	=	distance to an object from either the fire center or from fire surface	(m)
S	=	Also used to represent the turbulent flame velocity with respect to	(m/s)

		unburnt gases	
T_a	=	Air temperature	(K)
T_F	=	Radiative temperature of the fire	(K)
U_{wind}	=	Wind speed	(m/s)
U*	=	Dimensionless wind speed	
V_f	=	Volume of "pure" vapor at STP conditions before combustion	(m^3)
V_p	=	Volume of products of combustion at the local gas temperature	(m^3)
W_∞	=	Steady state (or asymptotic) width of the vapor fire burning zone	(m)
x	=	Distance along the axis of a jet fire	(m)
$\dot{y}$	=	Liquid regression or linear evaporation rate (steady state)	(m/s)
z	=	Vertical distance or distance along the axis of a tilted pool fire	(m)
β	=	Mass fraction of air that is entrained up to any height Z that burns stoichiometrically with fuel	
δ	=	Equivalent pure vapor thickness in a vapor cloud before ignition	(m)
θ	=	Angle of tilt of the fire axis with respect to the vertical	(rad)
λ	=	Wavelength	(μm)
χ_R	=	Fraction of the combustion energy that is converted to radiant emission	
ρ_a	=	Density of air	(kg/m^3)
ρ_l	=	Density of evaporating liquid	(kg/m^3)
ρ_v	=	Density of vapor just above the liquid surface before combustion	(kg/m^3)
ν_{air}	=	Kinematic viscosity of air	(m^2/s)
ψ	=	Ratio of "clean burn zone" axial length to mean fire plume length = L_C/L_F	
σ	=	Stefan-Boltzmann constant = 56.697×10^{-12}	(kW/m^2K^4)
τ	=	Atmospheric transmissivity for radiant heat	
τ_s	=	Transmissivity of smoke	
ω	=	Inverse volumetric expansion ratio of combustion gases relative to unburnt gases	

Appendix A

Assessment of the Point Source Thermal Radiation Hazard Model

A.1 Background

The requirements for calculating the exclusion distance from potential LNG fires in an impoundment are indicated in § 5.2.5.3 in NFPA 59A (2006) edition. While the pamphlet identifies three methods any one of which can be used to determine the safety distance (at the discretion of the user), not all of the models give the same hazard distance for identical fire conditions.

One of the models indicated in NFPA 59A pamphlet is the point source model for calculating the hazard distance from LNG fires in an impoundment. In this Appendix the point source model hazard distance results for people exposure and wood ignition are compared with the results from traditional "Solid Fire" models. The solid fire models are been based on experimental data and represent the fire more realistically than in the point source model.

In this Appendix, first, the point source model as indicated in NFPA 59A is presented. It is then compared to the DOT authorized LNGFIRE 3 model in equivalent terms. Results are also obtained using the model discussed in Chapter 4 ("PoFMISE" model). Conclusions are provided based on the comparison of the results.

A.2 Point source and solid fire models

A.2.1 NFPA model:

The NFPA model for exclusion distance to people exposure criterion (1600 Btu/hr ft^2 or 5 kW/m^2) indicated in § 5.2.5.3 (1) of NFPA 59A is as follows.

$$S^* = 3\,\mathrm{sqrt}(A) \quad \text{for hazard flux} = 5\ \mathrm{kW/m^2} \qquad \text{(A-1a)}$$

$$S^* = 0.8\,\mathrm{sqrt}(A) \quad \text{for hazard flux} = 31.5\ \mathrm{kW/m^2} \qquad \text{(A-1b)}$$

or

$$\frac{S}{R} = \left(\frac{S^*}{R}+1\right) = 6.3174 \quad \text{for hazard flux} = 5\ \mathrm{kW/m^2} \qquad \text{(A-2a)}$$

$$\frac{S}{R} = \left(\frac{S^*}{R}+1\right) = 2.418 \quad \text{for hazard flux} = 31.55\ \mathrm{kW/m^2} \qquad \text{(A-2b)}$$

where,

S* = Safety distance for person exposure from the dike edge (m)
A = Area of impoundment (m^2)
S = Safety distance for person exposure from the dike center (m)
R = Radius of an equivalent circle of area A (m)

A.2.2 LNGFIRE 3 model

This model was developed under the GRI sponsorship and referenced for use in NFPA 59A [§ 5.2.5.3 (1)] uses a solid flame model in which the LNG fire in an impoundment is represented by a cylindrical fire with uniform emissive power[16] (E) over the entire surface area of the fire. The actual emission rate in this model is dependent on the fire diameter (and is again assumed constant over the entire fire). This emissive power is given by,

$$E = E_f\ [1-\exp(0.3 * D)] \quad ; D \text{ in meters} \qquad \text{(A-3)}$$

In LNG FIRE III, the value of E_f is set to 190 kW/m^2. (A-4)

For circular pools, the flame is assumed to be a tilted cylinder with a visible flame length that is calculated from the equation developed by Thomas:

$$\frac{L_f}{D} = 42\left[\frac{m''}{\rho_a \sqrt{gD}}\right]^{0.61} \qquad \text{(A-5)}$$

Where L_f = Flame length (m)
D = Pool diameter (m)
$\dot{m}''$ = Mass burning rate
= 0.11 kg/m^2 s [@ wind speed = 0 & rectangular or circular pool] (A-6)
ρ_a = Ambient air density = 1.2 kg/m^3

Experimental fire data: The data from the 15 m China Lake and 35 m Montoir LNG fire tests have indicated that as the fire size increases the fire becomes more and more smoky and that the emissive power varies from the bottom to the top. It is also noticed that the visible fire plume length is given by Thomas' modified fire length correlation (see below)

$$\frac{L_F}{D} = 55\left\{\frac{\dot{m}''}{\rho_a \sqrt{gD}}\right\}^{\frac{2}{3}} \qquad \text{(A-7)}$$

and the measured value for $\dot{m}'' = 0.14\ kg/m^2$ s (A-8)

Calculations based on China Lake tests (Raj, et al 1979), Montoir tests (Nedelka, 1989) and recent calculations (Raj, 2006), based on a model developed with the Montoir test data, indicate

[16] Emissive power is the radiant heat flux emanating from each unit surface area of the "equivalent cylindrical fire" and is expressed in kW/m^2.

that the mean constant-over-the-fire cylindrical surface emissive power, defined on the basis of fire length from equation A-7 are as follows:

E_f = 220 kW/m^2 for 15 m diameter fires (A-9)
E_f = 165 kW/m^2 for 35 m diameter fires
E_f = 115 kW/m^2 for 100 m diameter fires
E_f = 107 kW/m^2 for 300 m diameter fires

It is noted that the mean emissive power decreases as fire size increases. The hazard distance values to ground level targets calculated from three different models for different fire diameters, with two hazard heat fluxes, no atmospheric absorption of radiant heat and zero wind (vertical fires with bases on the ground) are indicated in Table A-1. The results in Table A-1 are plotted in Figure A-1 and Figure A-2, respectively for heat flux values of 5 kWm^2 and 31.5 kW/m^2.

The three models used for comparison are (i) the NPFA 59A point source model as specified in **§ 5.2.5.3 (1),** (ii) the LNGFIRE 3 model specified both in NFPA 59A and in US DOT Regulations, 49 CFR part 193, and (iii) A recent LNG pool fire model ("Pool Fire Model Including Smoke Effects- PoFMISE). The NFPA model is, by the very construct of the model, is inferred to be applicable to vertical plane elements on the ground, under no atmospheric absorption and zero wind conditions. These conditions are imposed on the other two models also so that the results can be compared on the same basis.

Figure A-1 shows the calculated hazard distances by the three models for the 5 kW/m^2 heat flux criterion to a vertical element on the ground receiving heat when no heat is absorbed in the atmosphere and the fire plume is vertical (no wind). Figure A-2 shows similar results for the case of heat flux at 31.5 kW/m^2.

It is noted from the results that the point source model does not give conservative results. In fact, the distances predicted by the point source model are consistently less than that predicted by LNGFIRE 3 model. If there is a wind, the down wind hazard distances calculated by LNGFIRE 3 will be even greater than that presented in Figures A-1 and Figure A-2 making, whereas there will be no effect on the values calculated by the point source model. Under these conditions, the difference between the two models will become even more pronounced.

The comparison between the results in Figure A-1 from the LNGFIRE 3 and PoMISE models indicates that except for very small fires (< 40 m diameter) the former model gives larger hazard distances. In fact, for larger diameter fires LNG FIRE 3 predicts a hazard distance that is higher, by almost 25%, compared to that predicted by PoMISE. This is because, in the LNGFIRE 3 model the overall surface emissive power remains the same irrespective of the fire size, whereas, in the PoMISE model the fire becomes sootier with increase in diameter, and therefore the SEP over the fire surface decreases.

Table A-1
Comparison of hazard distances predicted by different models

	Distance in **meters** from fire center to ground level vertical element					
	q_{Haz} = 5 kW/m^2			q_{Haz} = 31.5 kW/m^2		
Fire Diameter (D) **m**	NFPA 59A Point Source Model (S) m	LNGFIRE 3 (S) m	Smokey fire PoMISE (S) m	NFPA 59A Point Source Model (S) m	LNGFIRE 3 (S) m	Smokey fire PoMISE (S) m
20	63.2	96.2	103.1	24.2	31.7	33.6
30	94.8	136.9	147.7	36.3	46.5	51.0
50	157.9	213.2	212.9	60.5	75.1	80.1
100	315.9	388.2	339.8	120.9	143.0	136.7
200	631.7	706.7	570.3	241.8	270.8	242.2
300	947.6	1003.0	785.2	362.7	392.8	339.8

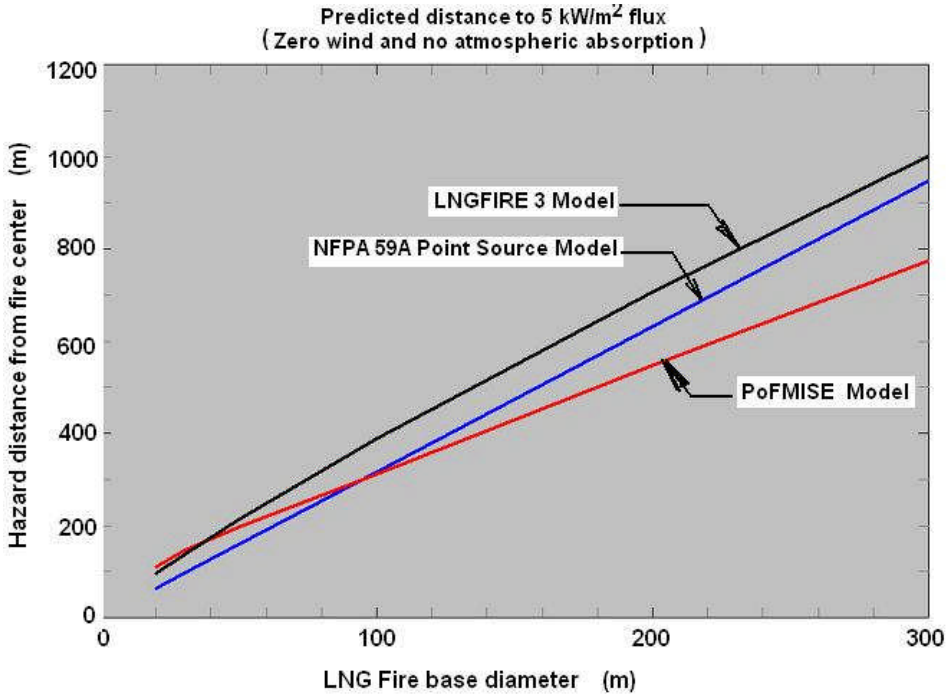

Figure A-1: Comparison of hazard distances to 5 kW/m^2 heat flux predicted by point source and solid fire models

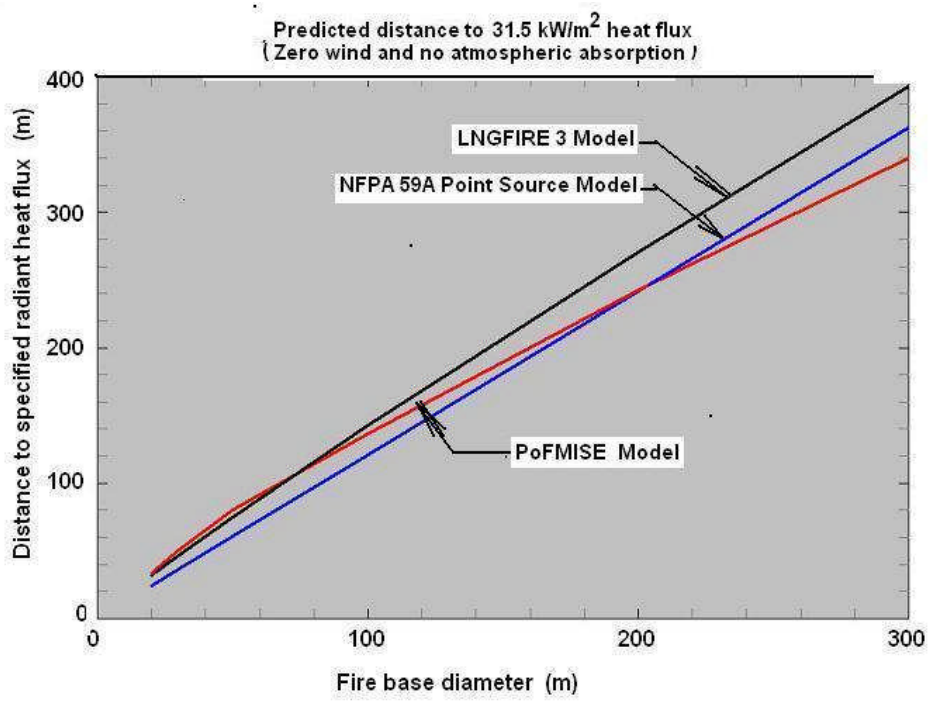

Figure A-2: Comparison of hazard distances to 31.5 kW/m^2 heat flux predicted by point source and solid fire models

Appendix B

Relationship between Visible Fire Plume Height, Diameter and Burning Rate

B.1 Introduction

Observations from fire experiments as well as accidental fires over burning pools of hydrocarbon liquid fuels indicate that the visible fire plume is very columnar, for fires up to about 50 m diameter. That is, the visible fire looks very much like a vertical (in low wind conditions), burning and radiating plume. The visible plume height is not fixed in time but pulsates up and down about a mean height. The pulsation rates change with the diameter. Also, as the fire diameter becomes larger, the entire dynamics of burning in the upper layers change due to the formation of a toroidal vortex. The puff type burning, with the toroidal vortex, results in recirculation of the burnt gases, dilution of air and formation of smoke, which is brought out to the surface by the toroidal circulation. The net effect of this is to make the combustion less efficient at the upper layers of larger fires. While the height up to which the combustible gases burn inside the fire may not be affected (other than by the air entrainment dynamics), the thermal radiation output from the upper layers is considerably reduced.

The observation that liquid pool fires burn in a long column of relatively same diameter from the base to the tip of the observable flame sheet is used in formulating the physical problem described below. Also used in the analysis below is the concept that only a fraction (β) of the mass of air entrained up to a given height "burns" with its stoichiometric equivalent fuel. This "inefficiency in combustion" continues until there is no more fuel vapor left in the air-fuel mixture to burn. The height at which all of the fuel is exhausted is considered to be the top of the visible flame height. This concept has been successfully used (Raj [1981) in a mathematical model to explain the experimentally measured centerline temperature and gas velocity variation with height in a 15.2 m diameter JP-4 pool fire.

B.2 Analysis

A fire shown, schematically, in Figure B-1 is considered. The vertical extent of the visible plume of the fire is represented by a flame height L_F. The "Control volume" for the analysis is assumed to be a cylinder formed by the base diameter of the fire and the "visible" fire height (L_f).

Air for combustion is entrained from the atmosphere along the sides of the visible plume boundary. A part of the air entrained "burns" in stoichiometric proportion with fuel vapor flowing at that height. The remainder of the fuel vapor traveling up in the fire plume burns with the same fraction of air entrained in the next layer. The top of the visible plume is represented by the height at which all of the fuel mass emanating at the "pool surface" is stoichometrically burned with air. That is, the gases that are in the updraft at the level of the top of the visible fire plume consist of products of combustion and excess air only.

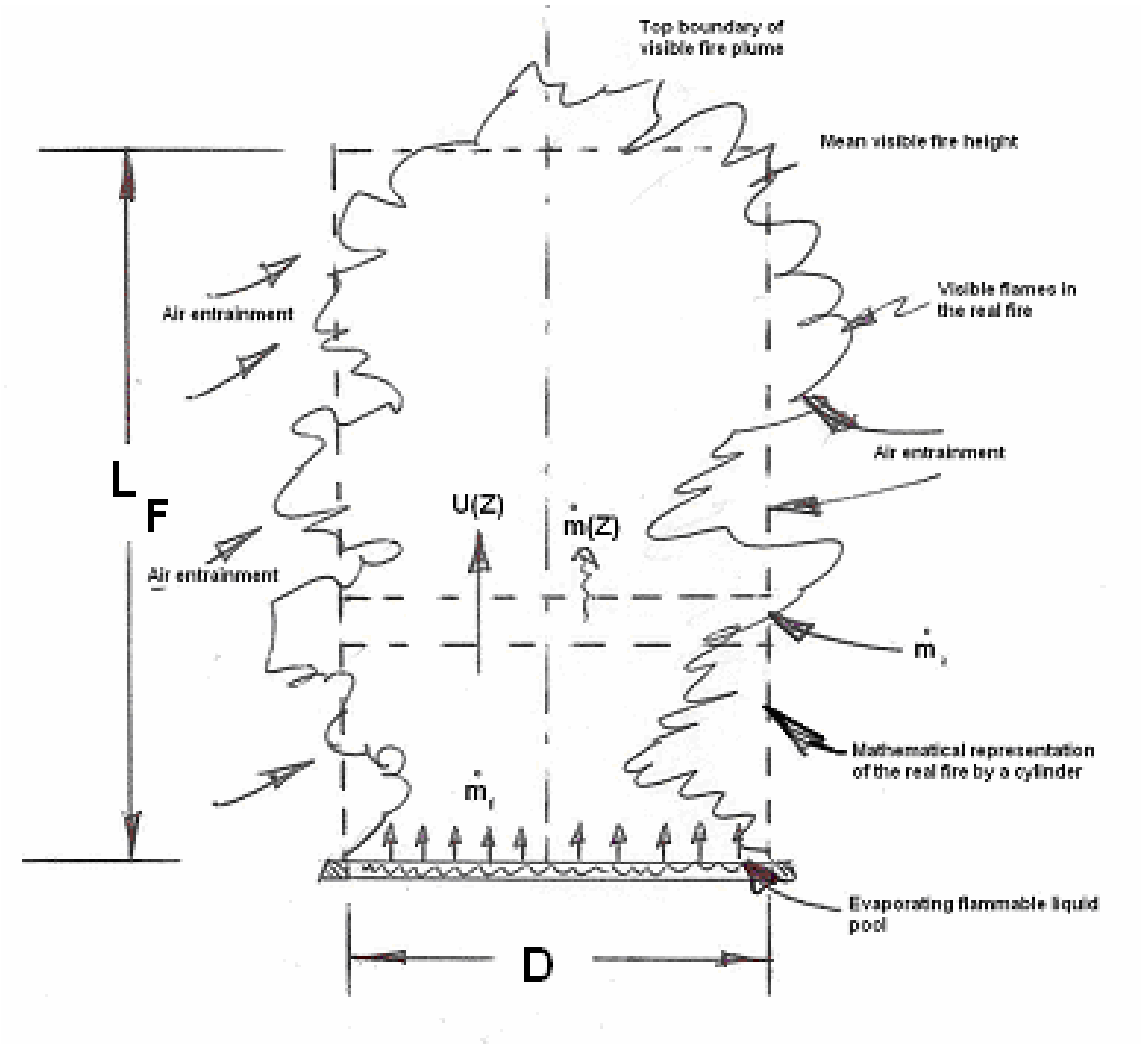

Figure B-1: Schematic representation of the air entrainment into a circular base fire for developing fire plume height correlation

In addition to the physical description above (and the assumptions that are part of the description) the following additional phenomena are assumed.

1 The entrainment of air occurs at the periphery of the column fire

2 The air entrainment rate at any horizontal section (at height Z) is proportional to the local mean vertical upward velocity of gases at that height. The local upward velocity used for entrainment is the velocity of gases averaged over the horizontal section of fire at height z.

3 The mean upward velocity of gases at any height Z is proportional to the square root of Z. (This is borne out of large field tests with other hydrocarbon fires where such velocity measurements have been made, Raj [1981]).

B.2.1 Model equations

Referring to Figure B-1, we write the mass flow rate of gases within the visible plume, at any height Z above the base of the fire[17]

$$\dot{m}(Z) = \dot{m}_f + \dot{m}_a(Z) \qquad \text{(B-1)}$$

Where

$\dot{m}(Z)$ = Mass flow rate at section at height Z

$\dot{m}_f$ = Mass flow rate of fuel at fire base

$\dot{m}_a(Z)$ = Mass rate of air entrainment up to height Z

It can be shown from the assumption on the entrainment rate that

$$\dot{m}_a(Z) = \rho_a \alpha \int_{z=0}^{z=Z} U(Z)\, \pi D\, dZ \quad = \rho_a \alpha \bar{U}(Z)\, \pi D Z \qquad \text{(B-2)}$$

where,

α = Air entrainment coefficient (of the order of 0.1)

U(Z) = Mean upward velocity of gases at section Z

$\bar{U}(Z)$ = Mean velocity of gases over the height 0 to Z

The last term on the RHS of equation B-2 represents the side area of the fire over which air is entrained. It is known from the literature and analyses (Raj [1981]) that the mean upward velocity of gases at any height is given by the expression

$$\bar{U}(Z) = \frac{2}{3}\sqrt{2g\frac{\Delta\rho}{\rho_a}Z} \qquad \text{(B-3)}$$

with

$$\frac{\Delta\rho}{\rho_a} = \frac{\rho_a - \rho}{\rho_a} \qquad \text{(B-4)}$$

The term $\Delta\rho/\rho_a$ represents the fractional decrease in the density of gases due to combustion. It is shown later that this term is a constant and does not vary (to the accuracy of our assumptions) in the Z -direction within the fire. The constancy of this term is a result of the

[17] See the section on "Nomenclature" for the definition of symbols.

assumption that a mass fraction β of the mass of air entrained up to a height Z "burns" with its equivalent stoichiometric mass of fuel vapor.

The top of the visible flame represents the section by which all of the fuel generated at the base of the fire is consumed by burning. That is at $Z = L_F$ we have,

$$r\,\dot{m}_f = \beta\,\dot{m}_a(L_F) \qquad \text{(B-5)}$$

where,

r = Stoichiometric air to fuel mass ratio (17.17 for CH_4)

β = Mass fraction of air entrained that burns with fuel, stoichiometrically

Substituting equation B-2 and equation B-3 in equation B-5 and setting $Z=L_F$, and rearranging we get

$$\beta\,\alpha\,\rho_a\left(\frac{2}{3}\right)\sqrt{2g\,\frac{\Delta\rho}{\rho_a}L}\;\left(\pi D L_F\right) = r\,\dot{m}_f''\,\frac{\pi}{4}D^2 \qquad \text{(B-6)}$$

with $\dot{m}_f''$ representing the mass evaporation rate from the pool per unit area. Equation B-6 can be written in a modified way as follows.

$$\frac{L_F}{D} = \left[\frac{3r}{8\sqrt{2}\,\beta\alpha\sqrt{\frac{\Delta\rho}{\rho_a}}}\right]^{\frac{2}{3}}\left(\frac{\dot{m}_f''}{\rho_a\sqrt{gD}}\right)^{\frac{2}{3}} \qquad \text{(B-7)}$$

B.2.2 <u>Evaluation of the fractional density deviation term</u> $\left(\frac{\Delta\rho}{\rho_a}\right)$

Assuming that the gases are perfect with the same molecular weight.

$$\frac{\Delta\rho}{\rho_a} = \frac{\frac{\Delta T}{T_a}}{1+\frac{\Delta T}{T_a}} \qquad \text{(B-8)}$$

where, $\Delta T = (T - T_a)$ temperature rise of the gases due to the heat generated by combustion. Hence, in the L/D correlation in equation B-6 the fractional increase in the temperature of the burnt gases and excess air mixture relative to the outside air temperature can be substituted (from equation B-8) for the fractional density decrease $\left(\frac{\Delta\rho}{\rho_a}\right)$.

Consider a horizontal plane at height Z above the base of the fire. Using the definition of the parameters indicated earlier we show that

$$\dot{m}_f(Z) = \beta \frac{\dot{m}_a}{r} \qquad \text{(B-9)}$$

where,

$\dot{m}_f(Z) =$ Mass rate of fuel burning up to height Z.

The total heat production rate by combustion up to height Z is therefore,

$$\dot{Q}(Z) = \dot{m}_f(Z)\,\Delta H_C = \beta \frac{\dot{m}_a}{r} \Delta H_C \qquad \text{(B-10)}$$

Assuming that all gases have the same mass specific heat, we write the enthalpy equation for the gases at a height Z plane,

$$\left\{\dot{m}_{f,0} + \dot{m}_a(Z)\right\} C_a\, T(Z) = \left\{\dot{m}_{f,0}\, C_f\, T_f(0) + \dot{m}_a(Z)\, C_a\, T_a\right\} + \dot{Q} \qquad \text{(B-11)}$$

where,

$\dot{m}_{f,0} =$ Mass flow rate of fuel at the base of the fire

Assuming (without significant loss of generality) that $C_f\, T_f(0) = C_a T_a$, using equation B-8, substituting equation B-10 in equation B-11 and rearranging we show that

$$\frac{\beta}{r} \frac{\Delta H_c}{C_p T_a} \frac{\dot{m}_a}{\left(\dot{m}_{f,0} + \dot{m}_a\right)} = \frac{T(Z) - T_a}{T_a} = \frac{\Delta T}{T_a} \qquad \text{(B-12)}$$

It is known that the mass of air entrained up to any height Z (for Z>0.1 D) is substantially larger than the mass flow rate of vapors at the fire base (For example, the total mass of air flowing through the top of the visible flame is estimated to be an order of magnitude higher than the stoichiometric value of r =17.17; that is, the air entrainment is about 170 times the mass flow rate of vapors at the surface of the pool). Hence, the ratio $\dot{m}_a / \left(\dot{m}_{f,0} + \dot{m}_a\right)$ can be considered to be unity. In this case, equation B-12 indicates that the ratio of temperature rise of the gases and air temperature is constant for all heights.

Equation B-6 is written in a non-dimensional form as follows[18]:

[18] If the fire plume is assumed to be an inverted frustum of a cone with base diameter equal to the fire diameter and the cone angle is α then it can be shown that the equation A13 changes to

$$\frac{L_F}{D}\left\{1 + \frac{\alpha}{2}\left(\frac{L_F}{D}\right)\right\}^{(2/3)} = A\, F^{2/3}$$

$$\frac{L_F}{D} = A F^{2/3} \qquad \text{(B-13)}$$

where,

$$\text{F} = \text{Froude Number} = \left(\frac{\dot{m}''_f}{\rho_a \sqrt{gD}} \right) \qquad \text{(B-14a)}$$

$$\text{A} = \text{Constant Factor} = \left[\frac{3r}{8\sqrt{2}\,\beta\alpha \sqrt{\frac{\Delta\rho}{\rho_a}}} \right]^{\frac{2}{3}} \qquad \text{(B-14b)}$$

We now define,

$$\mathcal{D} = \text{Damkohler number} = \frac{\Delta H_c}{C_a T_a} \qquad \text{(B-15)}$$

Substituting results of equation B-8, equation B-12 and equation B-15 in equation B-14b we get,

$$A = \left[\frac{9}{128\,\alpha^2 \mathcal{D}} \right]^{(1/3)} \frac{r}{\beta} (1 + \mathcal{D}\,\frac{\beta}{r})^{1/3} \qquad \text{(B-16)}$$

Equation B-13 shows that L_F/D ratio of the fire varies as the 2/3 power of the non-dimensional burning rate or the combustion Froude number. This exactly the result indicated by Thomas [1965]. Heskestad [1983] also has published the correlations for the L_F/D ratio for a wide range of Froude number; his correlation, though has a different mathematical formula, follows the 2/3 law in the applicable values (for large fires) of the Froude number. The correlation of Thomas indicates the following

$$\text{A} = 55 \qquad \text{(B-17)}$$

The above value is based on wood crib fire experimental data. This value of A is used below to estimate the value of the combustion efficiency factor β.

B.2.3 Combustion efficiency factor (β)

The following values for the thermal and combustion properties of methane and other parameters are used.

r	=	Air to fuel mass ratio for stoichiometric combustion	= 17.1674
ΔH_c	=	Heat of combustion	= 50.02 MJ/kg

For most fires of interest with L_F/D in the 0.5 to 3 range, and $\alpha = 0.1$, the second term in the { } brackets is small compared to 1 and can be neglected.

C_a	=	Specific heat of air	= 1000 J/kg/ K
T_a	=	Air temperature	= 293 K
α	=	Air entrainment coefficient	= 0.1
$\mathcal{D}$	=	Damkohler number = $\Delta H_c/(C_a T_a)$	= 170.05

Substituting the above values on the RHS of equation B- and setting A = 55 results in a value of $\beta = 0.1454$. That is, by the time the combustion of all of the fuel is complete about $1/\beta = 6.88$ times the stoichiometric mass of air is ingested into the fire. This is in keeping with the experimental observations reported by Thomas that an order of magnitude more air than the stoichiometric mass is entrained into the fire. The same approach when used with the JP-4 fire data results in $\beta = 0.06$. Hence, there is some uncertainty as to where the "visible fire plume" ends on a statistical mean basis.

Also, it can be shown from the above value of β and the relationships in equation B-8 and equation B-12 that

$$\frac{\Delta T}{T_a} = \frac{\beta}{r} N_E = 1.44 \quad \text{and} \quad \frac{\Delta \rho}{\rho_a} = 0.59 \qquad \text{(B-18)}$$

B.3 Conclusions

1 The analysis above shows clearly that for most liquid pool fires of hydrocarbon fuels that may occur due to accidents the height of the visible plume can be estimated by an equation (Thomas' modified equation). The L/D ratio of the fire varies as the 2/3 power of the combustion Froude number.

2 The model developed provides a means of estimating the value of the constant factor for different fuels with known properties of the fuel and assumed efficiency of combustion.

3 The model presented does not provide any means of indicating how the radiation output from the fire varies with height nor does it predict the chemistry that occurs within the fire (due to combustion inefficiencies).

Nomenclature (for Appendix B)

A	=	A fuel property and dynamics dependent constant	
D	=	Diameter of the base of the fire (or liquid pool diameter)	(m)
F_c	=	Combustion Froude Number = $\left(\frac{\dot{m}''_f}{\rho_a \sqrt{gD}} \right)$	
g	=	Acceleration due to gravity	(m/s^2)
L	**=**	**Length (height) of the visible fire plume**	**(m)**
ΔH_c	=	Heat of combustion of the fuel	(J/kg)
C_a	=	Specific heat of air (assumed the same for all gases)	(J/kg K)
$\dot{m}(Z)$	=	Total mass flow rate of gases at any height Z	(kg/s)
$\dot{m}_a(Z)$	=	Mass rate of entrainment of air up to height Z	(kg/s)
$\dot{m}_{f,0}$	=	Mass rate of fuel feed into the fire at the base	(kg/s)
$\dot{m}''_{f,0}$	=	Mass flux of fuel vapor at the base of fire	(kg/s m^2)
$\dot{m}_f(Z)$	=	Mass rate of fuel burning up to height Z.	(kg/s)
N_E	=	Emmons' number = $\Delta H_c/(C_a T_a)$	
r	**=**	**Air to fuel mass ratio for stoichiometric combustion**	
$\dot{Q}(Z)$	**=**	**Heat produced by combustion of fuel up to height Z**	**(W)**
T_a	=	Air temperature	(K)
T(Z)	=	Mean temperature of the gases at any height Z	(K)
U(Z)	=	Cross sectional average upward velocity of gases at any height Z	(m/s)
$\bar{U}(Z)$	=	Vertical height averaged upward gas velocity up to height Z	(m/s)
α	=	Air entrainment coefficient	
β	=	Mass fraction of air that is entrained up to any height Z that burns stoichiometrically with fuel	
ρ	=	Density of gases	(kg/m^3)
ρ_a	=	Density of air	(kg/m^3)

Subscripts

a	=	Air
c	=	Combustion condition
f	=	Fuel vapors
0	=	Fire base condition

Chapter C

Analysis of Risks from LNG Fires - A Protocol for Using the Models

C.1 Introduction

In many industries, decisions on the acceptability of a project are routinely based on the magnitude of risks posed by the project to the public, the workers and the investors. The US military uses a screening risk assessment methodology, specified in MIL Std 882C, to perform preliminary assessments. The Nuclear Regulatory Commission requires[19] the performance of a detailed Quantitative Risk Assessment (QRA) for siting nuclear power plants. Risk based decisions on alternative LNG transportation routes have been made in the past {ADL, 1978]. However, the current codes and regulations in the US related to LNG plant siting are prescriptive in specifications. As a minor part of this project a preliminary assessment was undertaken to develop a risk based protocol for considering, specifically, the LNG fire risks.

It is found that in the context of regulatory and/or code requirements for chemical and other plant risk assessment that two types of risks are identified. These are, (i) "Individual Risk," i.e., risk to an individual potentially affected by the detrimental effects of a release of a chemical, and (ii) "Societal Risk," in which the totality of the number of persons potentially exposed and the frequency of exposure are determined and compared with some acceptability criteria. "Risk" itself is defined as the combination (not necessarily the product) of the frequency of occurrence and the consequential (detrimental) effects on the public or other entities arising from an industrial activity in which an accidental release of a chemical into the environment is a possibility. In Europe, the requirements for risk analysis as the basis of decision-making by regulatory agencies are promulgated in the "Seveso II" directive [SEVESO II, 2003]. In England, the Seveso II directive is implemented under the COMAH Regulations [COMAH, 2005]. The Health and Safety Executive (HSE), in England, administers the processes related to facility application review, inspection and certification protocol in these regulations. HSE has issued a guidance document detailing the steps to be used in performing the risk analyses required under the regulations [HSE, 2001].

The focus of the risk assessment required by the European regulations is the "**Societal Risk**," although "**Individual Risk**" also needs to be evaluated. The definition of these types of people risks as given by Ball & Floyd [1992] are indicated below:

"Individual Risk *is the frequency with which an individual may be expected to sustain a given level of harm from the realization of specified hazards*." And

"***Societal Risk*** *is the relationship between the frequency and the number of people suffering from a specified level of harm in a given population from the realization of specified hazards.*"

[19] 10 CFR, § 52.47.

In general, the European regulations consider only the fatalities as the measure of consequence; that is, all calculations of hazard are geared towards determining the number of persons suffering potential fatalities. The risk itself is calculated by selecting a set of potential "credible, high consequence, low probability" release scenarios in the facility or plant. For each release scenario the probability of occurrence of the scenario is calculated (number of incidents/year or probability of occurrence per year) as also the extent of the hazards, subject to different conditional probabilities of occurrence (weather, ignitability, modes of behavior of the material released, etc). The number of persons exposed to a given level of hazard is calculated by counting the actual number of persons within a zone (radius) of hazard. Mitigating circumstances are considered, such as the fraction of the time a person is inside a shelter (building), protected by clothing, or is able to take evasive action to reduce the detrimental effects of the hazard. An example of this consideration is say, 100 people are residents within a given zone of fire thermal hazard for skin burn exposure, but only 15% of them are outside the buildings at any given time. Then the consequence count for this event will be counted as 15 and not 100.

HSE has established levels of acceptability of risks [HSPAG, 2004]. These risk regions are classified as (i) Broadly Acceptable, (ii) Tolerable Risk and, (iii) Unacceptable. These risk regions are indicated in the following figure with the specified numerical risk values.

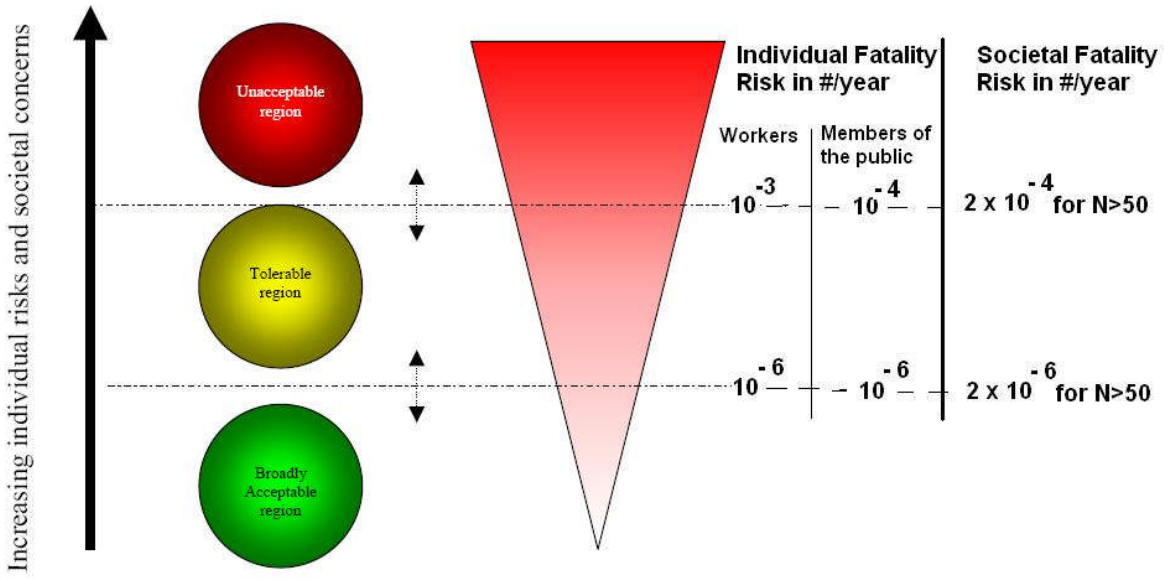

***Source: HSPAG** (2004)*

Figure C-1: Tolerability of risk framework according to HSE

The societal risk is generally illustrated on the F vs. N diagram (F stands for frequency per year of exceeding a consequence involving N or more persons affected by the consequence). In general, in safety studies related to the potential hazards arising from a chemical plant or an energy fluid storage facility (such as an LNG or LPG terminal) injury or fatality is used as a metric to measure the consequence. The HSE based acceptability criteria for societal risks are illustrated in Figure C-2.

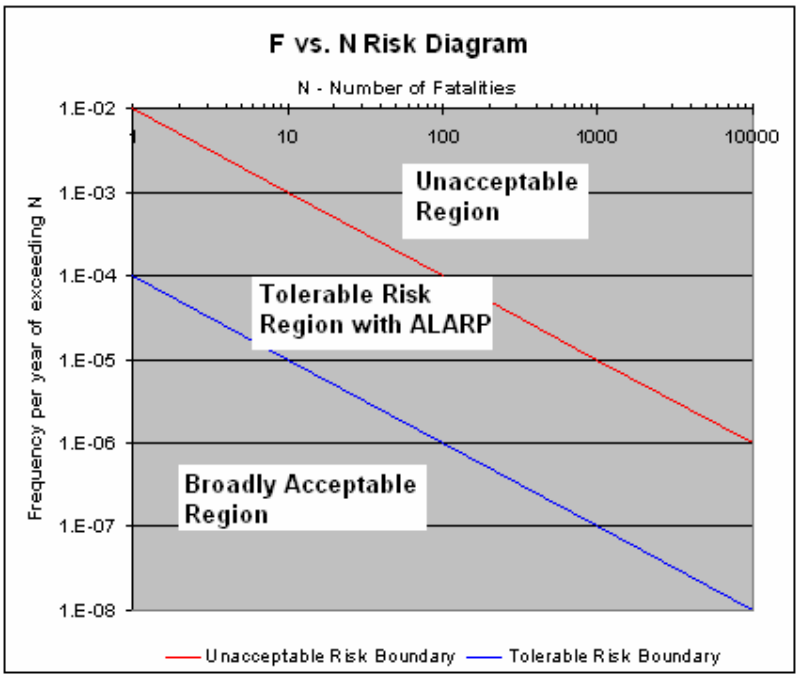

***Source**: HSE (2001)*

Figure C-2: Diagram showing the acceptable & unacceptable regions for societal risk

C.2 Risk Analysis application to LNG facilities

Risk analysis results for a project/facility (similar to an LNG facility) are plotted on the F-N diagram. Based on the location of the "F-N curve" for the project its acceptability can be determined using criteria similar to the one promulgated by the HSE (see Figure C-2). It is noted that for projects whose F-N curve falls within the "tolerable region," it is required for the project to demonstrate that all safety enhancing systems and procedures have been implemented to ensure that the risks are "As Low As Reasonably Practicable (ALARP)." This is the principle upon which most of the European regulations are based.

As mentioned earlier, the US regulations applicable to LNG facilities are not risk based. In any development of risk-based Regulations the following questions need to be answered before a risk based regulatory framework can be developed. The questions include whether to:

a) Prescribe unacceptable, tolerable and broadly acceptable risk-regions (in a diagram similar or same as the F-N diagram) in any future US regulations for LNG or any other industrial activity. Also there is a need to address how these "acceptable values" (and any associated judgmental considerations) are to be developed.

b) Consider only high consequence – low probability events for the determination of risk.

c) Limit the calculation of risks to only the off-site populations or include the facility workers also.

d) Impose criteria based purely on indices of hazard (ex, for thermal radiation either the intensity in kW/m^2 or the modified dosage units (MDU), etc) or whether the regulations allow consideration of the effects of hazard-reducing circumstances such as buildings and shelters, workday patterns, emergency response, ability of people to take evasive action in an emergency, etc.

e) Consider the failure criteria for buildings and structures based on their functions and the physical and thermal properties rather than specifying a single thermal incident flux criterion (as is the case at present).

f) Allow the reduction in individual risk by considering the % of time that an average person spends inside a building or in some such shelter.

g) Base decisions on the basis of individual risk values or societal risk values.

h) Specify fatality or injury as the hazard criterion. How should potential injuries (and the levels of injuries) be considered for presenting the overall risk from a project?

C.3 Risk calculation protocol for assessing fire risks from a LNG facility

The evaluation of the overall fire risks from a LNG facility involves a number of different calculations. The risk assessment consists of three important phases, namely (i) Data collection phase, (ii) Release scenario development phase and (iii) Risk determination phase

C.3.1 Data collection

In this phase the various physical and operational data for the facility should be colleted. These data include, but are not limited to,

1 Sizes and volumes of storage tanks, dike details, sizes of transfer piping, pumping or flow rates, pipeline pressures in each type of piping,

2 Details of the surrounding community including the topography, population density and location of houses, industrial and commercial centers, locations of sensitive populations, distribution and sizes of buildings, and any emergency shelters, etc.

3 Local meteorological conditions.

4 Any systems or procedures available for mitigating the occurrence of or effect of LNG fires.

5 Historical data, if available, on the modes of failures of components and systems used in LNG facilities or in ships or in the docks for unloading ships.

6 Other relevant information such as the criteria used for hazards (heat fluxes or burn injury levels, structural failures stresses or temperatures, etc).

C.3.2 Release scenarios

The various potential scenarios of LNG release leading to a fire should be identified. The cause of release may be either accidents or intentional acts. In addition, the scenarios must be described quantitatively in terms of rates of release, duration of release, total quantity of release, etc.

Table C-1 shows a possible list of scenarios of LNG release due to accidents in a facility that could lead to the occurrence of a fire. Similarly, the various scenarios of fire that may occur due to the release of LNG from intentional acts (sabotage, terror attack) in an LNG facility are indicated in Table C-2. The scenarios identified in these two tables are to be considered only as illustrations and not the entire spectrum of events that can occur in either accidents or from intentional acts. Each scenario may lead to different types and sizes of LNG fires or in some cases a sequence of different types of fires based on when the flammable vapors are ignited.

C.3.3 Risk determination

This phase of risk analysis includes the identification/determination of the probabilities of occurrence (including conditional probabilities of occurrence of sub-events) and the calculation of the consequences.

Event(s) probability identification: The annual probability of each type of release (identified in Tables C-1 and C-2) must be quantified either from historical data, HAZOP studies, and failure analysis or based on engineering judgment. Each principal release scenario may have sub-scenarios of behavior of the released LNG resulting in different types of fires. These sub-scenarios must be evaluated and the conditional probability of occurrence of each must be developed, again from historical data, if such are available, or from "engineering experience and assessments."

The purpose of developing Tables similar to Table C-1 or Table C-2 is to identify the probabilities with which the named events (including the sub events) occur in a year. The difficulty in filling these tables with proper probability values is well recognized, especially in the LNG facility or ship transportation matters since, and very fortunately, there are no historical data of accidents in or intentional acts against the industry. Therefore, in any risk assessment of the LNG facility it should be recognized that there are considerable error margins (even as high as one order of magnitude) in the estimation of the probabilities of occurrence of various fire scenarios.

Table C-1
Identification of LNG release scenarios in a plant
(Accidental releases)

Principal Release Scenario	Annual Probability of Principal Scenario	Sub-Scenario	Conditional Prob. of Sub-scenario	Quantities of release and description fire type				
				Rate of release (kg/s)	Duration of release (s)	Total quantity released (kg)	Types of fires	Conditional prob. of fire type
Ship-to-shore pipeline damage	P_1	Gasket leak or weld crack	$P_{1,1}$	----	----	----	Jet fire	1
		Impact by an object – small hole on pipe wall	$P_{1,2}$	----	----	----	Jet fire	1
		Guillotine break due to a large vehicle impact	$P_{1,3}$	----	----	----	Jet fire	0.3
							Pool fire	0.7
Send out pipe damage	P_2	Small release	$P_{2,1}$				Jet fire	
		Large release	$P_{2,2}$				Pool fire	
Vaporizer damage	P_3	Small release	$P_{3,1}$				Jet fire	
		Large release	$P_{3,2}$				Pool fire	
Truck fill station releases*	P_4	Uncoupling of transfer hose	$P_{4,1}$				Impoundment Pool fire (Immediate ignition)	
			$P_{4,2}$				Fireball & pool fire (slightly delayed ignition)	
			$P_{4,3}$				Vapor fire (very delayed ignition)	

* Assuming that a truck fill station exists

Table C-2
Identification of LNG release scenarios in a plant
(Occurring due to intentional acts of sabotage or terror)

Principal Release Scenario	Annual Probability of Principal Scenario	Sub-Scenario	Conditional Prob. of Sub-scenario	Quantities of release and description fire type				
				Rate of release (kg/s)	Duration of release (s)	Total quantity released (kg)	Types of fires	Conditional prob. of fire type
Ship-to-shore pipeline damage	P_1	Small arms penetration of pipeline	$P_{1,1}$	----	----	----	Jet fire	1
		Ramming of a vehicle onto the pipeline	$P_{1,2}$				Vapor fire and pool fire	
							Pool fire only	
		Explosive pipeline severance-Guillotine break	$P_{1,3}$	----	----	----	Pool fire	1
Missile impacting a LNG storage tank	P_2	Small release	$P_{2,1}$				Liquid Jet Fire & pool fire in the impoundment	
							Pool fire in the impoundment	
		Large release	$P_{2,2}$				Spreading Pool fire outside impoundment	
							Pool fire in the impoundment	
Vaporizer damage	P_3	Small release	$P_{3,1}$				Jet fire	
		Large release	$P_{3,2}$				Pool fire	
Truck fill station releases*	P_4	Deliberate uncoupling of transfer hose	$P_{4,1}$				Impoundment Pool fire (Immediate ignition)	
			$P_{4,2}$				Fireball & pool fire (slightly delayed ignition)	
			$P_{4,3}$				Vapor fire (very delayed ignition)	

Fire consequence analysis:

The purpose of the consequence analysis is to determine the number of persons that may be susceptible to the fire hazard for a given size and type of fire. The hazard to people outside the direct fire-flame zone will be due to radiant heat effects. In the case of vapor fires, the area occupied by the vapor with concentration at ground level above the lower flammable limit (5%) will form the direct vapor fire hazard area in addition to the radiant heat effects area outside this cloud. If ignition occurs before the cloud is established (to its maximum 5% contour area on the ground), then the area of the cloud from the ignition point to the source will constitute the hazard area. In the case of the jet fire, the direct impingement area of the flame together with the radiant heat area surrounding the fire in which the radiant heat flux is above a critical value will constitute the hazard area. In general, the latter is expected to be very small in comparison to the pool fire or the vapor fire hazard area. The criterion used in the US for evaluating the fire radiant thermal hazard to people is the second-degree burn over more than 10% of the body.

Using the fire models discussed in this report (Chapter 3 and Chapter 4) the areas of hazard between different radiant heat exposure flux values can be determined. For example, for a LNG pool fire of a given diameter and for specified wind speed, atmospheric temperature and relative humidity conditions the contour area around the fire for a specified heat flux can be determined. By calculating such areas for different levels of radiant heat fluxes the hazard area between, say, heat flux q_1 and heat flux q_2 can be determined. These are schematically illustrated in Figure C-3. It is assumed that the duration for the onset of 2^{nd} degree burn hazard due to radiant heat is dependent on the magnitude of the incident heat flux. Once this relationship between the heat flux and burn injury critical time is known, then the number of persons that may suffer second degree burns and the conditional probability (given that an exposure to the given level of heat flux occurs) and therefore the number of injuries can be determined. This procedure is illustrated with an example below.

C.4 Determination of the probability and number of radiant heat caused injuries - An illustrative example

Consider the schematic representation of the location of residences and other buildings within the heat flux contours q_1 and q_2. The assessment of the burn injuries to people located within the two contours is made by determining the type of population that “resides” within the zone, the fraction of the persons that may be outside the buildings and unsheltered during a fire incident, the probability of injury to a person given that he/she is exposed to the specified level of heat flux, etc.

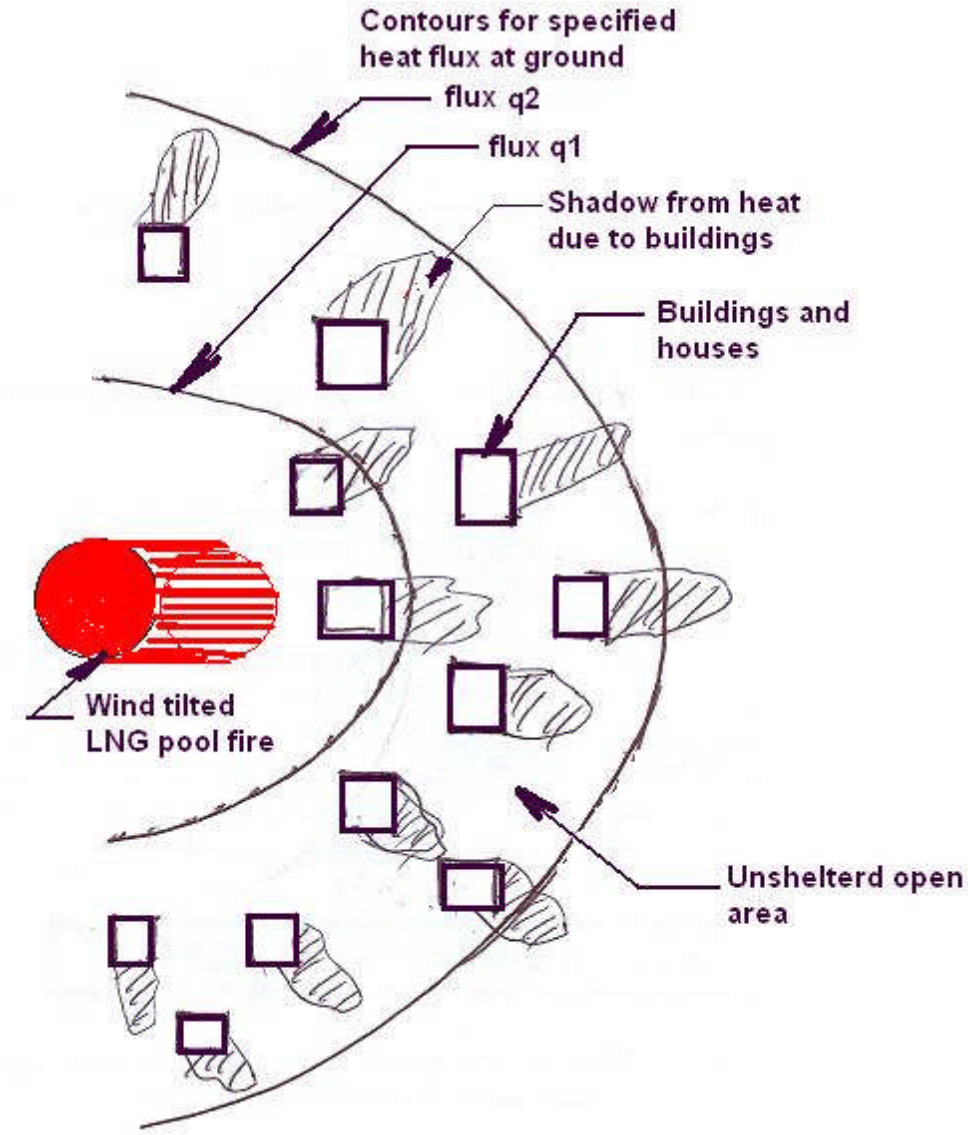

Figure C-3: Diagram of an example distribution of buildings, building shadows (shelters) and potential exposure areas for burn injury to people from fire radiant heat effects

In order to perform these risk calculations the following parameters are defined.

A_H	=	Average foot print area of a building or residence	(km^2)
A_S	=	Average area of the shadow (for radiant heat) behind a building or a residence	(km^2)
N_{burn}	=	Number of persons suffering burn injuries per km^2	(#/km^2)
N_H	=	Number density of houses/buildings per square km	(#/km^2)
N_P	=	Normal population density in the area	(# of persons/km^2)
F_O	=	Average fraction of the population that is outside buildings at any time	
F_{pop}	=	Fraction of the total population representing each "type" of population	
p_{burn}	=	Conditional probability of suffering a burn injury by exposure to the radiant heat flux q.	
R	=	Average distance that a person has to move before he/she can be in the shadow of building or go into a building for cover.	(m)
$t_{cri}(q)$	=	A critical time of exposure to cause 2nd degree burn injury (this time is dependent upon the radiant heat flux q)	(s)
$t_S(pop)$	=	Time in which a person will be able to seek shelter	(s)
U(pop)	=	Ambulation speed of a person in an emergency to seek shelter (This speed depends upon the age and other attributes of a specified group of persons, eg., children, physically challenged persons, older citizens, normal adults, etc)	(m/s)

Consider an area of 1 square km within the contours bounded by q_1 and q_2.

Average number of persons outside at any given time in this area $= f N_P$ (C-1)

Total area/km^2 that is in the open and outside the shadows $= [1- N_H (A_H+A_S)]$ (C-2)

Mean un sheltered area per house/building $= N_H/[1- N_H (A_H+A_S)]$ (C-3)

Mean radius of unsheltered area $= R = \sqrt{\frac{[1- N_H (A_H + A_S)]}{\pi N_H}}$ (C-4)

Therefore,

$$t_S = R/U(pop) \quad \text{(C-5)}$$

It can be argued that a person will suffer the 2nd degree and the probability of burn injury is 1 when

$$t_S(pop) >= t_{cri}(q) \quad \text{(C-6)}$$

In the case $t_S < t_{cri}$ the probability of burn injury varies between 0 and 1. We can therefore postulate a probability of burn depending upon the population type, heat flux and the mean distance of movement by the following formula,

$$p_{burn} = \frac{t_S(pop)}{t_{cri}} \quad for \quad t_S(pop) \le t_{cri} \qquad \text{(C-7a)}$$

and

$$p_{burn} = 1 \quad for \quad t_S(pop) > t_{cri} \qquad \text{(C-7b)}$$

The number of persons injured in 1 km^2, N_{burn} is given by

$$N_{burn} = N_P \, F_{pop} \, F_O \, [1-(A_H + A_S)] \qquad \text{(C-8)}$$

Equations 8 and 7 give, respectively, the number of persons injured of a specific population type and the corresponding conditional probability of injury given that a fire has occurred and the exposure is within the contours q_1 and q_2. The actual number injured in the contours will be the value given by equation 8 multiplied by the area within the contour.

The above calculations are repeated for various heat flux level contour pairs, sizes of “pool fires” and wind and weather conditions (if necessary). The resulting pairs of conditional probabilities of injury and number potentially suffering burn injury is accumulated in a database from which a f-N curve similar to that shown in Figure C-2 can be developed.

Similar calculation procedures can be implemented to determine the probabilities and radiant heat burn injuries and other types of injuries from vapor fires and jet fires. The combined procedures of such calculation as indicated above will constitute a protocol for determining the overall risk from an LNG facility. In the case of LNG spills from ships similar procedure can be adopted with different models used for calculating the sizes of pool fires, vapor fires and their probabilities of occurrence.